Reusable Rocket Upper Stage

Development of a Multidisciplinary Design Optimisation Tool to Determine the Feasibility of Upper Stage Reusability

L. Pepermans

Technische Universiteit Delft

TU Delft

Reusable Rocket Upper Stage

Development of a Multidisciplinary Design Optimisation Tool to Determine the Feasibility of Upper Stage Reusability

by

L. Pepermans

to obtain the degree of Master of Science
at the Delft University of Technology,
to be defended publicly on Wednesday October 30, 2019 at 14:30 AM.

Student number:	4144538	
Project duration:	September 1, 2018 – October 30, 2019	
Thesis committee:	Ir. B.T.C Zandbergen ,	TU Delft, supervisor
	Prof. E.K.A Gill,	TU Delft
	Dr.ir. D. Dirkx,	TU Delft

This thesis is confidential and cannot be made public until October 30, 2019.

An electronic version of this thesis is available at `http://repository.tudelft.nl/`.

Cover image: S-IVB upper stage of Skylab 3 mission in orbit [23]

TU Delft

Preface

Before you lies my thesis to graduate from Delft University of Technology on the feasibility and cost-effectiveness of reusable upper stages. During the accompanying literature study, it was determined that the technology readiness level is sufficiently high for upper stage reusability. However, it was unsure whether a cost-effective system could be build.

I have been interested in the field of Entry, Descent, and Landing ever since I joined the Capsule Team of Delft Aerospace Rocket Engineering (DARE). During my time within the team, it split up in the Structures Team and Recovery Team. In September 2016, I became Chief Recovery for the Stratos III student-built sounding rocket. During this time, I realised that there was a lack of fundamental knowledge in aerodynamic decelerators within DARE. This lead to the merger of the DARE Recovery Team and the Stratos III Recovery Team into the Parachute Research Group (PRG).
After the Stratos III launch, PRG proposed the Supersonic Parachute Experiment Aboard REXUS (SPEAR) for the 12th cycle of the REXUS/BEXUS project. This experiment was accepted in December 2018 and is set to fly in March 2020.
The research performed for Stratos, SPEAR and PRG in general culminated in the publication of several articles at the AIAA 2018 Aviation Forum, IAC 2018, EUCASS 2019, SSEA 2019, FAR 2019, and the IAC 2019. Going to these conferences and discussing our work has provided quite some insights into recovery and reusability and additionally provided a platform to discuss the thesis topic with the industry.

I would like to thank B.T.C Zandbergen for supervising my thesis and giving critical but justified feedback. Furthermore, I would like to thank all DARE members involved in the Aether, Stratos, and SPEAR projects for making the projects possible. I want to thank my teammates from the Parachute Research Group for the research and development work over the last years, providing me with a treasure of knowledge, data and experience.
In particular, I would like to thank Mark Rozemeijer for this work in the development of ParSim, which was of great help during the thesis.
Last but not least, I would like to thank Esmée Menting and my family for helping me during my studies and thesis and keeping me sane.

L. Pepermans
Delft, October 16, 2019

Summary

As of 2005, the number of launches into space has gone up every year. This trend is, in part, accompanied by a decrease in launch costs. In 1995 the Space Shuttle saw a launch cost of 26.884 USD/kg, where an Atlas V551 launch cost about 5.685 USD/kg in 2016. SpaceX with their Falcon 9 however, offered flights for about 1.891 USD/kg in 2017 [37]. Cost reductions can be achieved by smart choices in the design, such as reusing existing designs or standardising the launcher. Finally one can consider reusability of the launcher.
At the moment of writing, research is done on the recovery and reuse of strap-on boosters and first stages. Examples of this are the Falcon 9 and Ariane Next launchers. However, reusability of the upper stage is not mentioned often. The USA Space Shuttle is a classic example of a reusable upper stage which uses a gliding entry and horizontal landing. Furthermore, research has been done on the unflown Kistler K1, which would have used a system of parachute clusters and airbags for a safe landing. Reusability of launchers or elements of launchers is done for several reasons. These reasons include the reduction of launch costs, an increase in launch rate and a reduction of environmental impact. Making a stage reusable has the disadvantages of, amongst others, increasing the total hardware cost of the stage and decreasing the performance of the stage as recovery hardware is added. Overall a reusable stage is only advantageous if the cost per kilogram payload decreases compared to the expendable variant.

The reuse of an upper stage starts with a de-orbit manoeuvre towards the desired entry point. Due to the aerothermal heating of an object entering the atmosphere with high velocity, some form of thermal protection is usually required. This thermal protection comes either in the form of a conventional, solid heat shield or as an inflatable heat shield. To ensure a safe landing, descent and landing hardware elements are included. The landing hardware has to absorb the kinetic energy of the stage and is limited by a given maximum allowable terminal velocity of the stage. To ensure the terminal velocity of the stage falls within the allowable range, descent hardware can be required.

To determine if a combination of Entry, Descent, and Landing (EDL) hardware can be made to recover an upper stage while allowing for a decrease in launch cost, a tool is developed. This tool, called Conceptual Reusability Design Tool (CRDT), is developed in MATLAB and uses a modified version of the DARE ParSim v3 tool to determine the trajectory of the stage. ParSim is modified to include mass and cost models and has been upgraded with a dynamics model for drag plates and engine burns as a method of deceleration.
The modified version of ParSim is wrapped in a genetic optimisation algorithm to determine an optimal solution. Genetic optimisation was chosen due to the mixed integer nonlinear nature of the Reuse Index, which is used as the optimisation function. When a solution is found, CRDT performs several sensitivity analyses to determine the stability of the found configuration.
The mass and cost models used in CRDT originate from literature, previous research or historical data. Where this was not possible, a bottom-up model was created for this research. These models were validated with historical data to get insights into the accuracy of the model. Where no or limited historical data was available, verification was done using analytical data to demonstrate whether the model implementation is correct.

Finally, a run of the Atlas V Centaur launcher was done to find a solution for making the Centaur stage reusable. The Centaur stage has been chosen as it is lightweight, the RL-10 engine is relatively expensive, and most importantly the engine is proven reusable. The Centaur case is ran from LEO, SSO, MEO, and GTO with different initial masses. The results show the sensitivity to the inputs and finally concludes on the feasibility of upper stage reusability.
It can be concluded that reusability of the Centaur stage for MEO or GTO flights is not feasible as the de-orbit manoeuvre requires to much propellants. It is however feasible to recover and reuse a Centaur stage from LEO. The computations have been done for both a 400 km and 800 km circular orbit with 15 reuses. Here a cost reduction of 29 to 14% can be reached on the stage hardware. The solutions were be found to be most sensitive to the uncertainties in the entry conditions. The most significant uncertainty in the models used in CRDT comes from the number of manhours required for the operations and the cost per manhour. Therefore, it is recommended that this is looked into in more detail in the future.
Reusability of launcher elements is a feasible and good way to reduce the launch costs. Together with other cost reduction methods, such as standardisation, it can make space more affordable and thus more accessible.

Contents

List of Figures

List of Tables

List of Abbreviations, Definitions, Symbols, and Subscripts

The list of symbols gives an overview of the symbols and abbreviations used later on in the report. When deviated from the below list it will be indicated in the text.

Abbreviations

ADCS	Attitude Determination and Control system.
AIAA	American Institute of Aeronautics and Astronautics.
CFD	Computational Fluid Dynamics.
CoDR	Conceptual Design Review.
COTS	Commercial Off-The-Shelf.
CRDT	Conceptual Reusability Design Tool.
CSV	Comma Separated Value.
DARE	Delft Aerospace Rocket Engineering.
EDL	Entry, Descent, and Landing.
ESA	European Space Agency.
EUCAS	European Conference for Aeronautics and Space Sciences.
EUR	Euro.
FAR	International Conference on Flight vehicles, Aerothermodynamics and Re-entry Missions and Engineering.
GNC	Guidance Navigation and Control.
GTO	Geostationary Transfer Orbit.
GUI	Graphical User Interface.
HEART	High-Energy Atmospheric Reentry Test.
HIAD	Hypersonic Inflatable Aerodynamic Decelerator.
IAC	International Astronautical Congress.
IRDT	Inflatable Re-entry Demonstrator Technology.
IRVE	Inflatable Re-entry Vehicle Experiment.
LEO	Low Earth Orbit.
LOFTID	Low-Earth Orbit Flight Test of an Inflatable Decelerator.
MAR	Mid-Air Retrieval.
MEO	Medium Earth Orbit.
NLR	National Aerospace Laboratory.

ODE	Ordinary Differential Equation.	
ParSim	Parachute Simulation Tool.	
PDR	Preliminary Design Review.	
PRG	Parachute Research Group.	
REQ	Requirement.	
SMILE	SMall Innovative Launcher for Europe.	
SSO	Sun-Synchronous Orbit.	
TPS	Thermal Protection System.	
TRL	Technological Readiness Level.	
TumSim	Tumbling body Simulation Tool.	
ULA	United Launch Alliance.	
USD	United States Dollar.	
Definitions		
Configuration	Newly developed reusable stage with addition of Entry Descent and Landing hardware.	
Expendable	Stage or hardware that is used only once.	
Hybrid	Stage that contains both reusable and expendable hardware elements.	
Modification	Any change to the existing system to allow for reusability.	
Restriction	A user inputted limitation to the configuration.	
Reusable	Stage or hardware that is reused for multiple flights.	
Variant	Variants of the original launcher, such as added boosters or increased fairing size.	
Greek Symbols		
α	Angle of attack	deg
ϵ	Specific orbital energy	J/kg
γ	Flight path angle	deg
λ	Time between failures	$flights$
μ	Earth Gravitational Constant	m^3/s^2
ψ	Auxiliary angle	deg
ρ	Density	kg/m^3
σ	Complimentary angle	deg
Latin Symbols		
$\dot{m}$	Mass flow	kg/s
A	Area	m^2
a	Acceleration	m/s^2
A_e	Area of nozzle exit	m^2

c	Cost	USD
$C(B)$	The production cost of the hardware to be reused	USD
$C(RHW)$	The reused portion of the cost to recover and reuse (Recovery hardware, etc.)	USD
$C(RR)$	The expended portion of the cost to recover (Operational costs, refurbishment, etc.)	USD
C_D	Drag coefficient	–
C_f	Inflation load coefficient	–
C_L	Lift coefficient	–
C_x	Reduction coefficient	–
$c_{expendable}$	Cost of the expendable launcher	USD
c_{MY}	Cost per manyear	USD
$c_{reusable}$	Cost of the reusable launcher	USD
D	Drag force	N
F	Force	N
f	Development cost factor	–
$F_{t_{vac}}$	Thrust in vacuum	–
F_{unit}	Factor representing the producing unit cost increase when production decreases with a factor n	–
h	Altitude of the stage ($R_e - R$)	m
I	Reuse Index	–
Isp_{vac}	Specific Impulse in vacuum	s
k	Fraction of production cost of the hardware to be reused to the total cost of the expendable launcher	–
L	Lift force	N
M	Mach number	–
m	Mass	kg
m_b	Mass of the stage	kg
m_f	Fraction of stage propellant required for de-orbit maneuver	–
m_p	Propellant mass	kg
m_s	Structural mass	kg
m_u	Payload mass	kg
m_{earth}	Mass of the earth	kg
n	Number of reuses	–
n_y	Number of flights per year	–
OF	Oxidiser Fuel ratio	–
P	Pressure	Pa

p	Payload reduction factor	$-$
P_c	Engine chamber pressure	Pa
P_{inf}	Free stream pressure	Pa
q	Dynamic pressure	Pa
q_c	Convective heat flux	Wcm^{-2}
q_r	Radiative heat flux	Wcm^{-2}
R	Radius	m
r	Distance between upper stage and the centre of the Earth	m
r_a	Distance between apoapsis and the centre of the Earth	m
R_e	Radius of the Earth	m
R_n	Radius of the nose cone	m
r_p	Distance between periapsis and the centre of the Earth	m
$R_{specific}$	Molar-weight-specific gas constant	$Jkg^{-1}K^{-1}$
T	Temperature	K
t	Time	s
T_s	Throttle setting	$-$
U	Exhaust velocity	m/s
U_e	Effective exhaust velocity	m/s
V	Velocity	m/s
W	Weight	N

Subscripts

0	Initial configuration/value.
1	fFinal configuration/value.
a	Apoapsis.
E	Entry.
e	Earth.
inf	Free stream flow.
MY	Man year.
p	Periapsis.
sl	Sea level.
u	Useful, payload.
vac	Vacuum.

1
Introduction

Space missions are notoriously expensive. One of the costs of a space mission is the cost of the launch to orbit. This high launch cost is a barrier for companies, universities, and governments to launch space research missions. Reducing the launch costs enables easier access to space. For a launch provider, a cheaper launch vehicle implies a better position in the commercial launch market. Therefore, for both parties a reduction in launch cost is favourable.
To lower the cost of launch to orbit many steps can be taken such as simplification of the launch vehicle, implementation of 'commercial of-the-shelve' elements, increase production rates, standardisation of parts, reduction of manufacturing costs, and reusing launcher elements [31]. The latter is a method considered in launch vehicles such as the Falcon9, Space Shuttle, Kistler K1, and recently Electron. The philosophy of reusability is that one can divide the initial hardware cost of a launch vehicle over multiple flights thus reducing the price per launch. At the moment of writing, there is a trend in launch vehicles to consider reusing the first stage, either entirely or partially and reusing strap on boosters. Upon reading the various mission proposals and publications, I began to wonder if upper stage reusability would be technologically and economically feasible. This led first to a literature study and now the subsequent thesis that lies in front of you.

The goal of this thesis is to determine whether an existing upper stage can be modified to incorporate reusability to reduce the launch costs. During the literature study preceding the thesis, it was determined that sufficient systems are available to re-enter and land an upper stage safely. Furthermore, it was shown that most rocket stages and rocket engines could be reused. However, it remained unclear if a combination of Entry, Descent, and Landing (EDL) systems could be found that would reduce the hardware costs, and therefore, the total cost per flight. In other words, it remained to be shown that upper stage reusability is economically attractive. This leads to the following need statement:

There is a need to develop a tool that allows to investigate whether the launch cost can be reduced by making the upper stage reusable.

The central research question of this thesis is as follows:
Can a 10% reduction in launch cost be obtained by reusing the upper stage of a medium launcher to LEO?.

In order to provide an answer, the following four questions need to be addressed.

1. Which strategy for upper stage recovery is most effective in terms of mass?
2. What are the costs involved in upper stage refurbishment?
3. What is the performance loss of the upper stage when recovered and reused?
4. After how many flights does reuse of the upper stage become profitable?

Reusability is the act of reusing a launch vehicle, or parts of a launch vehicle, with the primary goal of reducing launch cost. Previous work in the fields of entry, descent, and landing has been performed by many agencies and organisations. In the research, information can be found in the aerothermal effects of entry, the performance of decelerators and landing hardware.

Besides cost reductions, there are two other advantages to reusability. The first is the decreased environmental impact as rocket stages are not left in orbit or are dumped in the ocean. Second, reusability can allow for higher launch rates in case the launch rates are limited by the production capabilities of a company [19]. From Falcon 9 and others, one can see reusability requires the de-orbit, recovery and refurbishment of the upper stage.
External work shows most upper stages perform a de-orbit manoeuvre that is in agreement with the ESA guidelines against space debris [17]. Research performed by United Launch Alliance in 2014 showed that about half of their launches already performed a de-orbit manoeuvre [24] and research from JAXA showed that modifications to de-orbit the upper stage of an H-IIB were small and included [59]:

- Application of thermal protection tape
- Addition of a function to receive the de-orbit approval command
- Addition of a helium bottle to pressurise the hydrogen tank

External work shows that there are two categories of reusable upper stages: lift generating and ballistic stages. The first requires the creation of a new and dedicated upper stage, as was done for the Space Shuttle. Due to the long development time and high development cost, this was deemed unfeasible for the research of this thesis. Therefore, this research focuses solely on an add-on system for current, existing upper stages returning ballistically. The Atlas V Centaur has been chosen as the primary vehicle for this research. The Centaur is a stage with quite some flight heritage, it has been the topic of a previous reusability study [26], and the stage has been elongated thus allowing for mass and cost predictions when modifying the stage.
In the field of entry, descent and landing the most prominent external work found is the 'Parachute Recovery Systems Design Manual' by T.W. Knacke [34]. As the work focuses mainly on feasibility and thus the conceptual design of a reusable upper stage, little focus is placed on Guidance Navigation and Control (GNC) and Attitude Determination and Control Systems (ADCS). With this in mind any work on steerable parachutes or precision landing systems is not included. Furthermore, the scope of the thesis is narrowed down with the assumption that any hardware selected shall be commercial of-the-shelve and therefore limited research and development is needed. For the development costs a simplified Transcost model is used [36].
Work done previously within Delft University of Technology includes "Solstice, small orbital launch systems, a tentative initial cost estimate" by Nigel T. Drenthe [16] and "Cost effectiveness of the first stage recovery of a small satellite launcher" by Merle Snijders [53]. The first will be used in combination with the United Launch Alliance Reuse Index to determine the economic feasibility of upper stage reusability. The latter provided the baseline for the method used in the research, in particular the selection of the optimisation algorithm.
Work previously done by Delft Aerospace Rocket Engineering (DARE) includes the development of the ParSim simulation tool. This tool, developed for the recovery Stratos III mission, can help engineers to quickly make calculations regarding the trajectory of an entry vehicle and the loads applied by the parachute system onto the structure. Due to the modular and fast nature of this tool, it was chosen as the baseline for the dynamics model for this thesis.

Besides the work done externally or by the university, the author has other reports and papers in the field of Entry, Descent, and Landing. These include the papers "Systematic Design of a Parachute Recovery System for the Stratos III Student Built Sounding Rocket", "Flight Simulations of the Stratos III Parachute Recovery System" and "Comparison of Various Parachute Deployment Systems for Full Rocket Recovery of Sounding Rockets" all conference papers published under the DARE Parachute Research Group. Furthermore, this thesis is preceded by the literature study "The Reusable Upper Stage". Finally, the design work of the Stratos III recovery system, together with the design documents of the Supersonic Parachute Experiment Aboard REXUS can be made available upon request.

The thesis report is broken down in seven chapters. After the introduction, the report gives some background on the recovery and reusability in general. It shows the mission and flight phases of a reusable upper stage together with some earlier work done on the Centaur stage and the Kistler K1. The Reuse Index is introduced together with the various effects of reusability on the mission and the launcher. The chapter ends with the general requirements this information places on the thesis tool.
The third chapter breaks down the requirements into the basics of the tool. This chapter identifies the different models required to fulfil the requirements.
This is followed by chapter 4, which shows all models identified in chapter 3 in more detail. The models are distributed into categories. These categories are made on either flight phase or hardware type and include

upper stage modelling, de-orbit manoeuvre, dynamics model, aerothermal model, mass models, and cost models. The chapter ends with an overview of all models showing: the origin of the model, the range of the model, and the accuracy of the model.

The fifth chapter gives a more detailed overview of the tool now called Conceptual Reusability Design Tool (CRDT). It covers the various inputs and outputs that CRDT requires for a run. Furthermore, it gives an overview of how the genetic algorithm and Monte Carlo algorithm have been combined with the modified ParSim tool to form CRDT. In the chapter screenshots of the tool are added showing what the user sees during a run.

Chapter 6 contain the steps done to verify and validate the program, and what was done to prove the ParSim modifications were implemented correctly. This was done by running the same case in both CRDT and ParSim v3 and comparing the results. Every mass and cost model is presented against available data for validation. Where no validation data was available, the models are compared to each other and the behaviour of the model is discussed.

The final chapter, chapter 7, shows the cases ran for the Atlas V Centaur configuration and indicates a potential configuration to reduce the hardware cost per flight. The cases considered are from a low earth orbit, as well as medium earth orbits and geostationary transfer orbits. For the found solutions, a sensitivity analysis is performed showing it's stability.

The report closes with the conclusion and recommendations that follow from the research and the lessons learned.

2
Background

The gives a background on the recovery and reusability of objects, in particular upper stages. It shows some of the conclusions of the literature study and how these are implemented in CRDT. Furthermore, it shows the flight phases required for an upper stage to be recovered and reused, followed by a more detailed description of the aspects of recovery and reusability. Based upon these findings an overview is made of the required mass and cost models. The chapter ends with a generic breakdown of the expandable and reusable upper stage.

2.1. Mission of a Reusable Upper Stage

The mission of a reusable upper stage is to bring and release a payload to the orbit desired by the customer. The recovery and reuse of the stage only apply after the primary mission has been for filled and shall thus not effect the primary mission. This means that the reusable upper stage only effects the launch in terms of the payload capacity it can lift to orbit. These mission requirements can be found in Table 2.1.

Table 2.1: Reusable Upper Stage Mission Requirements

ID	Requirement
MIS - 01	The reusable upper stage shall deploy a payload to a desired orbit
MIS - 02	A launch cost per kilogram reduction of 10 % shall be achieved with respect to the expendable variant
MIS - 03	The addition of reusability shall only impact the stage performance in terms of payload capacity

2.2. Earlier Work on Reusable Upper Stages

Two previous reports on upper stage reusability have been found to be interesting for this thesis. The first being "Reusable Centaur Stage" [26] and the second "Landing system design summary of the K-1 reusable launch vehicle" [60].
The mission of the reusable Centaur stage was to fly to and from orbit in the Space Shuttle cargo bay. The This removed any form of entry descent and landing hardware as the vehicle was protected by the Space Shuttle cargo bay. For the orbital manoeuvres, the following lessons were learned.

- Number of engine burns increased from 4 to 5
- Total dry mass increased to between 400 to 680 kg
- Reliability decreased from 0.984 to between 0.951 and 0.751
- Production unit cost increased from 5.2 M$ to between 8.1 and 11.9 M$
- Turnaround cost estimated to be between 0.9 and 1.7 M$
- Reusable Centaur used between 50 and 85 % of the original Centaur stage

The researched of the Kistler K-1 showed a recovery system using a solid heat shield, parachutes and an airbag landing system. The parachute system of the upper stage was estimated to be 520 kg, where the airbag system was estimated to be 44.4 kg. It should be noted that the parachute system of the K-1, developed by Airborne Systems, was a very lightweight system. It should be noted that the Kistler K1 has never flown to orbit. During the development, parachute drop tests have been performed validating the systems performance.

2.3. Reusable Upper Stage Mission Phases

The mission phases that a reusable upper stage goes through can be found in Figure 2.1. Here one can see the different phases in the rectangular boxes and the actions to be taken by the stage by the diamond shape boxes. The Figure 2.1 is supported by Figure 2.2 which shows the altitudes and velocity regimes corresponding with the mission phases and Figure 2.3, which shows a schematic overview of the different orbits the stage will fly.

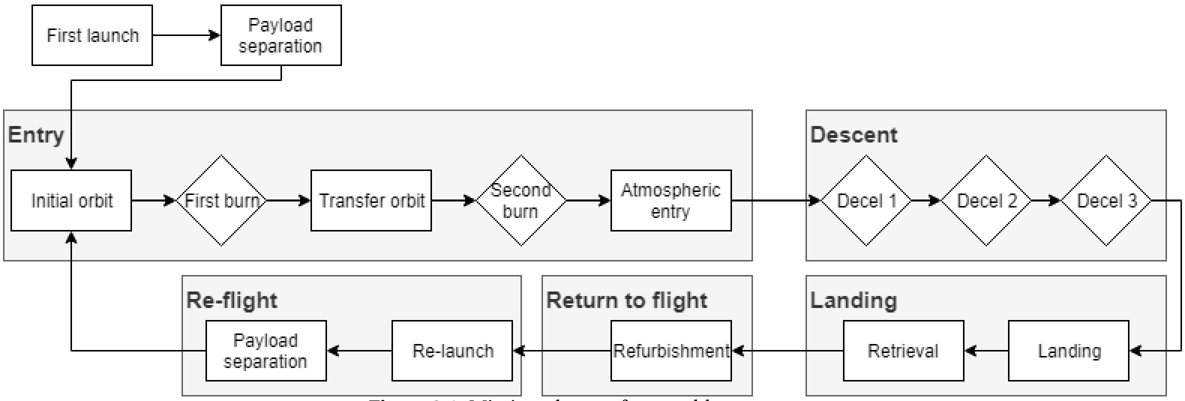

Figure 2.1: Mission phases of a reusable upper stage

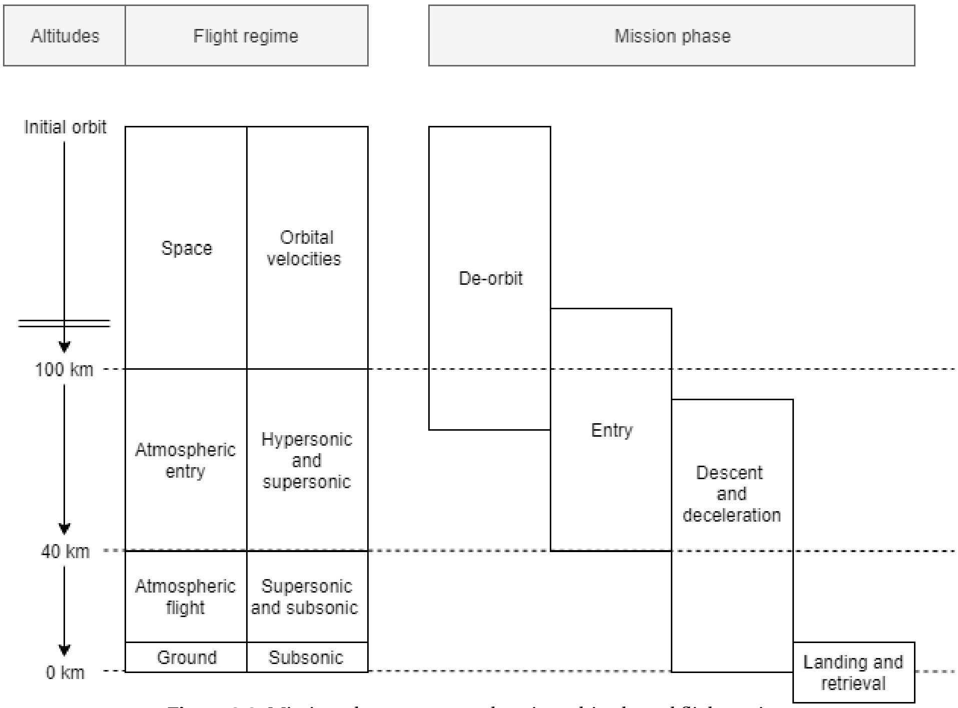

Figure 2.2: Mission phases presented against altitude and flight regime

The return flight begins with a de-orbit phase that includes two engine burns. One burn is required to lower the periapsis, where the second burn controls the entry point. When the stage reaches the atmosphere, the final phase identified as "Entry Descent and Landing" or EDL is begun. In this phase the stage will reduce its kinetic energy such that the final terminal velocity is lower than the acceptable landing velocity. After landing, the stage is retrieved and refurbished so it can be re-flown for a new mission.

Figure 2.2 shows the mission phases shown in Figure 2.1 against the altitudes and velocities. As can be seen, there is some overlap in the altitudes at which one phase ends and another begins.

2.3.1. De-Orbit

As can be seen in Figure 2.3, the stage will first go from the initial orbit to a transfer orbit with a low periapsis. The initial orbit is represented by the "long, short, short dashed line" and the low orbit is represented by the "dashed line". This orbit has the apoapsis on the original orbit and the periapsis at the entry point. This change in orbit requires a single-engine burn at apoapsis. When the stage reaches the periapsis of the low orbit, a second engine burn is performed to match the required entry point.

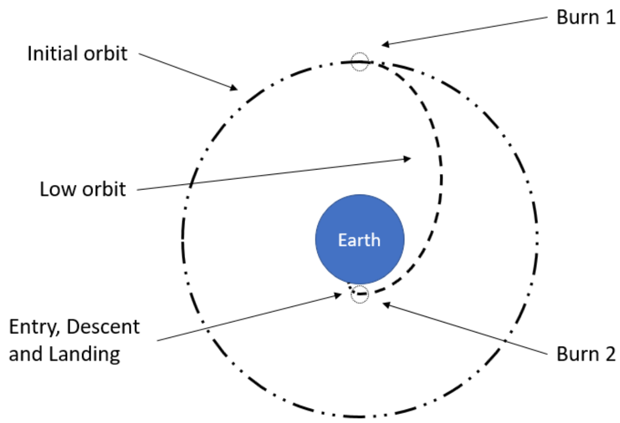

Figure 2.3: Systematic overview of the various orbits the reusable upper stage will encounter

To demonstrate the influence of the initial orbit on the de-orbit manoeuvre, the orbital velocity at periapsis (v in m/s) is shown in Table 2.2. This table also shows the specific orbital energy, ϵ. These values have been calculated using Equation 2.1 and Equation 2.2 [9]. In this equation the r_a and r_p are the distances between the apoapsis and the periapsis of the orbit respectively to the centre of the Earth in m. The orbits considered are a circular 400x400km Low Earth Orbit (LEO), a circular 800x800 km Sun Synchronise Orbit (SSO), a 22000x22000 km Medium Earth Orbit (MEO), and an elliptical 35786x400 km Geostationary Transfer Orbit (GTO).

$$v = \sqrt{\mu\left(\frac{2}{r_p} - \frac{2}{(r_a + r_p)}\right)} \tag{2.1}$$

$$\epsilon = \epsilon_k + \epsilon_p = \frac{V^2}{2} - \frac{\mu}{r} \tag{2.2}$$

Table 2.2: Overview of the Various Orbits Considered

Orbit	Apoapsis - Periapsis altitude [km]	Velocity at periapsis [m/s]	Specific orbital energy at periapsis $[MJ/kg]$
LEO	400 - 400	7677.0	-29.46
SSO	800 - 800	7459.8	-27.82
MEO	22000 - 22000	3750.2	-7.03
GTO	35786 - 400	10078	-8.15

2.3.2. Entry

The atmospheric entry can be done using several methods and strategies [46]. During the literature study, it was determined that it was unfeasible to perform a skipping or gliding entry as the stage does not generate significant lift. As the development of an entirely new stage is time-consuming and expensive, it was deemed unfeasible for this research. Therefore, a ballistic entry is performed in all cases. During the entry phase no deceleration elements are added and is discussed in the section Descent hardware.

For the entry flight it is assumed that the on-board Guidance Navigation and Control systems (GNC) are capable of determining the stage's state and controlling the entry point. As the stage is required to rotate to ensure the de-orbit burns are given in the correct orientation, one requires an Attitude Determination and Control System (ADCS). It is assumed that the stage has sufficient ADCS capabilities to perform this operation. When assuming the Centaur stage is a hollow cylinder and requires the full rotation in 600 seconds, one finds a propellant mass required of 1.8 kg. This is assumed to be negligible.

During the entry flight, the stage experiences a heat flux due to aerothermal heating. The aerothermal heating is mitigated by either altering the entry velocity or the addition of a thermal protection system. The thermal protection can either be a conventional solid heat shield or an inflatable heat shield [39, 49].
Inflatable heat shields are relatively new pieces of technology to replace conventional heat shields ,e.g. for landing heavy payloads on Mars. As they can be larger in frontal area than the original body, they allow for engineers to change the ballistic coefficient of the vehicle. By doing this it is possible to reduce the vehicle's velocity at the main parachute deployment. This in term it lowers inflation loads on the main parachute. Besides this advantage, it also combines the functioning of the drogue parachute with the function of the heat shield. This allows for a significant reduction of mass of the total vehicle. The solid heat shield on the other hand allows for a more conventional form of thermal protection.
The entry is simulated as a ballistic entry which generally have a high deceleration [30]. However, both the solid and inflatable heat shield allow for an offset between the centre of gravity and the centre of pressure. This offset leads to the stage generating lift, thus decreasing the maximum deceleration. This can be done when the deceleration constraint is breached [4].

2.3.3. Descent

During the descent phase three different deceleration methods can be used: parachutes, drag plates, and engine burns. The literature study identified a rotor landing as a possible deceleration option, however the technology readiness level was deemed too low [46, 13].
The parachutes identified to be of use for this research are ballistic, non-steerable parachutes. These parachutes come in three categories: ballute, ribbon parachutes, and Ringsail parachutes. The ballute's primary function is stabilisation of the stage and is used when the upper stage is unstable during the flight. The ribbon parachutes are assumed to be supersonic drogue parachutes where the Ringsail parachutes are mainly used for final descent or main parachutes. [34]. Parachutes are used for a safe landing for almost every manned mission. The choice of parachutes is based upon the deployment altitude:

- 100000 m - 60000 m - Ballute
- 60000 m - 7500 m - Ribbon parachute
- 7500 m - 0 m - Ringsail parachute

The drag plates are deployable, solid drag enhancement surfaces. These surfaces increase the drag of the body to decrease the terminal velocity. Drag plates can also provide aerodynamic control, although this is not considered in this research [64].

Engine burns are an air-independent method of deceleration. This means that it can help with decreasing the maximum dynamic pressure and heat flux on the stage during the atmospheric flight. When a concept separates the engines and propellant tanks, engine burns are not possible after separation. The deceleration burn can also be seen in the entry and landing trajectory of the Falcon 9.

2.3.4. Landing and Retrieval

The landing hardware is tasked with nullifying the final velocity and thus bringing the stage to a standstill. For landing it is assumed that the stage always performs a safe landing as long as the stage terminal velocity of the stage is within the allowable range. Five landing options are considered here [34].

- Retrorocket landing on land (Soyuz)
- Airbag landing on land (Starliner)
- Water landing (Gemini, Mercury, Apollo)
- Mid-air retrieval (spy satellite data, Genesis probe)
- Rotor landing

During the literature study, it was determined that any form of precision landing would be too complex in terms of guidance navigation and control and thus removed from the design options tree. Therefore, all options are non-precision landing options. Even though the rotor landing nicely combines the decelerator and landing options, the technology readiness level is not sufficient for current applications and thus not considered [13].
To allow for a land landing one requires either a soft landing using retrorockets to reduce the final velocity to zero, or an airbag to dissolve the remaining kinetic energy. A crushable structure such as a honeycomb has

been discarded as they typically cause a deceleration above 20 g [34, p. 6-104].

Both the retrorockets and airbags are used for a dry landing; this can either be on land or a ship. The retrorocket solution equips the stage with small solid rocket engines that are fired just before the stage hits the ground. The advantage of this system is that the maximum allowable terminal velocity is assumed to be 100 m/s. As there is no limit imposed by the rocket engines, the 100m/s limit is based upon the Phoenix Mars Lander [29]. The airbag system has a lower maximum acceptable landing velocity of 10 m/s [34]. A land landing with retrorockets is used for the Soyuz missions, where the airbags can be seen in the Boeing Starliner capsule. During a land landing, the stage is retrieved by a truck with a crane.

When the stage lands in the water, it is assumed that any landing is safe when the landing velocity is below 20 m/s, comparable to the landing velocity of the Space Shuttle Boosters [34]. The added mass and cost comes from the flotation devices required to keep the stage afloat and protect the engine against saltwater. For a water landing the stage is retrieved using a ship, comparable to the SpaceX Dragon capsule.

During a mid-air retrieval, the stage is intercepted in flight by a helicopter. This means that no additional hardware is required for landing. It only imposes the requirement that the final decelerator stage is a parachute system [34].

2.3.5. Overview of Considered Hardware

An overview of the considered hardware and a schematic representation of each element can be found in Table 2.3 and Figure 2.4. The de-orbit manoeuvre is in all cases done using two engine burns. Through previous missions it could be seen that some form of thermal protection would be required, this is either a conventional or inflatable heat shield. For the descent and landing, there are multiple possible combinations. For any configuration, one landing option is chosen with up to three descent elements preceding it.

Table 2.3: Overview of Hardware Options per Mission Phase

Phase	Design options
1) De-orbit	Two burn de-orbit
2) Atmospheric entry	Conventional heat shield Inflatable heat shield
3) Descent	Aerodynamic deceleration (no hardware)
	Ballute Ribbon parachute Ringsail parachute Drag plate Engine burns
4) Landing	None Airbag Retrorocket Water landing Mid-air recovery
5) Retrieval and Refurbishment	

To help visualise the different stage phases, the icons shown in Figure 2.4 are used in the developed tool, CRDT.

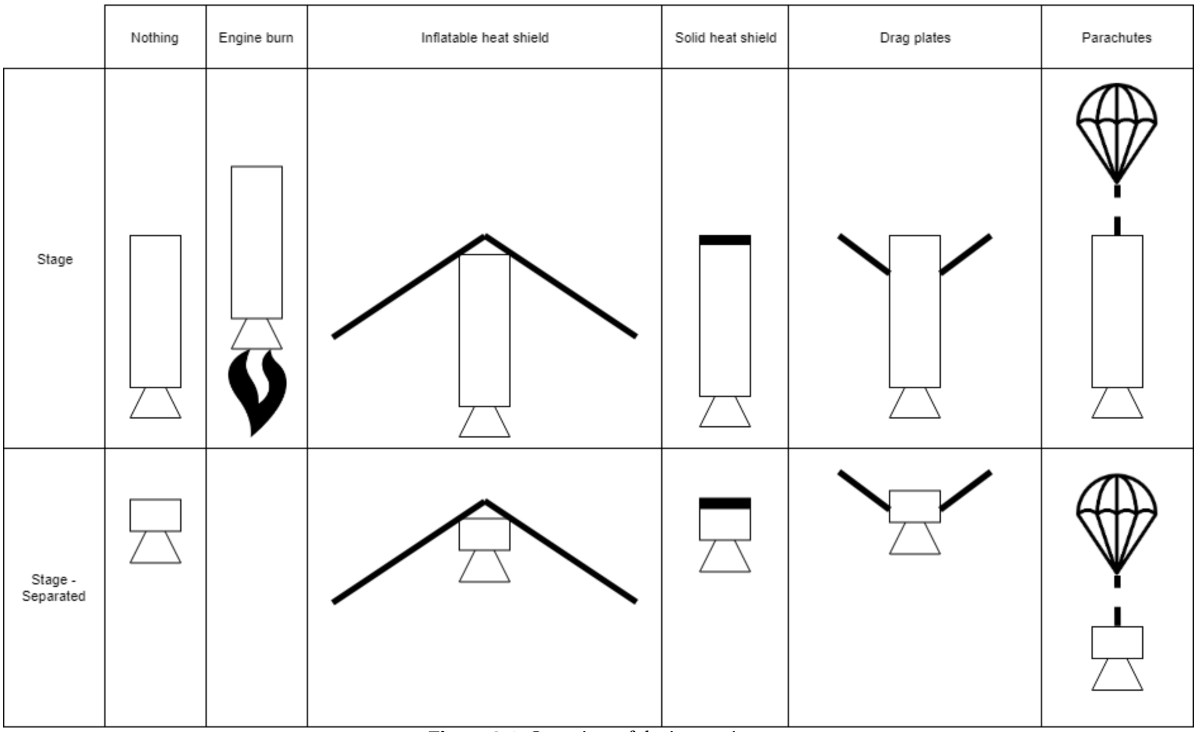

Figure 2.4: Overview of design options

2.4. Launcher with Reusable Upper Stage

The launcher is the focal point of this research. This section describes the assumptions made in order to analyse the launcher including an upper stage.

2.4.1. Mission cost breakdown

The cost of a launch vehicle is build up out of three elements. These are the operational costs, amortisation charge, and average unit manufacturing cost. The operational costs cover any single use cost for the operations and manhours required for a space launch. Where the amortisation charge covers the development costs, and is the total development cost divided over the number of launches. Finally, the average unit manufacturing costs cover the hardware costs. As the name suggest, these costs are a function of the number of produced units. This will later be demonstrated in section 2.5. For a launch vehicle it can be assumed that the amortisation charge is about 10%, where the operation costs and the manufacturing costs are about 20% and 70% respectively. This breakdown, including the profit margin, can be seen in Figure 2.5.

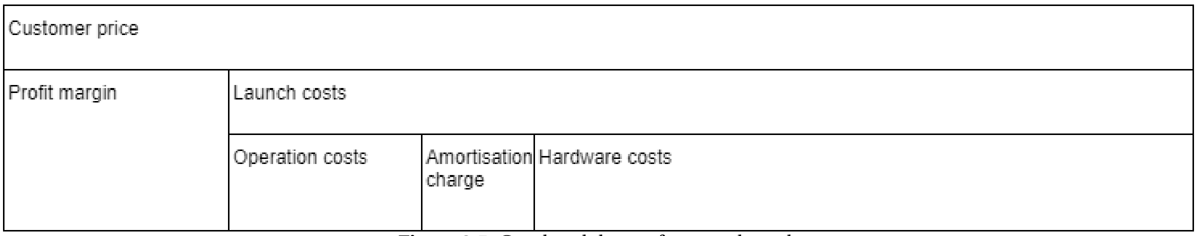

Figure 2.5: Cost breakdown of a space launch

2.4.2. Expendable Stage Breakdown

In the accompanying literature study, it was found that the upper stage of the Atlas V Centaur is about 25 % of the total empty mass of the launcher, whilst it is 30 % of the hardware cost. A detailed breakdown can be found in Table 2.4 and Figure 2.6.

Table 2.4: Comparison between the mass and cost breakdown of the first and second stage of the Atlas V Centaur

	Mass		Cost	
	Stage 1	Stage 2	Stage 1	Stage 2
Total	0.75	0.25	0.7	0.3
Electronics	0.05	0.2	0.075	0.25
Structure	0.6	0.5	0.2	0.25
Engine	0.2	0.1	0.6	0.25
Engine feed system	0.15	0.2	0.075	0.15
Payload	-	-	0.05	0.1

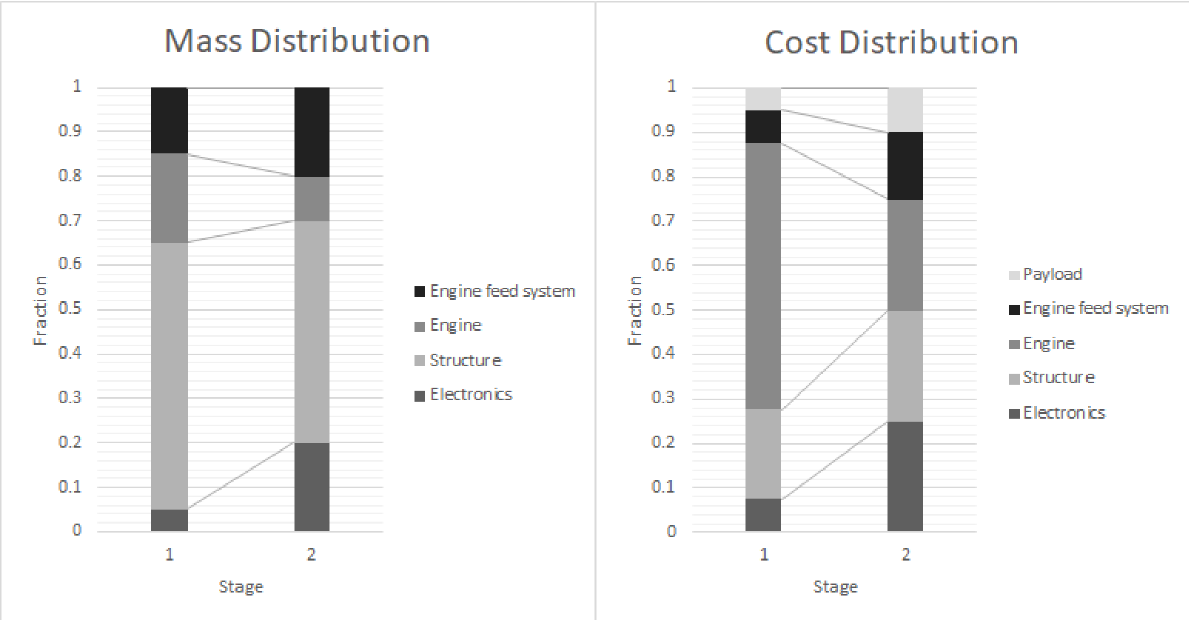

Figure 2.6: Comparison Between the Mass and Cost Breakdown of the First and Second Stage of the Bare Atlas V Centaur

From this breakdown it can be seen that the upper stage has a higher cost to mass ratio than the first stage. This is advantageous for recovery, as a lower stage mass results into a lower EDL system mass.

2.4.3. Stage Breakdown

The upper stage can be broken down into subsystems. These subsystems can be systems that were already on the Centaur stage, such as the engines, or systems that have to be added to make the stage reusable, such as EDL hardware. A breakdown of the reusable Centaur upper stage can be found below. When making a configuration for the reusable Centaur stage one adds a combination of EDL systems. The system breakdown can be found in Figure 2.7.

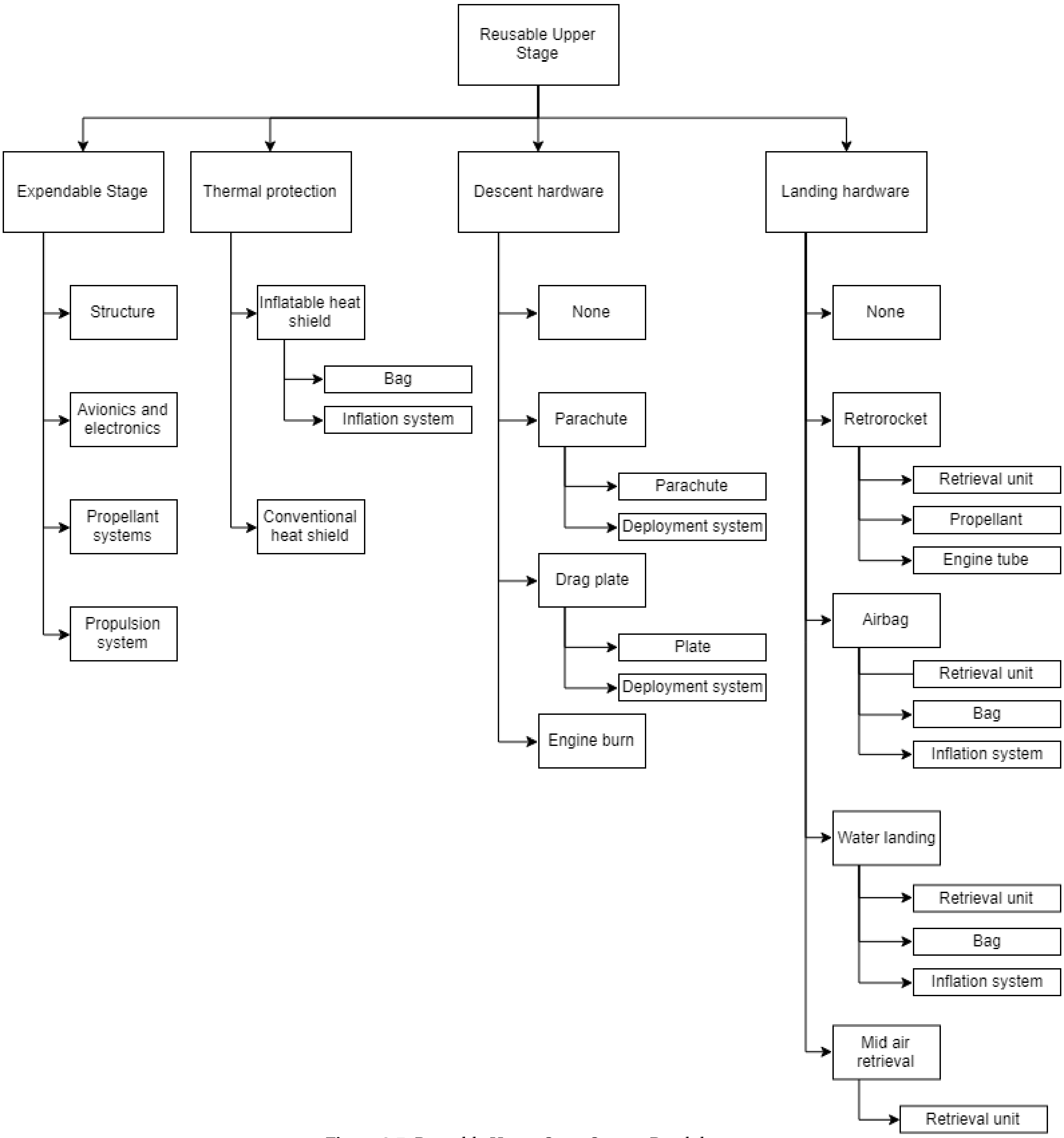

Figure 2.7: Reusable Upper Stage System Breakdown

2.5. Reusability

By enabling reusability, one does accept a reduction in payload capability as the added hardware is, in case of an upper stage, one-on-one deducted from the payload capabilities. Furthermore, reusability increases the complexity of the mission and the vehicle, leading to an increase in operational costs.

In general, a reusable rocket stage is an economically feasible alternative if and only if it is cheaper than the expendable variant. This is reflected in the Reuse Index, defined in Equation 2.3. The dimensionless Reuse Index is a function of a reusable and expendable stage cost per kilogram. For this research all costs are transferred to 2019 USD. When denoting 2019 USD, it will be shown as USD.

$$I = \frac{c_{reusable}/m_{u_{reusable}}}{c_{expendable}/m_{u_{expendable}}} \tag{2.3}$$

The cost of the expendable stage variant can be found in Equation 2.4 and the cost of the reusable variant can be found in Equation 2.5. The cost of the expendable variant is written as a function of the to be reused hardware cost (C(B)) and the fraction of reused and non-reused hardware cost, k.
The cost of the reusable stage is the sum of the added hardware, the cost of the original stage, and the cost of the rebuild and refurbishment. The added hardware costs are divided in reusable and non-reusable hardware or C(RHW) and C(RR) respectively.

$$c_{expendable} = \frac{C(B)}{k} \tag{2.4}$$

$$c_{reusable} = c_{reusable\ reuse\ hardware} + c_{expendable\ reuse\ hardware} + c_{Initial} + c_{Re-build} \tag{2.5a}$$

$$c_{reusable} = \frac{C(RHW)}{n} + C(RR) + \frac{C(B)}{n}F_{unit} + \frac{C(B)}{k}(1-k) \tag{2.5b}$$

$$I = \frac{c_{reusable}/m_{u_{reusable}}}{c_{expendable}/m_{u_{expendable}}} = p\left(k\left(\frac{F_{unit}}{n} + \frac{1}{n}\left(\frac{C(RHW)}{C(B)}\right) + \frac{C(RR)}{C(B)}\right) + (1-k)\right) \tag{2.6}$$

The following parameters are used in the Reuse Index:

- I - Reuse index.
- p - The ratio of the payload capacity of the expandable system to the payload capacity of the comparable reusable system.
- k - Fraction of production cost of the hardware to be reused to the total cost of the expendable launcher.
- F_{unit} - Factor representing the production unit cost increase when production decreases with a factor n, Equation 2.7.
- n - Number of reuses.
- $C(RHW)$ - The reused portion of the cost to recover and reuse (Recovery hardware, etc.).
- $C(B)$ - The production cost of the hardware to be reused.
- $C(RR)$ - The expended portion of the cost to recover (Operational costs, refurbishment, etc.).

The Reuse Index only compares the flight of the reusable launcher to the flight of the expendable launcher. It assumes that every of the total n flights is reusable. It is more likely that an operator operates a fleet of rockets that fly a certain amount of time in reusable configuration, and then perform a final flight in the expendable configuration. This depends on the number of payloads that cannot be lifted with the reusable variant but can be lifted with the expendable variant [65]. This assumption in the Reuse Index also only allows for a single launcher type to be analysed for a single mission. When looking at, for instance, the Atlas V Centaur one can see that there is a wide variety in configurations, payload masses, and orbits.

2.5.1. Production cost decrease

The learning curve is used to determine the decrease of production cost due to mass production, this is shown in Equation 2.7. The cost reduction factor is estimated to be 90% [35, 16].

$$F_{unit} = n^{\left(\frac{ln(0.9)}{ln(2)}\right)} \tag{2.7}$$

2.5.2. Reduction of Payload

The loss of payload performance of the reusable upper stage can be calculated using the rocket equation. One can say that the delta-V of the expendable stage has to equal the delta-V delivered by the reusable stage. This can be seen in Equation 2.8. Using the rocket equation one can re-write this to Equation 2.9. Here m_u is the payload mass, m_s is the structural mass and m_p is the propellant mass. All masses are given in kg.

$$\Delta V_{expendable} = \Delta V_{reusable} \tag{2.8}$$

$$U_e\,ln\left(\frac{m_{s_{expendable}}+m_{u_{expendable}}+m_p}{m_{s_{expendable}}+m_{u_{expendable}}}\right)=U_e\,ln\left(\frac{m_{s_{reusable}}+m_{u_{reusable}}+m_p}{m_{s_{expendable}}+m_{u_{reusable}}+m_f*m_p}\right) \tag{2.9}$$

Where m_f is the fraction of the propellant that is saved for the EDL manoeuvres:

$$m_f=\frac{m_{p_{deorbit}}}{m_p} \tag{2.10}$$

This leads to the payload capacity of the reusable alternative launcher to be:

$$m_{u_{reusable}}=m_{u_{expendable}}-m_f(m_p+m_{s_{expendable}}+m_{u_{expendable}})+m_{s_{expendable}}-m_{s_{reusable}} \tag{2.11}$$

Now the ratio p is given as shown in Equation 2.12

$$p=\frac{m_{u_{expendable}}}{m_{u_{reusable}}} \tag{2.12}$$

Given the Reuse Index shown in Equation 2.6, one can see the following desired characteristics of a solution.

1. Minimal reduction in payload performance, thus minimum added hardware mass
2. Maximise fraction of the stage that is reused
3. Minimise cost of added hardware
4. Maximise fraction of reusable cost (C(RHW)) of the cost of added hardware

2.5.3. Hybrid Reusable Stage

Some studies indicate it to be advantageous to recovery and reuse only parts of a rocket stage. Only of these proposals is the ULA SMART system to be used on the Vulcan first stage [25]. This method is referred to as a hybrid reusable stage. This means that only the engine section of the upper stage is recovered. The higher cost to mass ratio of the engine section compared to the entire stage, together with the lower mass of just the engine section could make this a desirable solution. If separation is chosen, it is done after the second de-orbit burn at a variable altitude. Hybrid reusability has the following advantage:

- Reduction of the to be recovered mass leads to a lower recovery system mass [34].
- Upper stages are generally unstable during free flight, recovering only the engines puts the centre of gravity lower, allowing for easier stabilisation [3].

The chosen separation system in case of hybrid reusability is the clamp band separation systeem. The clamp band is used on almost every launcher to separate the payload from the upper stage. It is ideal as it allows a clear path on the inside of the vehicle for plumbing and wiring and is considered a low shock, low-cost system with high stiffness [18, 15].

2.5.4. Refurbishment

The last step of a reusable stage is that it needs to be refurbished for re-flight. SpaceX suggests that the refurbishment of a rocket stage is done in three steps [12]. These are as follows:

1. Replace broken/discarded elements
2. Inspection
3. One full engine burn as flight acceptance

2.6. Tool Requirements

Based upon the previous sections, one can generate requirements for the simulation tool. The mass and cost uncertainty of 10% has been chosen to be in line with the AIAA recommendations on PDR level designs for a space mission based upon existing hardware (REQ-Tool-01/02/03/04) [6]. Given that CRDT can be used to both find a configuration with the lowest Reuse Index, as analyse the stability of the found solution, it is essential that the tool can do both within an acceptable time and present the results in a clear overview to the user. (REQ-Tool-05/06/07/08/09). Finally, CRDT should be based upon ParSim v3 as this was identified to be a good basis for the tool (REQ-Tool-10) [46] and that the tool should be able to analyse different types of upper stages and thus the inputs should be changeable externally (REQ-Tool-11).

Table 2.5: Requirements on the tool

ID	Requirement
REQ - Tool - 01	The tool shall be able to determine the mass of the various EDL systems with 10 % accuracy
REQ - Tool - 02	The tool shall be able to determine the cost of the desired EDL systems with 10 % accuracy
REQ - Tool - 03	The tool shall be able to determine the performance of the various EDL system in terms of mechanical loads with 10 % accuracy
REQ - Tool - 04	The tool shall be able to determine the performance of the desired EDL system in terms of thermal loads with 10 % accuracy
REQ - Tool - 05	The tool shall be able to analyse a single configuration in less than 1 second
REQ - Tool - 06	The tool shall be able to analyse a single upper stage configuration
REQ - Tool - 07	The tool shall be able to find the configuration with the lowest Reuse Index given the users constraints
REQ - Tool - 08	The tool shall be able to analyse the sensitivity of a given configuration
REQ - Tool - 09	The tool shall present the results of an optimisation or sensitivity run to the user
REQ - Tool - 10	CRDT shall use a modified version of the DARE ParSim v3 to determine the stage performance
REQ - Tool - 11	Inputs shall be read from user modifiable files

3
Tool Basics

This chapter gives a basic overview of the tool developed for the thesis. This chapter gives a general overview of the tool, together with the various models required. These models include the dynamics model, mass, and cost models.

3.1. General Tool Layout

The objective of the tool is to find a reusable upper stage configuration that can reduce the launch cost to orbit, such that it becomes cheaper than the expendable alternative. For this, a tool, named Conceptual Reusability Design Tool (CRDT), has been written. Figure 3.1 shows a general breakdown of the tool.

One can see two major elements in the code: the genetic optimisation and the Monte Carlo analysis. Genetic optimisation has been chosen due to the mixed integer nonlinear nature of the Reuse Index [21]. One can select multiple hardware options (Figure 2.7) and configurations to achieve a safe entry, descent, and landing. All these design options have different variables such as surface area and deployment altitude. The complete list can be found in section 4.1.

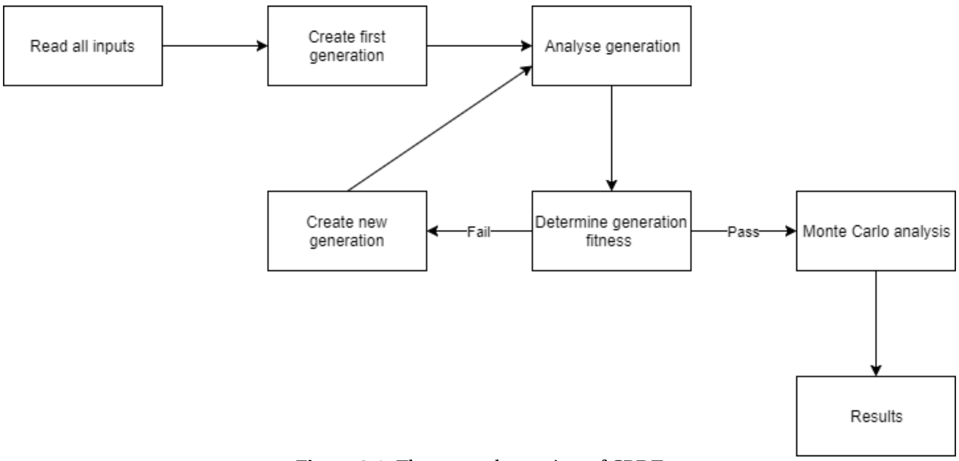

Figure 3.1: The general overview of CRDT

The tool starts with reading all general inputs provided by the user. This allows for flexibility and for the tool to be used on different types of upper stages. These inputs are shown in section 5.2. With these inputs, the tool will generate the first generation of configurations; this is done randomly but within limits imposed by the user. The first generation is analysed by a modified version of the DARE ParSim tool, which is discussed further in section 3.2. For each configuration, the Reuse Index is determined.

The optimisation is considered done, when it meets one of the set stop conditions. This can either be when the Reuse Index has not changed for a user defined number of generations, or when the maximum number of generations is reached.

In case a generation fails, thus not meets the criteria, it is passed on to the next generation and re-analysed. The creation of a new generation is further elaborated in section 5.4.

When a stop criterion has been met, the final generation is passed to the Monte Carlo analysis. Here the configurations with the lowest Reuse Index are analysed for their sensitivity and stability. The Monte Carlo analysis computes a passing rate. When the passing rate equals 1, all variations of the stage are feasible. The lower the passing rate, the less suitable a configuration is.

After the Monte Carlo analysis, the best configurations are presented to the user. Again the outputs can be found in section 5.2. Now the user can run a more detailed Monte Carlo analysis that splits the different uncertainties into four categories: uncertainty in stage geometry, trajectory uncertainty, errors in onboard state estimation, and uncertainties in mass and cost models. The results of this analysis can be used to determine to which uncertainties the stage is most sensitive. More information on both Monte Carlo analyses can be found in section 5.5.

3.2. Dynamics model

The dynamics model used by CDRT to analyse the re-entry flight of a configuration, is the DARE Parachute Simulation Tool, or ParSim for short. It was developed to assist the DARE Parachute Research Group in the development of the recovery system of the Stratos III student built sounding rocket. ParSim was primarily required to generate the structural loads on the system together with the inflation conditions of the parachutes. Furthermore, the tool was capable of presenting altitude-time and velocity-time plots. The tool was subjected to extensive verification and validation, which is presented in the IAC paper "Flight Simulations of the Stratos III Parachute Recovery System" [47].

ParSim has been written in MATLAB as this was the most available and familiar programming language for the team at the moment. It is, in essence, an integrator that determines the aerodynamic force on the body per time step and uses that to determine the deceleration in this time step to determine the new velocity. The integrators used are the ODE113 and ODE15s integrators standard in MATLAB; more details on the code can be found in the aforementioned paper. As the code is a relatively simple ODE solver, it is possible to add the required modifications to the code. These modifications are to allow for the addition of drag plates and propulsive deceleration.

3.3. Mass and Cost Models

Based on the flight phases identified in Figure 2.1 and the hardware elements identified in subsection 2.3.3, one can identify where additional hardware is necessary. The addition of hardware means an increase in mass and cost, the required mass and cost models can be found in Figure 3.2. Each mass and cost estimate has a certain factor that it has to be multiplied with. This factor is determined using the Transcost model and is depended on the Technology Readiness Level.

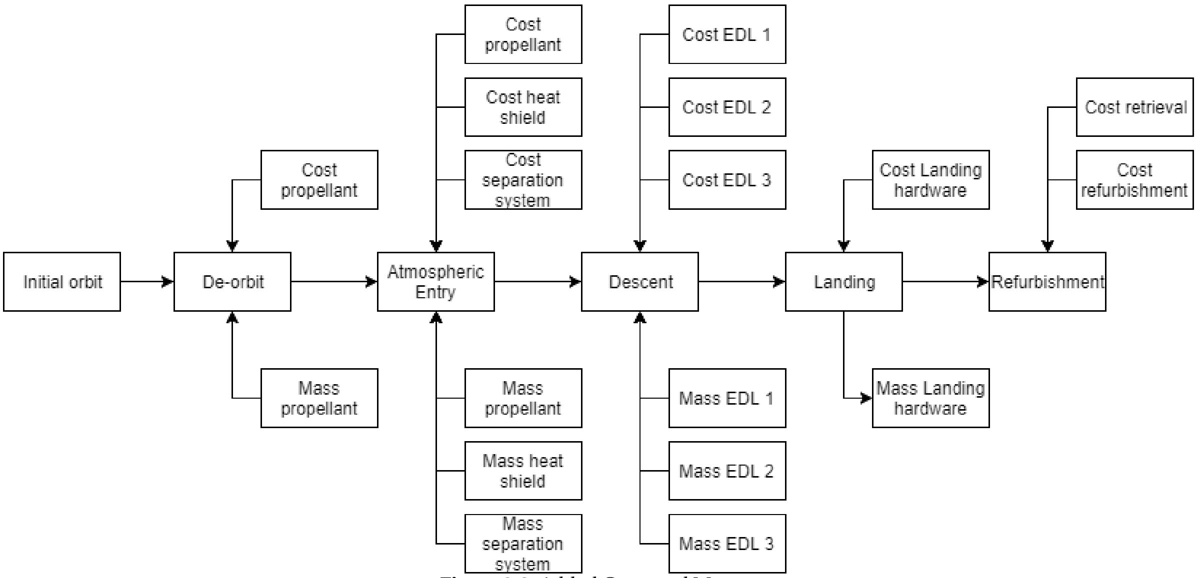

Figure 3.2: Added Costs and Masses

The total mass and costs are computed as the sum of the elements. This can be found in Equation 3.1, Equation 3.2, and Equation 3.3. The individual models can be found in chapter 4.
As can be seen, the mass of the upper stage is the sum of the stage mass, plus the propellant mass. Finally, the masses of all the additional hardware elements are added. Here the decelerator hardware is noted down as Decel1, Decel2, and Decel3. The costs are divided into the reusable recovery hardware cost (RHW) and the expendable recovery hardware cost (RR). It is assumed that the thermal protection, parachutes, drag plates and landing hardware can be reused. The separation system, propellants and operations, however, are single use only.

$$m_{s_{reusable}} = m_{stage} + m_{propellant} + m_{separation} + m_{TPS} + m_{Decel1} + m_{Decel2} + m_{Decel3} + m_{landing} \tag{3.1}$$

$$C(RHW) = c_{TPS} + c_{parachute} + c_{plates} + c_{landing} \tag{3.2}$$

$$C(RR) = c_{separation} + c_{propellant} + c_{operations} \tag{3.3}$$

3.3.1. Cost Models

The cost for any piece of hardware comes from three sources. These are Hardware cost, Development cost, and Operational costs. The total cost equal the hardware cost multiplied with a factor showing the development effort plus the cost of the operations. This can be seen in Equation 3.4. Unless otherwise mentioned the cost is given in 2019 USD; the exchange rates used can be found in Appendix B.

$$c_{Element} = c_{hardware} * f_{development} + c_{operations} \tag{3.4}$$

The factor of the development effort is based upon the Transcost model [36]. Transcost assumes a basic cost and multiplies this with three dimensionless factors as can be seen in Equation 3.5. For CRDT, the f2 is set to 1 as no new vehicle is developed. The values of the factors can be found in Table 3.1 [36]. The operational costs are estimated as the required amount of manhours multiplied by the cost of a manhour.

$$f_{development} = f1 * f3 * f3 \tag{3.5}$$

Table 3.1: f-factor for costs

Parameter	Status	Value	Criterion
f_1 - Correction factor for the overall technical development status	1	1.25	First generation system
	2	0.8	Flight proven system
f_3 - Team experience factor	1	0.6	Company with relevant experience
	2	1	Company with some related experience
	3	1.3	New company or team

3.3.2. Mass Models

Similar to the cost, the masses are multiplied with a certain factor to take the uncertainty into account. This can be seen in equation 3.6, where the factor f_{mass} can be found in table 3.2 [6].

$$m_{Element} = m_{hardware} * f_{mass} \tag{3.6}$$

Table 3.2: f-factor for masses

f_{mass}	**Status**	**Criterion**
1.05	1	COTS parts
1.10	2	Part used for other space mission
1.20	3	New part

4

Models

This chapter gives an overview off how the problem of reusable upper stages is modelled in CRDT. The models are broken down into the launcher, the entry manoeuvre, the descent hardware, the landing hardware, retrieval, and refurbishment. Mass and cost models are presented as required.

4.1. Upper Stage

The upper stage has to be modelled and modified for the recovery flight. This is done by writing the stage configuration as a matrix, referred to as "the ID". The following section describes the assumptions and model used for the upper stage.

4.1.1. Assumptions

The following assumptions are made with respect to the launcher:

Table 4.1: Assumptions - Launch vehicle

ID	Assumption
Veh - 01	The only performance loss of the launch vehicle is in terms of payload mass to orbit
Veh - 02	The performance of the first stage is not affected by the reusable upper stage
Veh - 03	The performance of the strap-on boosters is not affected by the reusable upper stage
Veh - 04	The ascent trajectory is not affected by the reusable upper stage

Table 4.2: Assumptions - Upper Stage

ID	Assumption
Stage - 01	No mass is lost during re-entry other than propellant mass
Stage - 03	Refurbishment is sufficiently good to not influence launcher reliability
Stage - 04	The empty upper stage can operate in a user defined thermal range
Stage - 05	The empty upper stage can operate in a user defined dynamics pressure range

It is assumed that the launch trajectory of the launcher is not changed by the addition of a reusable upper stage. This means that the only effect the reusable upper stage has on the launcher is a reduction of payload capacity. Regarding the upper stage itself, it is assumed that the reliability of the stage does not decrease after multiple flights. Finally, it is assumed that the only constraints on the upper stage comes in terms of maximum dynamic pressure and maximum thermal load.

4.1.2. Stage ID

The upper stage is modelled as a combination of constants that are shown in the configuration ID. This ID is defined in the matrix found in Equation 4.1. A specific item in the matrix is defined as ID(Row,Column). This Stage ID defines a single configuration in the generation.

$$\begin{bmatrix} Number & EDL1 & EDL2 & EDL3 & Landing & Launcher \\ Entry\,velocity & EDLvar1 & EDLvar1 & EDLvar1 & Type\,heat\,shield & Orbit \\ Entry\,angle & EDLvar2 & EDLvar2 & EDLvar2 & Area\,heat\,shield & Modifications \\ Entry\,altitude & EDLvar3 & EDLvar3 & EDLvar3 & Separation\,altitude & Nr\,reuse \end{bmatrix} \tag{4.1}$$

This matrix uses the following parameters to vary the different upper stages:

- *Number* - Number of the current ID in the current generation.
- *Entry velocity* - Velocity in m/s at which the upper stage enters the atmosphere at entry altitude.
- *Entry angle* - Angle in degrees (downward negative) at which the upper stage enters the atmosphere at entry altitude.
- *Entry altitude* - altitude in m at which the stage performs the second engine burn
- *EDL1, ELD2, EDL3* -
  1. None
  2. Parachutes
  3. Drag plates
  4. Engine burn
- *Landing* -
  1. None
  2. Retrorockets
  3. Airbags
  4. Water landing, flotation device
  5. Mid-air retrieval
- *Type heat shield* -
  1. Conventional heat shield
  2. Inflatable heat shield
- *Area heat shield* - Parameter to define the frontal area of the heat shield in m^2. For "Type of heat shield = 1", the frontal area is the same as the stage.
- *Launcher* - Defines the version of the launcher when multiple versions are available. For the Atlas V Centaur the values are:

  1. 401
  2. 411
  3. 421
  4. 431
  5. 501
  6. 511
  7. 521
  8. 531
  9. 541
  10. 551

- *Separation altitude* - Altitude in m at which the tank and engine section separate. The parameter is 0 when no separation occurs in flight.
- *Orbit* - The orbit where the payload has been deployed.

  1. LEO
  2. SSO
  3. MEO
  4. GTO

- *Modifications* - Modifications made to the stage.
  1. No modifications
  2. Extra booster to the first stage
  3. Elongated propellant tanks of the upper stage
  4. Extra booster and elongated propellant tanks
- *Nr of reuses* - Number of times the stage shall be reused.

The different EDL systems are defined in Equation 4.2. Sketches of the various stage configurations can be found in Figure 2.4.

$$\begin{bmatrix} EDL \\ EDLvar1 \\ EDLvar2 \\ EDLvar3 \end{bmatrix} =$$

$$\begin{bmatrix} 0\,(none) \\ - \\ - \\ - \end{bmatrix} \vee \begin{bmatrix} 1\,(Parachute) \\ Deployment\ altitude\,[m] \\ Area\,[m^2] \\ - \end{bmatrix} \vee \begin{bmatrix} 2\,(Dragplate) \\ Deployment\ altitude\,[m] \\ Area\,[m^2] \\ - \end{bmatrix} \vee \begin{bmatrix} 3\,(Engine) \\ Deployment\ altitude\,[m] \\ Burn\ time\,[s] \\ Throttle\,[-] \end{bmatrix} \tag{4.2}$$

Every piece of hardware has a deployment altitude, this is the altitude in meters at which the element starts working. Both the parachute and the drag plates have an area that determines the drag. The engine burn has both the burn time in seconds, and the throttle setting as a fraction between 0 and 1.

4.1.3. Stage Modifications

Three modifications can be be made to the upper stage. These are: Increase performance to compensate for payload loss, addition of a separation system enabling hybrid reusability, addition of EDL hardware. Below these modifications are explained in some detail.

4.1.3.1 Increase Payload Performance

In order to accommodate for the additions to the stage, the user can opt to do one of four options compensate for the loss in payload capacity. These are as follows:

1. No modifications
2. Extra booster to the first stage
3. Elongated propellant tanks of the upper stage
4. Extra booster and elongated propellant tanks

As CRDT was written to determine the reusability of the Atlas V Centaur stage, the mass and cost functions implemented are for this launcher. When the user would like to change the launcher type, this can be done in the code.

For the Atlas V Centaur launcher it is quite well documented what the payload mass and launch cost for every version of the launcher is; this can be found in chapter 7. For the additional booster modification, the type of launcher is simply changed to the variant with one more booster. For the configurations 431 and 551 this cannot be done as the variants 441 and 561 do not exist. Whenever a ID shows up that does require a 441 or 561 configuration the ID is considered a lethal ID and thus killed. The mass and cost models used for the added booster can be found in Equation 4.3 and Equation 4.4. The cost of a solid booster equals the USD 6.8E6 described by ULA, the 20 million USD is the cost of the original Centaur stage [62]. As the boosters are added to the first stage, the mass of the upper stage is not changed and remains the original 2247 kg of the Centaur stage.

$$m_{EmptyStage} = 2247 \tag{4.3}$$

$$c_{EmptyStage} = 2E7 + 6.8E6 \tag{4.4}$$

The increased mass and cost of using elongated tanks is determined by looking at historic data. This can be done as the Centaur stage has had quite some upgrades and updates over its lifetime. The following relations are used where the empty mass of the stage ($m_{EmptyStage}$) is in kg and the cost of the stage (($c_{EmptyStage}$) is in 2018 USD. Again the 20 million USD is the cost of the original Centaur stage.

$$m_{EmptyStage} = 1051.6 + 0.0722 * m_p \tag{4.5}$$

$$c_{EmptyStage} = +2E7 + 470.88 * m_p \tag{4.6}$$

Whenever both an extra booster and elongated tanks are required, the modifications are superimposed.

4.1.3.2 Separation System

The mass of the clamp band system is obtained by interpolating from historic data from Sierra Nevada and RUAG Space [54, 55, 56, 7]. The costs of the separation system is estimated based upon the mass of the clamp band. It is assumed the stage is made out of aluminium and compensated for the complexity of the structure by a factor of 2.
When looking at the historical data of separation systems one finds that it is dependent primarily on the mass of the stage that needs to be separated. Given the small spread of the available low mass data points, this area treated as a single data point. This means only three usable data points are available, leading to a second degree polynomial fit. This fit can be seen in Figure 4.1. The mass of the separation system is modelled using a second degree polynomial and is limited to a stage mass of 7000 kg.

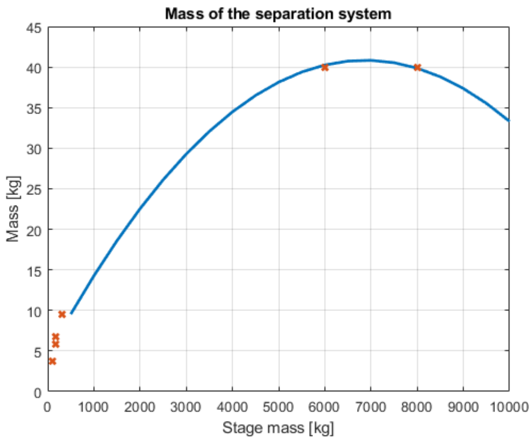

Figure 4.1: Second degree estimation

The mass of the separation system $m_{separation}$ is given in Equation 4.7 and is given in kg. The cost of the separation given in Equation 4.8 and is given in 2018 USD.

$$m_{separation} = -7.7064E - 7 * m_{EmptyStage}^2 + 0.0106 * m_{EmptyStage} + 4.4383 \tag{4.7}$$

$$c_{separation} = m_{separation} * c_{Aluminium} * 2 \tag{4.8}$$

4.1.3.3 Combinations of Entry Descent and Landing Hardware

Not all EDL options can be combined with each other. This can be found in Figure 4.2. In this figure, the options marked red are not feasible. As can be seen an engine burn cannot be done when the stage has separated. Furthermore, the separated stage with a conventional heat shield is considered to be unstable, and thus requires a ballute stabiliser. The combination of an inflatable heat shield together with drag plates is unfeasible as the drag plates are in the wake of the heat shield and thus do not generate drag.

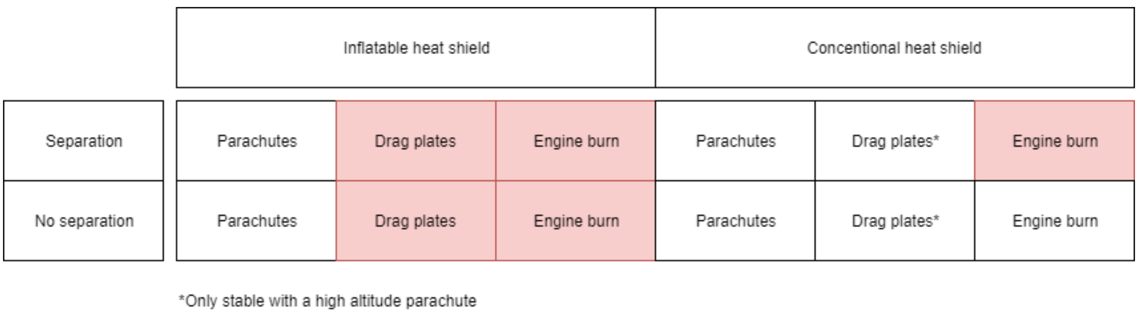

Figure 4.2: Allowed combinations of EDL hardware

- EDL items are not allowed to actuate within 500 meters from each other
- After separation, no engine burn is possible
- When using Mid Air Retrieval, the final decelerator option shall be a parachute
- When using a conventional heat shield either drag plates or parachutes are required to keep it stable
- Drag plates and engine burns are not possible in combination with the inflatable heat shield

4.2. De-orbit Manoeuvre

The de-orbit manoeuvre will bring the upper stage from the initial orbit, thus the orbit where the satellite is in, to an orbit where it can re-enter. This can be seen in Figure 2.3 on page 7. There are two burns required. The first will put the stage in an elliptic orbit where the periapsis equals ID(4,1), and the apoapsis equals the initial orbital altitude. The second burn will ensure the orientation and velocity specified in ID(2,1) and ID(3,1).

4.2.1. Assumptions

The following assumptions are made for the de-orbit manoeuvre:

Table 4.3: Assumptions - De-orbit

ID	Assumption
DO - 01	Two engine burns are sufficient for de-orbiting
DO - 02	The stage is de-orbited in half an orbit.
DO - 03	Atmospheric drag is negligible during the de-orbit manoeuvre
DO - 04	The bare stage has sufficient Attitude Determination and Control System capabilities to perform the de-orbit manoeuvre so modifications are not required
DO - 05	The engines can be started multiple times

It is assumed that the de-orbit manoeuvre is a relatively simple two burn de-orbit. This means that atmospheric drag is not taken into account during the de-orbit manoeuvre. These assumptions will result in a higher amount of required propellants, than a de-orbit manoeuvre where aerobraking is taken into account (DO-01 through 03 and 05). Finally, it is assumed that the stages on-board Attitude Determination and Control System is sufficient to keep the stage oriented correctly during the manoeuvres.

4.2.2. Model

In order to decelerate the upper stage to the desired entry conditions two burns are used. The first burn, to initiate the Hohmann transfer orbit, can be determined using Equation 4.9 [9]. In this equation r_1 is the radius of the departure orbit, and r_2 is the radius of the arrival orbit. Both parameters are in meters.

$$\Delta V_1 = \sqrt{\frac{\mu}{r_1}}\left(1 - \sqrt{\frac{2r_2}{r_1 + r_2}}\right) \tag{4.9}$$

The second burn, the entry manoeuvre, is used to change the entry angle and velocity to the required angle and velocity. A schematic of the manoeuvre can be found in figure 4.3. The delta-V equation can be found in Equation 4.10. In this equation the desired velocity vector is subtracted from the velocity vector at periapsis (V_p). The desired velocity vector is build up of the entry velocity in m/s (V_E) and entry angle in degrees (γ_E).

$$\Delta V_2 = V_1 - V_2 = \begin{bmatrix} V_x \\ V_y \end{bmatrix}_1 - \begin{bmatrix} V_x \\ V_y \end{bmatrix}_2 = \begin{bmatrix} V_{p_x} \\ V_{p_y} \end{bmatrix} - \begin{bmatrix} V_E * cos(\gamma) \\ V_E * sin(\gamma) \end{bmatrix} \tag{4.10}$$

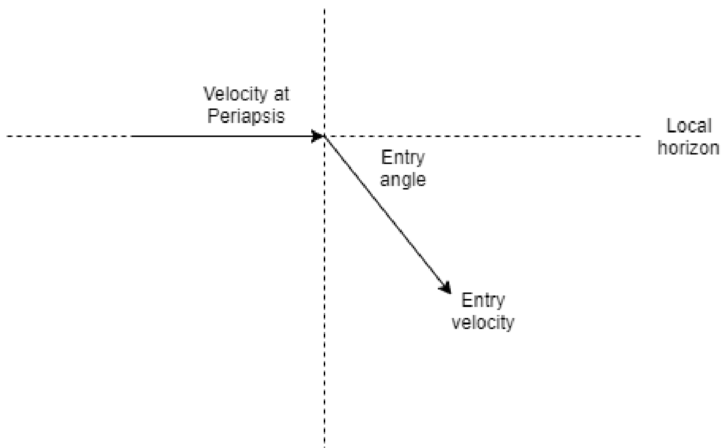

Figure 4.3: Entry manoeuvre visualised

The total delta-V can be determined by summing up ΔV_1 and ΔV_2. Using this required delta-V and the rocket equation, one can determine the total mass and cost of the propellants. This can be done using Equation 4.11 and Equation 4.13 respectively. The script used to determine the propellant mass as a function of delta-V can be found in Appendix C.

Here the mass flow ($\dot{m}$) is given in kg/s and is defined a the mass flow when 100% thrust is provided. It is assumed that one throttles the engine by restricting the mass flow, this is done by setting the factor T_s to a value between 0 and 1. Finally the burn time is included as t_{burn} in seconds.

$$m_{DeOrbit} = \dot{m}\ t_{burn}\ T_s = m_{ox} + m_{fuel} \tag{4.11}$$

$$c_{DeOrbit} = m_{ox} * c_{ox} + m_{fuel} * c_{fuel} \tag{4.12}$$

$$c_{DeOrbit} = m_{DeOrbit} \frac{OF}{1+OF} * c_{ox} + m_{DeOrbit} \frac{1}{1+OF} * c_{fuel} \tag{4.13}$$

4.3. Dynamics Model

The atmospheric entry phase of the mission is a phase where the stage is subjected to high velocities, high dynamic pressures, and high thermal loads. The phase starts at a given altitude and velocity and orientation.

The dynamic pressure and deceleration during the entry can be found in section 4.6 and are not further discussed in this section. This section will discuss the aerothermal model together with the solid and inflatable heat shield models.

4.3.1. Equations of Motion

The deceleration of the upper stage can be calculated using Newtons second law and basic physics. The force applied on the body is a combination of the attributions of the body drag and any EDL hardware.

The free body diagram of a general entry vehicle can be found in Figure 4.4 and the free body diagram of the axis system of ParSim v3 can be found in Figure 4.5. These free body diagrams lead to the equations of motion found in Equation 4.14.

Here the D is the drag force in Newtons, m_{stage} is the masses in kg of the stage. The parameter r equals the radius of the earth plus the altitude. The flight path angle γ in degrees shows the angle between the local horizon and the velocity vector. The gravitational constant of Earth (μ) is given in $m^3 s^{-2}$.

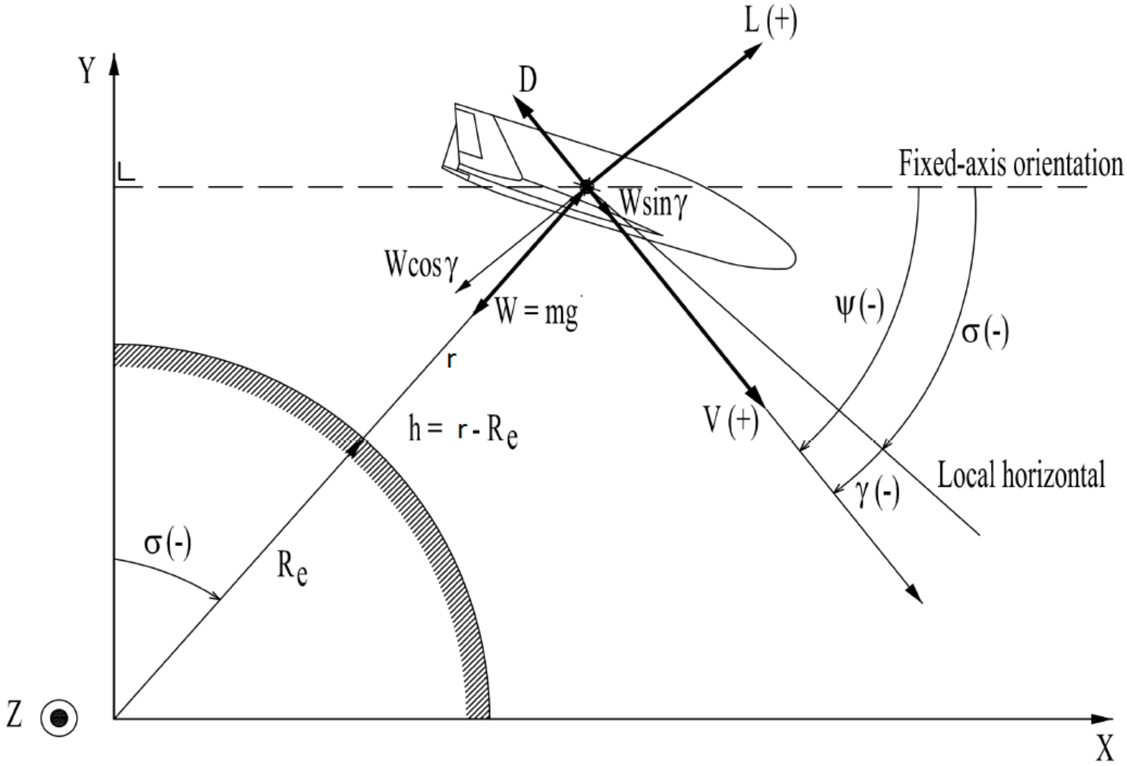

Figure 4.4: Two-dimensional planar motion of entry vehicle [43]

$$\begin{bmatrix} F_{x_E} \\ F_{z_E} \end{bmatrix} = \begin{bmatrix} -D\,cos\gamma \\ -m_{stage}\frac{\mu}{r^2} - D\,\sin\gamma \end{bmatrix} \tag{4.14}$$

$$D = F_{body} + F_{parachute} + F_{plates} + F_{prop} \tag{4.15}$$

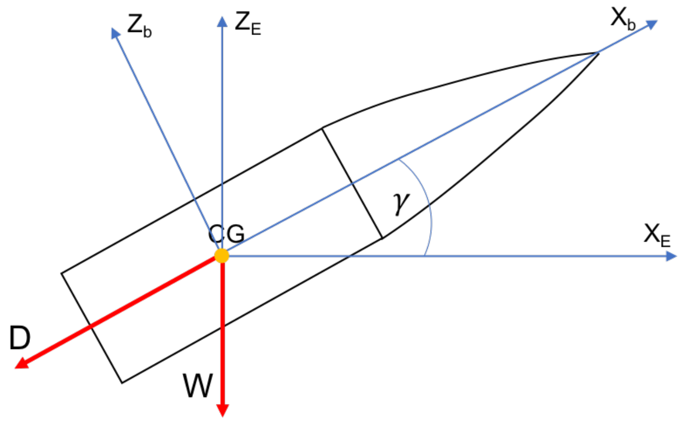

Figure 4.5: Free body diagram of ParSim for $\alpha = 0$ [47]

The force contributions of the respective body and EDL systems can be found in subsection 4.3.3, 4.3.4, 4.3.5 and 4.3.6.

4.3.2. Assumptions

The following assumptions are made for the entry dynamics model:

Table 4.4: Assumptions - Entry

ID	Assumption
AE - 01	There is no loss of mass during entry phase
AE - 02	The stage is aerodynamically stable during re-entry
AE - 03	A ballistic entry trajectory is flown
AE - 04	The stage is assumed to have sufficient GNC capabilities for the entry manoeuvre
AE - 05	The stage is assumed to have sufficient ADCS capabilities for the entry manoeuvre

Throughout the atmospheric entry it is assumed that the stage is aerodynamically stable, and does not loose mass. Finally, it is assumed that a ballistic entry flight is followed and that the stage has sufficient ADCS and GNC capabilities for the manoeuvres. The following assumptions are made for the decelerator model:

Table 4.5: Assumptions - Descent

ID	Assumption
Desc - Body - 01	The stage is aerodynamically stable during the descent
Desc - Body - 02	The stage has a constant angle of attack of 0 degrees during flight
Desc - Body - 03	The stage does not generate any lift (L=0)
Desc - EDL - 01	Figure 4.2 is followed
Desc - Para - 01	Parachute inflation force is taken as a constant factor
Desc - Para - 02	The parachutes are stable, thus the deceleration force is parallel to the velocity vector
Desc - Para - 03	Parachute lines are sufficiently long for the wake effects to be neglected
Desc - Para - 04	Vehicle angle of attack is zero when the parachute is deployed
Desc - Para - 05	No mass is lost during parachute deployment
Desc - Para - 06	The deployment altitude of the parachute determines what kind of parachute is used (h < 7500 m - Ringsail, h < 35000 m - Ribbon Parachute, h > 35000 m - Ballute)
Desc - Para - 07	Maximum Mach number of the Ringsail parachute equals 1.5
Desc - Para - 08	Maximum Mach number for the ribbon parachute equals 3
Desc - Para - 09	Ballute has no maximum Mach number
Desc - Para - 10	Dynamic pressure is no limit for parachutes
Desc - Plate - 01	Drag plate deployment is instantaneous
Desc - Plate - 02	Drag generated by the drag plates is symmetric
Desc - Plate - 03	Drag plates are not limited by Mach number
Desc - Plate - 04	Drag plates are not limited by dynamic pressure
Desc - Prop - 01	Engine has no start up behaviour, thus deliverers required thrust at t-0
Desc - Prop - 02	Engine thrust is always in line with the velocity vector
Desc - Prop - 03	Engine has no problems starting whilst wind blows into the engine
Desc - Prop - 04	Vehicle angle of attack is zero when the engine is fired
Desc - Prop - 05	No propellant is left behind after the engine burn

Assumption Desc-EDL-1 originates from the assumption AE-02 and Desc-Body-1 that the stage is aerodynamically stable during the flight. Furthermore, all the Desc-Body assumptions originate from the theory of ballistic entry [43].

The assumptions regarding the parachute systems focus on the limits used for the flight envelope [34]. Furthermore, it is assumed that both the body and the parachute are stable. The inflation is assumed to be only a function of time, and no effects such as flow separation are taken into account. Finally, wake effects are also neglected.

The drag plates are assumed to have no limits; thus, the plate is always sufficiently strong. Finally, the drag of the plates is assumed to be symmetric, and the deployment instantaneous.

It is assumed that, during an engine burn, the stage is stable. Furthermore, it is assumed that the engine has no start-up behaviour and thus ignites instantaneously. Finally, it is assumed that the stage uses all propellants such that no propellants are left behind.

4.3.3. Body Drag

The body drag is modelled as shown in Equation 4.16. As can be seen, the body drag coefficient is only a function of the Mach number and not the angle of attack (Desc-Body-02).

$$F_{body} = \frac{1}{2}\rho v^2 A_{body} C_{D_{body}}(M) \tag{4.16}$$

When an inflatable heat shield is used, the forward area of the stage is increased to the size of the heat shield. This can be found in Equation 4.17. When a solid heat shield is used the area and drag coefficient do not change.

$$F_{body} = \frac{1}{2}\rho v^2 A_{HeatShield} C_{D_{HeatShield}}(M) \tag{4.17}$$

4.3.4. Parachutes

Parachutes create a force by generating drag behind the vehicle. There should be a distinction between the equilibrium force and the dynamic force of the parachute [34]. These forces can be determined as follows:

Equilibrium force of the parachute:

$$F_{parachute} = \frac{1}{2}\rho v^2 A_{parachute} C_{D_{parachute}}(M) \tag{4.18}$$

Dynamic force of the parachute:

$$F_{parachute} = \frac{1}{2}\rho v^2 A_{parachute} C_{D_{parachute}}(M) C_f C_x \tag{4.19}$$

Combined forces of the parachute

$$F_{parachute} = (q_{equilibrium} + q_{dynamic} C_f C_x) A_{parachute} C_{D_{parachute}}(M) \tag{4.20}$$

Where:

$$q_{dynamic} = q_{total} - q_{equilibrium} \tag{4.21}$$

4.3.5. Drag Plates

The force of the drag plate can be calculated using Equation 4.22, and is superimposed on the body drag.

$$F_{plate} = \frac{1}{2}\rho v^2 A_{plate} C_{D_{plate}}(M) \tag{4.22}$$

4.3.6. Engine Burn

It is assumed that the upper stage has a vacuum optimised RL-10 engine. This means that the performance of the engine decreases in a higher density atmosphere. This relation can be seen in in Equation 4.23. By the system ID it can be determined that the engine could require throttling, thus the engine not performing at 100 percent performance. This is assumed to be done by reducing the mass flow of the engine. This can be found in Equation 4.24 [69].

$$U = U_{vac} + \frac{P_{inf} A}{\dot{m} T_s} \tag{4.23}$$

$$F_{prop} = U \dot{m} T_s \tag{4.24}$$

4.4. Aerothermal Model

The aerothermal model is based upon an analytical solution found during the literature study [5]. This model assumes that below 9.5 km/s only convective heating (q_c) is relevant, where above 9.5 km/s, also radiative heating (q_r) is taken into account. The total heat flux in W/cm^2 on the stage is shown in Equation 4.25.
In the aerothermal equations the ρ is the density of the atmosphere, V is the stage total velocity in m/s and R_n is the radius of the nose cone in m. The parameters a and $f(V)$ are supportive functions that can be found

in Equation 4.30 and Equation 4.32. The equations are valid up to 3 km/s, below this no aerothermal effects are taken into account.

$$q = q_c + q_r \tag{4.25}$$

Convective and radiative heating for 3 < V < 9.5 [km/s]

$$\dot{q}_c = 7.455E-9\,\rho^{0.4705}\,V^{3.089}\,R_n^{-0.52} \tag{4.26}$$

$$\dot{q}_r = 0 \tag{4.27}$$

Convective and radiative heating for 9.5 < V < 17 [km/s]

$$\dot{q}_c = 1.270E-6\,\rho^{0.4678}\,V^{2.524}\,R_n^{-0.52} \tag{4.28}$$

$$\dot{q}_r = 3.416E4\,R^a \rho^{1.261}\,f(V) \tag{4.29}$$

$$a = min(3.175E6\,V^{-1.80}\,\rho^{-0.1575}, amax) \tag{4.30}$$

$$amax = \begin{cases} 0.61 & \text{if } 0 < R_n < 0.5 \\ 1.23 & \text{if } 0.5 < R_n < 2 \\ 0.49 & \text{if } 2 < R_n < 10 \end{cases} \tag{4.31}$$

$$f(V) = -53.26 + \frac{6555}{1 + (16000/V)^{8.25}} \tag{4.32}$$

4.5. Thermal Protection System

The following section describes the mass and cost models used for the thermal protection systems. The two thermal protection systems considered are the solid and inflatable heat shield.

4.5.1. Solid Heat Shield

For the solid heat shield, it is assumed that it takes the same frontal area as the stage itself. Therefore the drag generated by the heat shield remains identical to the original body drag. This drag is calculated in section 4.6. The mass and cost estimates for the heat shield can be found in the article "Thermal Protection System Materials and Costs for Future Reusable Launch Vehicles" [49]. This article gives the mass and cost as a function of surface area. It shows a cost of 333 USD/ft^2 (3580 USD/m^2) and a mass of 0.62 lb/ft^2 (3.03 kg/m^2). Both models can be found in Equation 4.33 and Equation 4.34.

$$m_{TPS_{Solid}} = 3.03 * A_{Stage} \tag{4.33}$$

$$c_{TPS_{Solid}} = 3580 * A_{Stage} \tag{4.34}$$

4.5.2. Inflatable Heat Shield

When investigating the mass of inflatable thermal protection systems, one can find a low mass estimate of about 3 kg/m^2 [20]. The higher estimate for inflatable heat shield comes from a NASA document on the future of Entry Descent and Landing systems, here one can determine the higher mass estimates to be closer to 5 kg/m^2 [45].
Comparable to parachute systems the deployment system of an inflatable heat shield is about the same mass as the heat shield itself. This can be seen in the data gathered for validation in subsection 6.4.1. The mass of the inflatable heat shield can be found in Equation 4.35.

The cost of the inflatable aerodynamic decelerators is done using a bottom-up approach. The system is built up by the inflatable structure itself and the gas generator. From literature it can be found that the bag is made up of 40mm Nextel 440, 236mm (47 plies) Pyrogel3350, 1mm Kapton, and 5mm (10 plies) Kevlar [28].

The mass of the various materials can be found in table 4.6. A factor of 2 is applied to include the inflation system and attachment of the system. The model used for the inflatable heat shield cost can be found in Equation 4.36.

Table 4.6: HIAD material costs

Material	Cost	Source
Nextel	116 USD/kg	[8] [1]
Pyrogel	4.89 USD/ft^2	[48]
Kapton	5.678 USD/ft^2	[33]
Kevlar	20 USD/m^2	[66]

$$m_{TPS_{Inflatable}} = 3 * A_{Stage} \tag{4.35}$$

$$c_{TPS_{Inflatable}} = (m_{Nextel} * c_{nextel} + 47 * A_{Stage} * c_{Pyrogel} + A_{Stage} * c_{Kapton} + 10 * A_{Stage} * c_{Kevlar}) * 2 \tag{4.36}$$

4.6. Decelerator Systems

The following section shows the mass and cost models used for the decelerator hardware.

4.6.1. Parachutes

The mass of the parachutes is estimated using the historical relations mentioned in Knacke, which are presented in Figure 4.6 and Figure 4.7 [34]. These mass estimates are for Ringsail parachutes and ribbon parachutes. The estimates for the ballute are taken from historical data [42, 67].
Depending on the deployment altitude a type of parachute is automatically chosen by CRDT. The mass of the parachute system is about 50 % parachute, and 50 % deployment system. CRDT assumes this to be true and multiplies the parachute mass with a factor 2 to get the parachute system mass [34].

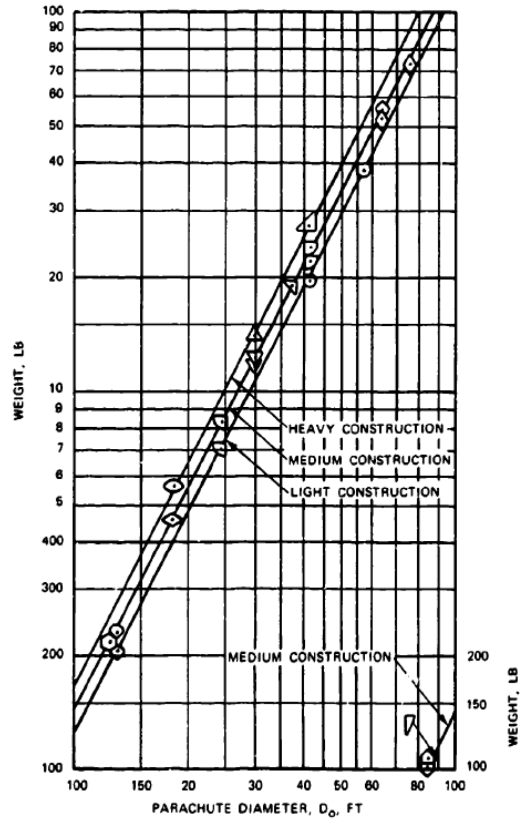

Figure 4.6: Mass of a Ringsail parachute [34]

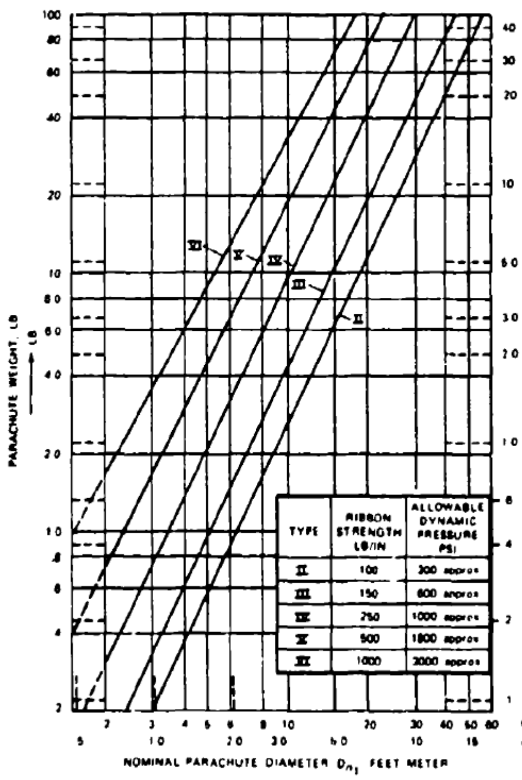

Figure 4.7: Mass of a ribbon parachute [34]

For both the ribbon parachute and the Ringsail parachute a log-log relation is used, this relation can be found in Equation 4.37. The parameters P(1) and P(2) are obtained from data points of Figure 4.6 and Figure 4.7.

For the ribbon parachute the "Type 2" ribbon has been chosen with a maximum dynamic pressure of 300 psi (2068 kPa). For the Ringsail the "Light construction" type parachute is used. As the data presented in Knacke originates form older research and technologies have advanced, this is deemed a valid assumption. The mass model can be found in Equation 4.37.

$$m_{D_{parachute}} = \left(2\sqrt{\frac{A_{parachute}}{\pi}}\right)^{P(1)} * exp(P(2)) * 2 \tag{4.37}$$

The cost models for all parachutes are built up using a bottom-up approach. This can be seen in Equation 4.38. It is assumed that the ballute and ribbon parachute are made out of aramids where the Ringsail is made out of nylon. Through personal communication with Gueth-Wolf the price per meter or square meter of both materials has been obtained. It is furthermore assumed that the riser and suspension lines are always made out of aramids in order to be more resistant to thermal loading. In this equation the costs of the individual materials are summed up and multiplied with 1.1, denoted as $c_{production}$. The 10% indicates the spare cost for the production process. The cost model can be found in Equation 4.38.

$$c_{D_{parachute}} = c_{production}(c_{canopy} + c_{suspension} + c_{riser}) \tag{4.38}$$

4.6.2. Drag Plates

The drag plates are assumed to be made out of Aluminium 7075. This type of aluminium has a density of 2810 kg/m^3 and a melting temperature of 635 deg C [41]. Furthermore, it is assumed that the plate is 0.01 m thick and the area is defined by the stage ID. Using the volume of the plate the mass and cost of the aluminium can be determined. A factor of 2 is applied to include the mass and cost of the hinge and hold down system. The models used can be found in Equation 4.39 and Equation 4.40.

$$m_{D_{plate}} = A_{plate} * 0.01 * \rho_{alu} * 2 \tag{4.39}$$

$$c_{D_{plate}} = m_{D_{plate}} * c_{aluminium} * 2 \tag{4.40}$$

4.6.3. Propulsive Deceleration

With the required thrust setting (T_s) and burn time (t_{burn}) stated in the configuration ID, CRDT can determine the total propellant mass and cost. This can be found in Equation 4.41 and Equation 4.43. Here the mass flow ($\dot{m}$) and total fuel and oxidiser mass, denoted as m_{fuel} and m_{ox}, are used. Finally the OF ratio, or Oxidiser to Fuel ratio, is used.

$$m_{D_{propellant}} = \dot{m}\ t_{burn}\ T_s \tag{4.41}$$

$$c_{D_{propellant}} = m_{ox} * c_{ox} + m_{fuel} * c_{fuel} \tag{4.42}$$

$$c_{D_{propellant}} = m_{D_{propellant}} \frac{OF}{1+OF} * c_{ox} + m_{D_{propellant}} \frac{1}{1+OF} * c_{fuel} \tag{4.43}$$

4.7. Landing Systems

The following section shows the mass and cost models used for the landing hardware. It shows the assumptions together with the models themselves.

4.7.1. Assumptions

The following assumptions have been made for the landing model:

Table 4.7: Assumptions - Landing

ID	Assumption
Land - 01	Landing system mass is a function of landing velocity, stage mass at landing, and landing system type
Land - 02	Maximum landing velocity of the landing system type is dependent on the landing system type
Land - 03	Mid-air retrieval is only possible in case a parachute is deployed at 5 km or higher
Land - 04	When using a landing system the vehicle always lands safely

It is assumed that the stage always lands safely as long as the terminal velocity of the stage is within the allowed velocity range of the landing hardware. Furthermore, the mass of the system is dependent on the stage mass and velocity at landing, as this defines the kinetic energy that needs to be nullified. Finally, the mid-air recovery requires a parachute to be caught by the helicopter.

4.7.2. Land Landing

As can be seen in Figure 4.8 there is an optimum for both deceleration systems. This figure was created for the USAF B-1 escape module which weighs about 7800 lb (about 3538 kg). CRDT takes the airbags or retrorocket curves into account when determining the mass of the landing system. Note that the y-axis of the graph shows the ratio between the recovery mass and the payload mass.

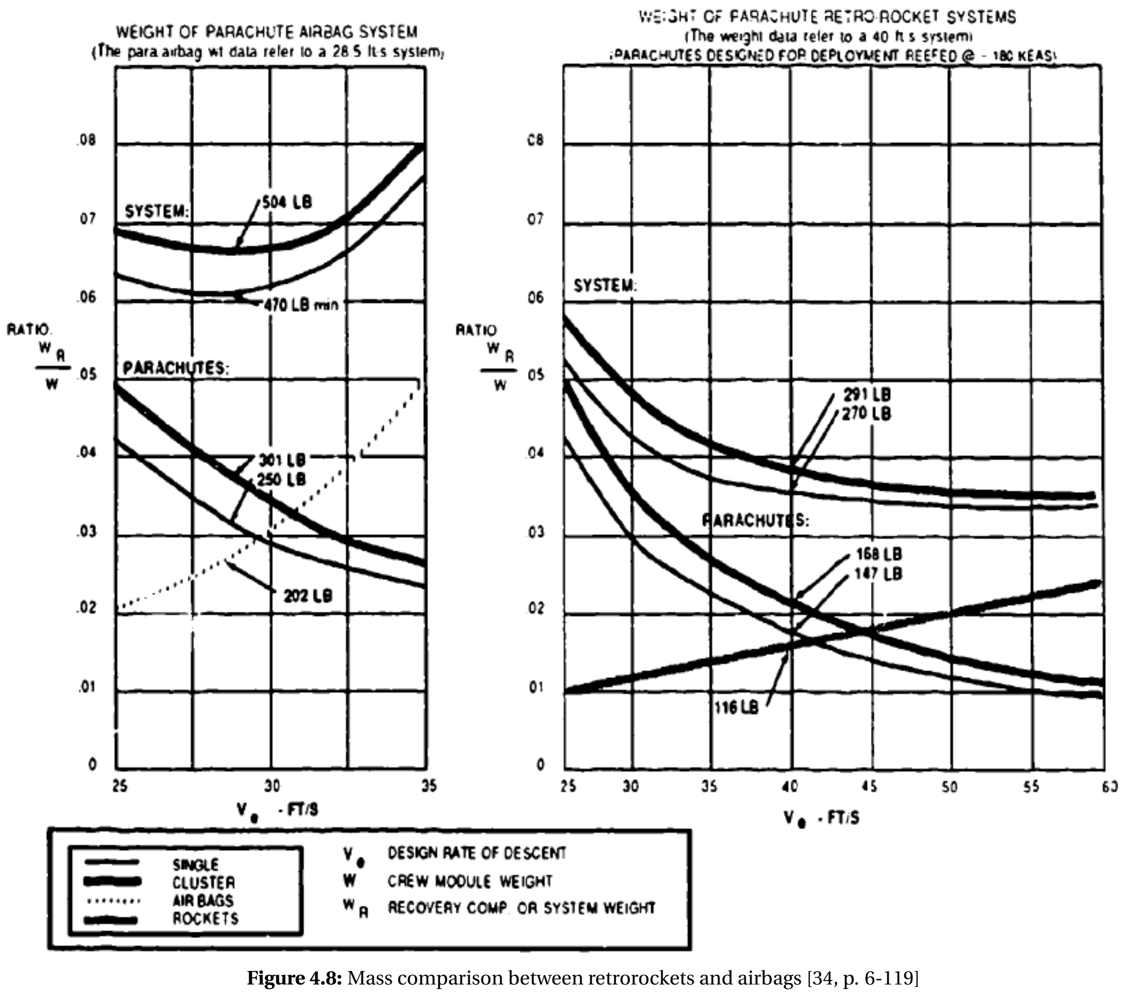

Figure 4.8: Mass comparison between retrorockets and airbags [34, p. 6-119]

The mass equations can be written as shown in Equation 4.44 and Equation 4.45. In line with Figure 4.8, the masses are in pounds and the landing velocity is in ft/s.

$$\frac{m_{L_{retrorocket}}}{m_{stage}} = 4E-4*V_{land} \tag{4.44}$$

$$\frac{m_{L_{airbag}}}{m_{stage}} = 4.57E-6*V_{land}^2 + -2.1143E-4*V_{land} + 3.2E-3 \tag{4.45}$$

The cost of the retrorocket landing system is broken up into the casing and the propellant. From Project Bellerophon of Purdue University, it can be seen that the cost of a solid engine can be broken into the cost of the propellant and the cost of the casing and nozzle [52]. This can be seen in Equation 4.46. From literature it can be seen that the dry mass of an average solid rocket booster is between 0.115 to 0.167 of the total mass. This mass fraction is shown as α [69]. Within CRDT a mass fraction of 0.115 is used.

$$c_{L_{retrorocket}} = 5*m_{propellant} + 1780*m_{dry}^{0.658} \tag{4.46a}$$

$$c_{L_{retrorocket}} = 5*m_{system}*(1-\alpha) + 1780*(m_{dry}*\alpha)^{0.658} \tag{4.46b}$$

The cost of the airbag system is calculated bottom up similarly to the inflatable heat shield. From the Mars Exploration Rovers Opportunity and Curiosity, it can be seen that the airbags are made out of Vectran for both the bladder and the abrasion layer. In total the mass of this system can be found to be 14.5 oz/m^2 (0.491 kg/m^2) and about 4500 yen/kg (40 USD/kg) [32, 27].

$$m_{L_{airbag}} = 4.57e-06v_{land}^3 - 2.11e-04v_{land}^2 + 0.0032v_{land} \tag{4.47}$$

$$c_{L_{airbag}} = m_{airbag}*c_{Vectran}*2 \tag{4.48}$$

4.7.3. Water Landing

For the reusable upper stage, it is assumed the stage has no buoyancy; thus a flotation device has to keep the stage afloat. Furthermore, it is assumed that the flotation device also closes off the engine such that salt water does not enter the inside. The required volume of trapped air can be determined using Archimedes' principle.

$$V_{air} = \frac{m_{stage}}{\rho_{water}} \tag{4.49}$$

With a mass of 2500 kg and a density of water of about 1000 kg/m^3 one only requires 2.5 m^3 of gas. This compares to a single sphere with a radius of 0.84 m. It is assumed there is no upper limit to this model as one can always add more flotation system. However, when production limits are reached one should add multiple flotation systems.
When looking at Hypalon, the material used for Rigid-hulled inflatable boats, one can find it to be about 68 GBP/m^2 and 1.3 kg/m^2. It is assumed that these prices can be used for space applications, as the airbag is deflated and protected during the space flight. The flotation device is only inflated just before the stage hits the water. The mass of the pressurisation gas required can be found when assuming a 2 bar pressure in the sphere and assuming the sphere is filled with CO_2. Now using the ideal gas law, one can determine the required mass of the gas as can be seen in Equation 4.50 and Equation 4.51.

$$m_{L_{flotation}} = (A_{flotation}*\rho_{Hypalon})*2 + \frac{P*V_{air}}{R_{specific}*T} \tag{4.50}$$

$$c_{L_{flotation}} = (A_{flotation}*\rho_{Hypalon}*c_{Hypalon})*2 \tag{4.51}$$

4.7.4. Mid-Air Retrieval

When opting for a mid-air retrieval (MAR) one does not require any particular hardware on the stage itself expect for a parachute as the final EDL system. Therefore it is assumed that no mass or cost is required for MAR. This can be seen in Equation 4.52 and Equation 4.53. The cost of operations and the helicopter are placed under the retrieval phase and can be found in section 4.8.

$$m_{L_{MAR}} = 0 \tag{4.52}$$

$$c_{L_{MAR}} = 0 \tag{4.53}$$

4.8. Retrieval Operations

Based upon the work done at Delft University of Technology by M. Snijder for the National Aerospace Laboratory (NLR) on first stage recovery for the "SMall Innovative Launcher for Europe" project (SMILE), the costs of ships and helicopters can be found. This work based the cost estimates on advice from (former) employees of Airbus Helicopters, Zwijnenburg Shipbuilding and Damen Shipyards. It estimated the cost of the retrieval ship to be EUR 760.000 per year for a water landing and the cost of the helicopter to be EUR 775.000 per year for mid-air retrieval [53]. The cost of a truck is estimated to be about USD 180.000 per year [61]. The costs of the retrieval unit (c_{unit}) is distributed over the amount of flights per year (n_y) as can be seen in Equation 4.54.

$$c_{Retrieval} = c_{unit}/n_y \tag{4.54}$$

4.9. Refurbishment Operations

Refurbishment is the act of preparing the launch vehicle for re-launch. During a presentation, SpaceX mentioned that it consists of three major elements, shown below [12]. The total cost for refurbishments are assumed to be as mentioned in Equation 4.55

1. Inspection
2. Replacement
3. Acceptance test

During the inspection phase, a team of workers is required to go over the vehicle and inspect for damages. The DC-X, a suborbital platform using RL-10 engines similar to the Centaur upper stage, showed a turnaround time of 26 hours [11]. This is similar to the 24 hour turnaround time goal of SpaceX Falcon 9 first stage [57]. However, both are suborbital vehicles. The unflown Kistler K-1 had a targeted turnaround time of nine days [10]. The turnaround of the Kistler K-1 included the inspection and clean up of both stages, the integration of the entire vehicle and the acceptance for re-flight.
As it is possible only to retrieve and reuse a part of the upper stage, it might be required to rebuild parts of the launcher. The cost of this is dependent on the k-factor found in the Reuse Index.
The acceptance test is assumed to be one full-length engine burn. For the Centaur upper stage, this would be a 700-second burn. During this test, the operations crew can confirm the stage to be in good health and thus accept it for re-flight.

$$c_{Refurbishment} = c_{Inspection} + (1-k) + c_{Acceptance} \tag{4.55}$$

4.10. Overview of Implemented Models

The following section contains an overview of the models used in CRDT. Table 4.8 shows the source of the various models, where Table 4.9 and Table 4.10 show the ranges in which the models are valid and the uncertainty. When performing the optimisation, CRDT assumes the nominal value of the mass and cost presented by the model. The uncertainty is only taken into account in the sensitivity analysis.

Table 4.8: Overview of Entry Descent and Landing (EDL) hardware

Hardware		**How implemented in the dynamics model**	**Mass model**	**Cost model**
Separation system		-	Historic data [54, 55, 56, 7]	Function of system mass
Thermal protection	Solid heat shield	-	Milos et all [49]	Milos et all [49]
	Inflatable heat shield	Change the frontal area of the stage to the area of the heat shield	Historic data [51, 45]	Bottom up model
Decelerators	Parachute	EDL force superimposed on the body drag force	Knacke [34]	Bottom up model
	Drag plates		Bottom up model	Bottom up model, function of system mass
	Engine burn		Function of burn time	Function of propellant mass
Landing	Retrorockets	Prescribed safe landing	Knacke [34]	Bottom up function of retrorocket mass. Mass divided in propellant and casing
	Airbags		Knacke [34]	Bottom up function of airbag mass
	Flotation device		Bottom up model	Bottom up, function of system mass
	Mid air retrieval		NA	NA

Table 4.9 and Table 4.10 shows the mass and cost models in more detail. It shows the parameters of which the mass function is dependent on. The parameters presented are only the variables in CRDT, elements that cannot be varied are not presented in the table below. The table shows the range in which every model is valid. For more information regarding the ranges of the model, the reader is directed to chapter 6 where the verification and validation activities are presented. If available the uncertainty of the model is shown in the table. Where the uncertainty is unknown, a 20% margin is assumed during the sensitivity studies, this is indicated with '± ~20%' where the tilde indicates an assumed range. Where other ranges are assumed that are not explained in chapter 4 or chapter 6 a footnote is added below the table.

Table 4.9: Mass Modelling of the EDL Hardware

Item	Mass model	Range	Uncertainty
Solid heat shield	Function of frontal area	Unknown	Unknown
Inflatable heat shield	Function of diameter	3 - 16 $[m^2]$	±25%
Separation system	Function of stage mass	0 - 7000 $[kg]$	0.0718 * stage mass
Ribbon parachute	Function of parachute diameter	1 - 24.3 $[m]$	± ~20%
Ringsail parachute	Function of parachute diameter	1 - 24.3 $[m]$	± ~20%
Ballute	Historic data, function of parachute diameter	1 - 20 $[m]$	± ~20%
Drag plates	Bottom up, function of drag plate area	2-5 $[m^2]$	± ~20%
Engine burn - 1	Function of required delta-V	0 - inf $[m/s]$	± ~20%
Engine burn - 2	Function of burn time and throttle setting	0 - inf $[s]$	± ~20%
Retrorocket	Function of landing velocity and stage mass	0 - 100 $[m/s]$	± ~20%
Airbags	Function of landing velocity and stage mass	3 - 10 $[m/s]$	± ~20%
Flotation device	Function of stage mass	Unknown	± ~20%
Mid air retrieval	NA	NA	NA
Retrieval	NA	NA	NA
Refurbishment	NA	NA	NA

The table below gives a more detailed overview of the cost functions. The same nomenclature as with the mass functions applies, when the uncertainty is unknown, this is indicated with ± ~20%.

Table 4.10: Cost Modelling of the EDL Hardware

Item	Cost model	Range	Uncertainty
Solid heat shield	Function of frontal area	Unknown	± ~20%
Inflatable heat shield	Function of frontal area	3 - 16 $[m^2]$	± ~20%
Separation system	Function of system mass	0 - 7000 $[kg]$	± ~20%
Parachutes	Function of frontal area	1 - 24.3 $[m]$	± ~20%
Ballute	Function of ballute diameter	1 - 20 $[m]$	± ~20%
Drag plates	Function of system mass	0-inf $[kg]$	± ~20%
Engine burn	Function of propellant mass	0 - inf $[kg]$	± ~20%
Retrorocket	Function of propellant + casing mass	Unknown	± ~20%
Airbags	Function of mass	Unknown	± ~20%
Flotation device	Function of system mass	Unknown	± ~20%
Mid-air retrieval	NA	NA	NA
Retrieval	Function of landing location	Unknown	± ~20%
Refurbishment	Function of inspection, replacement, and validation	Unknown	± ~20%

5
Development of the Tool

The Conceptual Reusability Design Tool, or CRDT for short, is the tool developed to determine whether reusability can reduce the costs of an upper stage. This chapter gives an overview of the tool itself and shows the requirements imposed on the tool. Furthermore, it shows the input and outputs CRDT requires and provides. The chapter shows the way the genetic optimisation algorithm and the Monte Carlo analysis have been implemented with the DARE ParSim tool. Furthermore, it shows the modifications made to the ParSim V3 tool.

5.1. Tool Overview

The following section gives an overview of the Conceptual Reusability Design Tool (CRDT). When making the initial simulation diagram, which can be found in Figure 5.1, one can see that the code consists of three pillars. The tool has been developed in MATLAB2018a released in March 2018 by MathWorks [40].

The most right column is called the "MDO column". This column is the core in the program and contains the code to create the first generation, run the genetic algorithm (section 5.4), and the Monte Carlo analysis (section 5.5).

The middle column is called the "ParSim column". This section of the code contains the integrator that determines the trajectory of a ballistic entry. More information can be found in section 5.3. This column also determines the dynamics of the various EDL hardware elements added to the stage.

The most left column is called the "Vehicle column". It contains the performance, mass and cost models of the various pieces of hardware (chapter 4). A more detailed overview of the tool with all the sub-blocks can be found in appendix C.

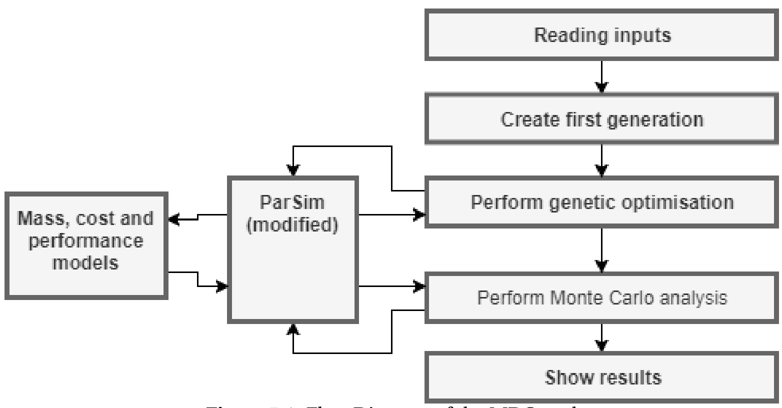

Figure 5.1: Flow Diagram of the MDO tool

5.2. Inputs and Outputs

the following section describes the inputs and outputs of CRDT and the categories they are divided into. A complete overview can be found in Appendix D.

5.2.1. Inputs

CRDT is developed with the Atlas V Centaur stage as the initial mission, however it is modular such that other launchers and upper stages can be implemented. Because of this, all inputs are put in external CSV files which can be modified through the Graphical User Interface (GUI).

There are 108 inputs divided over 12 categories. These categories can be seen in the list below. Below the categories, one can see the various CSV files CRDT uses.

- Constants
- Material Parameters
- Manhour costs
- Development parameters
- System limits
- Initial orbit
- Launcher performance
- Allowable range of variable parameters
- Stage definition
- Engine definition
- Stage costs
- GUI inputs

- Constants.csv - File that contains all constants
- Cost man.csv - File containing the manhour time estimates
- Cost Development - File containing the Transcost estimates
- Cost Material - File containing all material properties
- Launcher.csv - File that contains the launcher variants and orbits of interest.
- Orbits.csv - File containing the parameters for the initial orbits
- System constraints.csv - File containing the system limits by which the optimisation is limited, such as maximum area of a decelerator
- System Definition.csv - File containing the system overview in terms of stage size, engine performance and parachute performance
- System Limits.csv - Constraints imposed on the system such as maximum thermal flux

5.2.2. Outputs

There are 16 outputs divided over 4 categories. These are presented in the result tabs that automatically appear after a optimisation or sensitivity run. These categories are as follows:

- Stage mass breakdown
- Reuse Index inputs and results
- Sensitivity plot
- Figures showing trajectory of the stage

The outputs presented are chosen as they show the value of the Reuse Index, which indicates whether the reusable stage is cheaper compared to the expendable variant. To support the presented results, the input parameters of the Reuse Index such as mass and cost are presented. Boxplots showing the sensitivity of the results of the Monte Carlo analysis are presented. Finally, the trajectory plots are shown to demonstrate to the user that the constraints of the nominal case are not breached.

Screenshots of the GUI can be found in Figure 5.2 through 5.4. The tabs show the inputs for the genetic optimisation in Figure 5.2. Figure 5.3 and Figure 5.4 shows the check boxes that allow a user to select or unselect the various options.

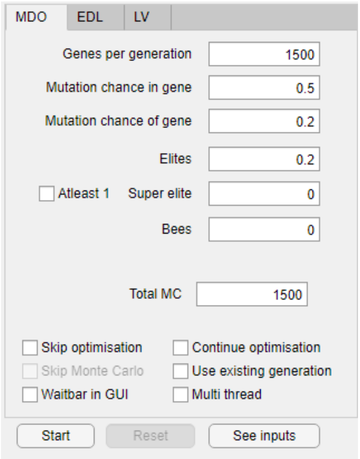

Figure 5.2: Input tab 1

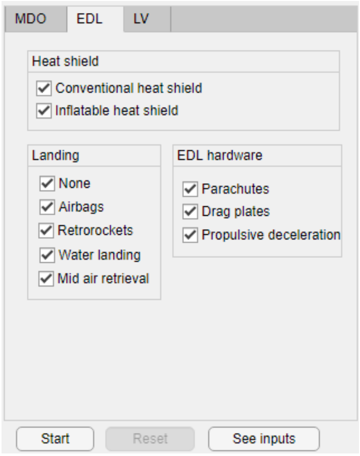

Figure 5.3: Input tab 2

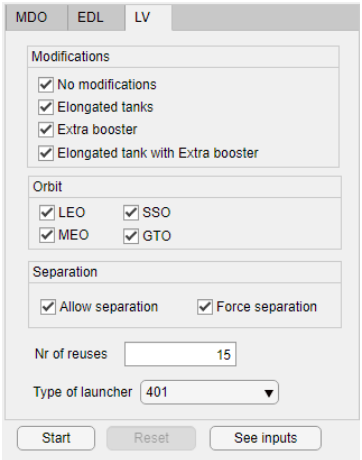

Figure 5.4: Input tab 3

5.3. Modified ParSim

With the open architecture of ParSim [47], it was relatively easy to modify the tool for the requirements of CRDT. Several modifications have been made to the tool:

- Allowed for three decelerator elements where ParSim only allows for two EDL elements
- Added drag plates as decelerator option
- Added propulsive deceleration as decelerator option
- Added landing hardware
- Added de-orbit code
- Added thermal protection system
- Added mass and cost models

5.4. The Genetic Optimisation Algorithm

The genetic optimisation algorithm is represented in Figure 5.1 in the block "Perform Genetic Optimisation". A schematic representation of how the creation of the new generation works can be found in subsection 5.4.1.

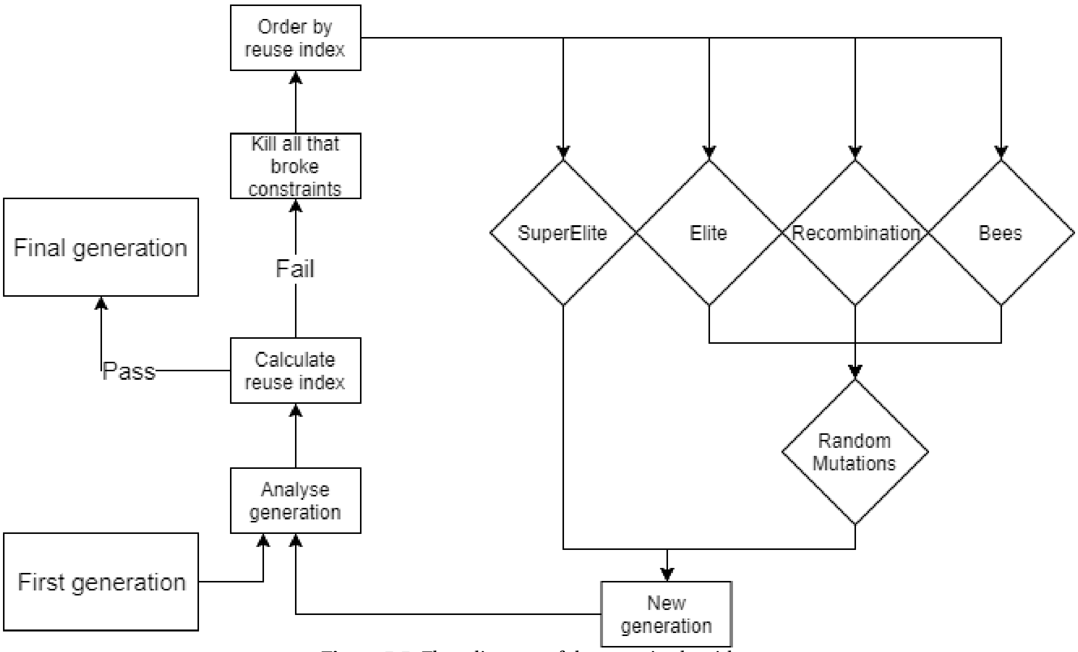

Figure 5.5: Flow diagram of the genetic algorithm

The genetic optimisation includes a modified version of the DARE ParSim tool to analyse the generation and to calculate the Reuse Index. The remainder of this block diagram is the genetic optimisation algorithm. This algorithm, developed for CRDT, includes a fairly standard genetic algorithm featuring a transfer of elites, recombination of parents and random mutations but also allows for the inclusion of SuperElite and Bees; the latter are discussed later in this section.

5.4.1. Creation of First Generation

The first generation is created at random, but within the limits imposed by the user. The general flow diagram can be found in Figure 5.6. The tool begins by creating a random configuration which is checked against the limits. When the created configuration passes, it is stored in the first generation. This process repeats until the first generation has been filled. The generation of the first generation is similar to the way bees are generated in the the creation of a new generation.

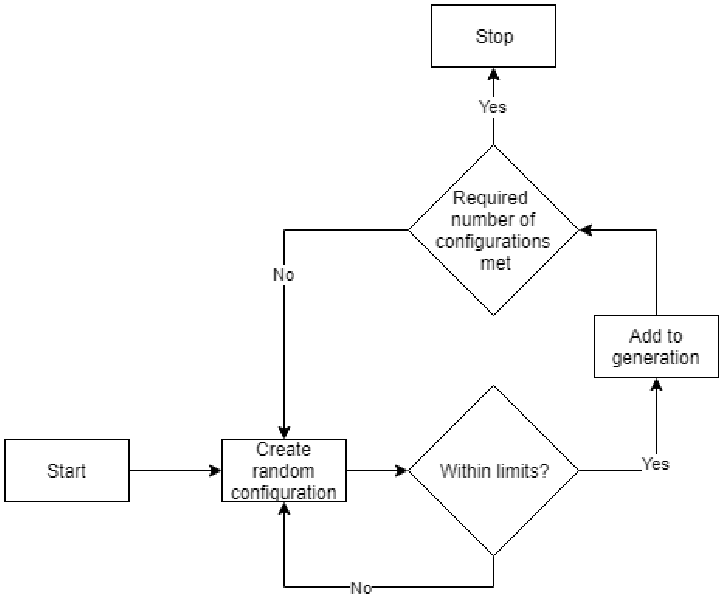

Figure 5.6: Schematic representation of the creation of a first generation

5.4.2. Creation of a New Generation

After all configurations in a generation have been analysed, the results are combined into a single structure. From this structure, the new generation is created. The creation of a new generation can be seen in Figure 5.7.

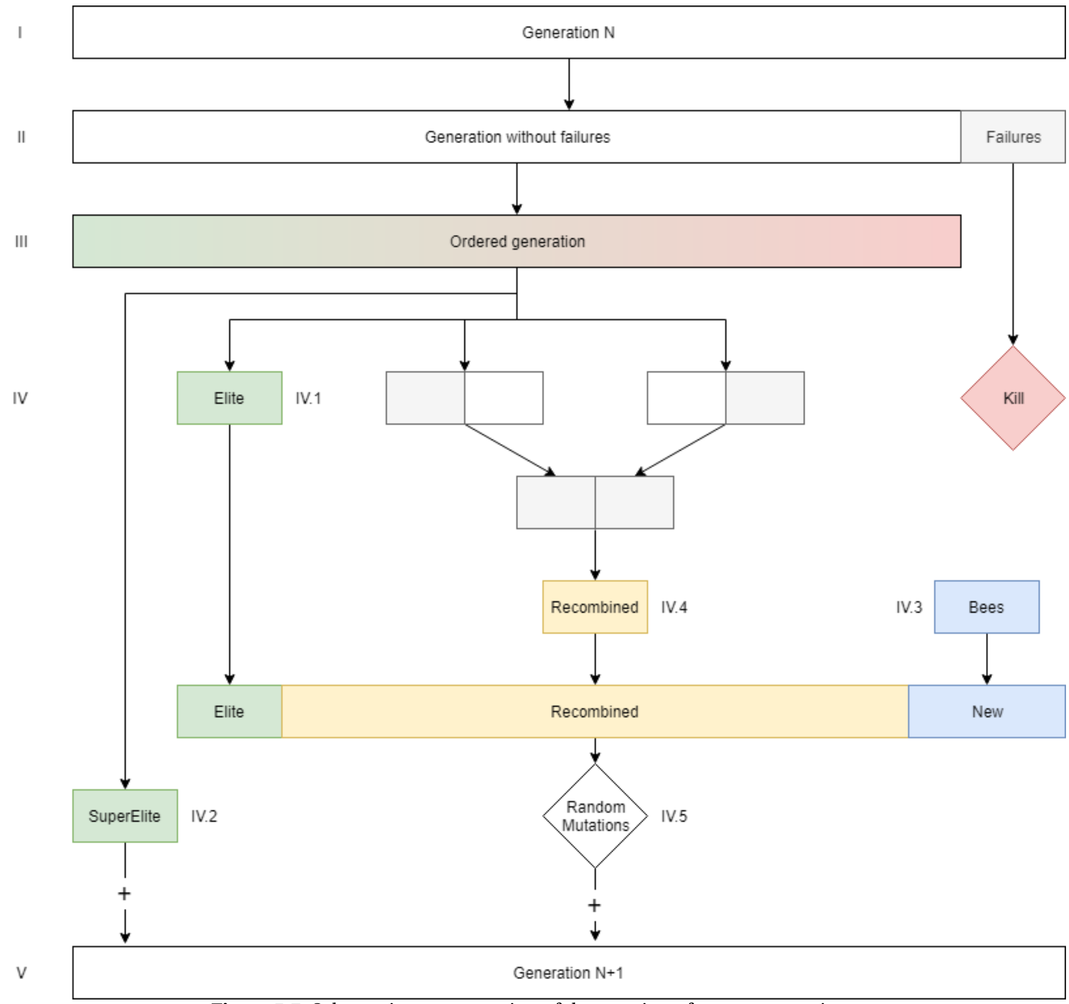

Figure 5.7: Schematic representation of the creation of a new generation

From the previous generation (I), all genes that breach the constraints set by the yser are put to zero, which effectively kills the configuration and does not allow transfer to a new generation (II). The remainder of the generation is ordered by Reuse Index in ascending order (III).

The creation of the new generation (IV) is done in four steps: transfer of elite transfer of SuperElite, creation of bees, and recombination.

From the generation, a certain percentage of elites are transferred to the new generation (IV.1). The user decides on this percentage. In case the user asks for more elites than there are non-zero results, all results are transferred. Depending on user input, some genes might be immune to mutations occurring in IV.5 and are referred to as SuperElites (IV.2). SuperElites cannot be influenced by mutations and are, by definition, transferred to the next generation. SuperElites can be used in functions where the optimum is very narrow and thus hard to find. An example of a function where SuperElites can be useful can be found in Figure 5.8.

Next, a group of bees, which are new random configurations, can be added to the generation (IV.3). The number of bees is determined by the input from the user together with the killed genes. Adding bees to the generation is done to keep a certain variety in the generation. This helps CRDT to keep a global overview. This is useful for when the target minimum is obscured by a non-global minimum. An example of a function where bees can be useful can be found in Figure 5.9.

The remainder of the new generation is filled up with recombinations of the old generation (IV.4). The re-combination is done by combining the first half the genes of a configuration with the second half of another

configuration.
Finally, there are random mutations performed on the generation (IV.5). These mutations are done on all elements of the configuration with the exception of the elements "EDL System 1", "EDL System 2", and "EDL System 3".

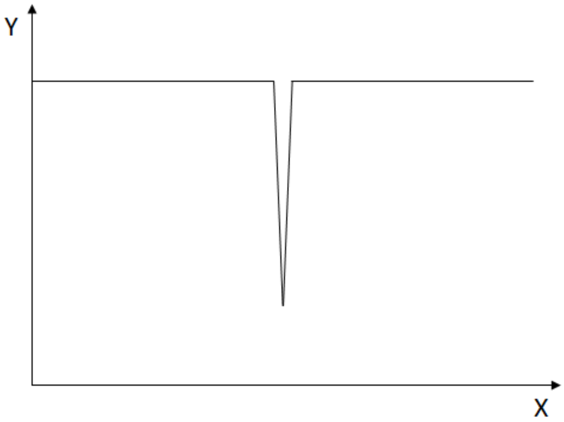

Figure 5.8: Example of a function where SuperElites can be used

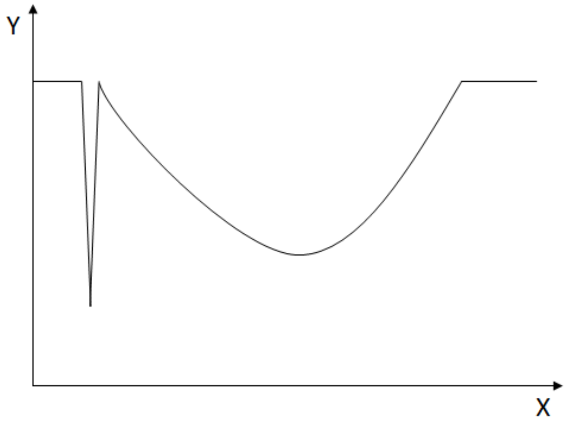

Figure 5.9: Example of a function where bees can be used

Example of a new generation
An example of a generation with 10 genes can be seen in Figure 5.10. Of these ten genes, there are two genes that are killed off. These are indicated in red in the second row.
As the elites have been set to 0.2, 2 genes are transferred as elites. With the tag "always one" activated, the first elite is transferred as a SuperElite. The user sets the bees to 0.1, as there are two kills, ten% would be 0.2 genes, rounding up gives one gene. The bees are indicated in blue.
The other genes are recombined into new genes. A white/grey configuration indicates this recombination. Finally, the genes are added and mutated. As can be seen, the SuperElite is immune, the others are, not. In this case, the user inputted that 0.5 of the genes are mutated, which can be seen by some genes remaining white, while others are receiving specks.

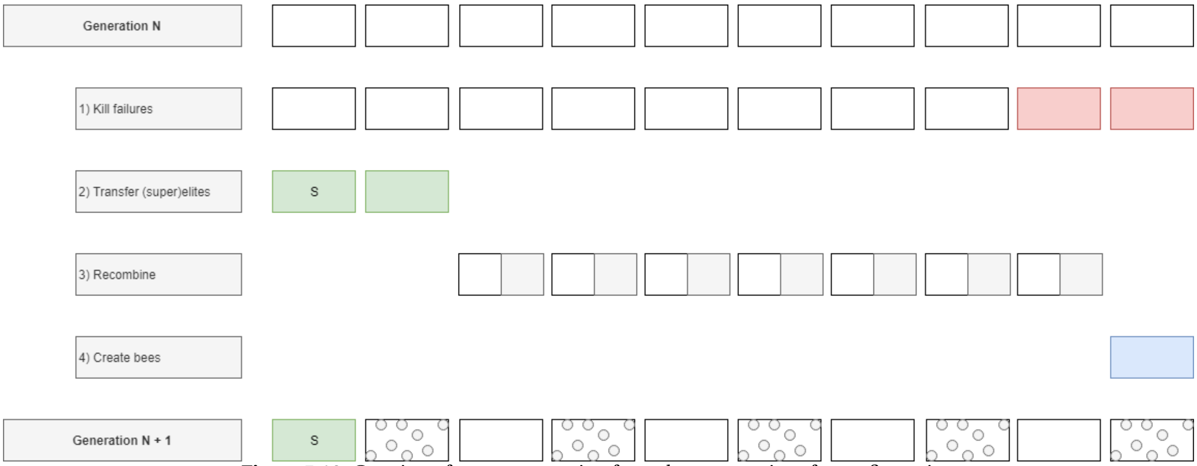

Figure 5.10: Creation of a new generation from the perspective of a configuration

5.4.3. Stop Criteria

This new generation is transferred back to the modified ParSim, where it is analysed. This loop continues until a pre-defined stop trigger is reached. Three stop conditions are included in CRDT. These can be found in Table 5.1.

Table 5.1: Overview Stop Criteria

Criteria	Definition
Maximum generations	Maximum number of generations reached
Crashed	Increase in minimum Reuses Index, whilst the number of non-zero genes decreases. When this is triggered, the user is warned and has the option to still continue the run or to abort the run.
Flatline	Fitness of generation remains the same for three generations

5.4.4. Status Updates During a Run

When the tool is running, the genetic optimisation algorithm shows the status and kills of a generation together with the total time required to determine the fitness of the generation. This is done in the Status vector (Equation 5.1) and Kill vector (Equation 5.2). These are as follows:

$$\begin{bmatrix} Actual\ number\ of\ Elites\ (Actual\ number\ of\ SuperElites) \\ Actual\ number\ of\ Recombinations \\ Actual\ numbers\ of\ Bees \\ Actual\ number\ of\ Mutations \end{bmatrix}^T \tag{5.1}$$

$$\begin{bmatrix} Total\ kills \\ Payload\ capacity\ reduced\ to\ zero \\ Payload\ capacity\ constraint\ violated \\ Mechanical\ constraint\ violated \\ Thermal\ constraint\ violated \\ Landing\ velocity\ constraint\ violated \end{bmatrix}^T \tag{5.2}$$

During a run, CRDT gives updates on the progress through four tabs. These are a text based log, a line plot showing the lowest Reuse Index over the generations, boxplots showing the Reuse Index distribution over multiple generations, and a configuration overview per generation.

Figure 5.11 shows a text based log. One can see that the run was performed on the 24th of September and was started at 11:45. From the outputs it can be seen that the creation of the first generation took only 8 seconds. This is due to the fact that all options were allowed, thus filling the generation is more easy. Each update, presented after a run, shows the number of elites transferred, number of recombinations, number of bees, and number of mutations. From the time required to analyse a single generation one can see that it takes about half a second to analyse a single configuration.

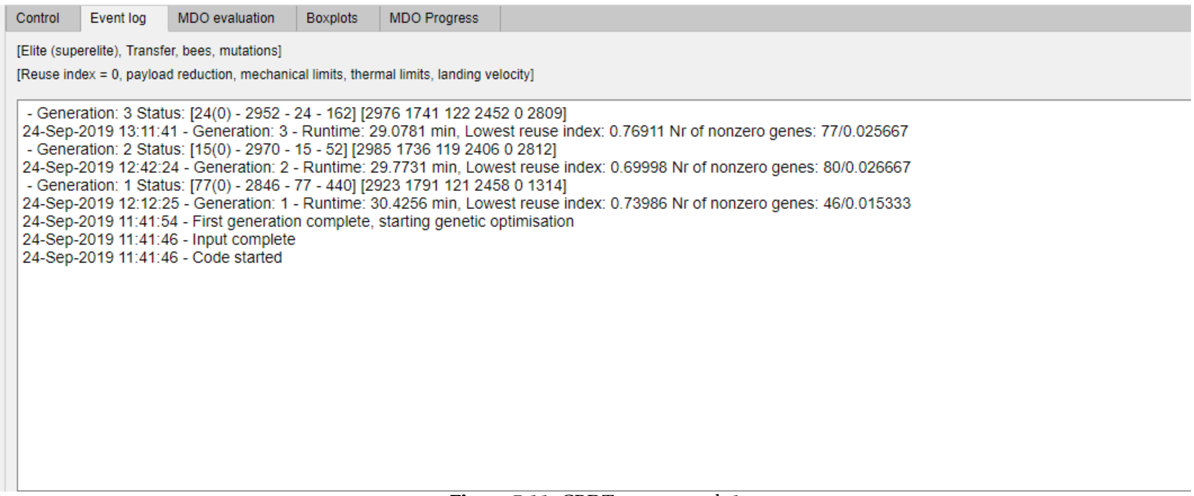

Figure 5.11: CRDT progress tab 1

The second tab, seen in Figure 5.12, shows the progress of the Reuse Index in a graph. Besides the lowest Reuse Index, it also shows the average Reuse Index of the generation and the average Reuse Index of the lowest ten genes. The final line is the number of non-zero genes. The plots show that over the generations, the number of "non-zero genes" goes up, whilst the average Reuse Index goes down. A non-zero configuration is a configuration that does not breach any constraint, and is therefore not killed.

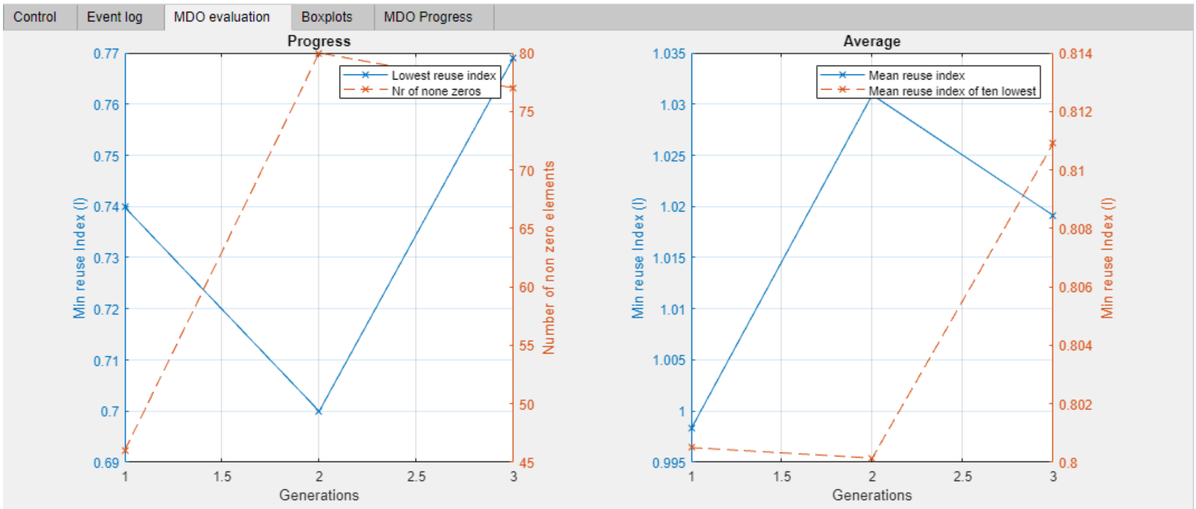

Figure 5.12: CRDT progress tab 2

Figure 5.13 shows the Reuse Index of every configuration in a certain generation, showing the spread. The figure on the right does the same, but then only for the surviving configurations. In this figure, it can be seen that the total spread decreases, and the mean Reuse Index decreases as well. In this figure one can clearly see that in any generation, there are many outliers (indicated with the red markers). In the figure on the right it can be seen that these outliers are killed and thus cannot pass to the next generation. In the right figure it can also be seen that the average Reuse Index of the generations decreases in line with Figure 5.12.

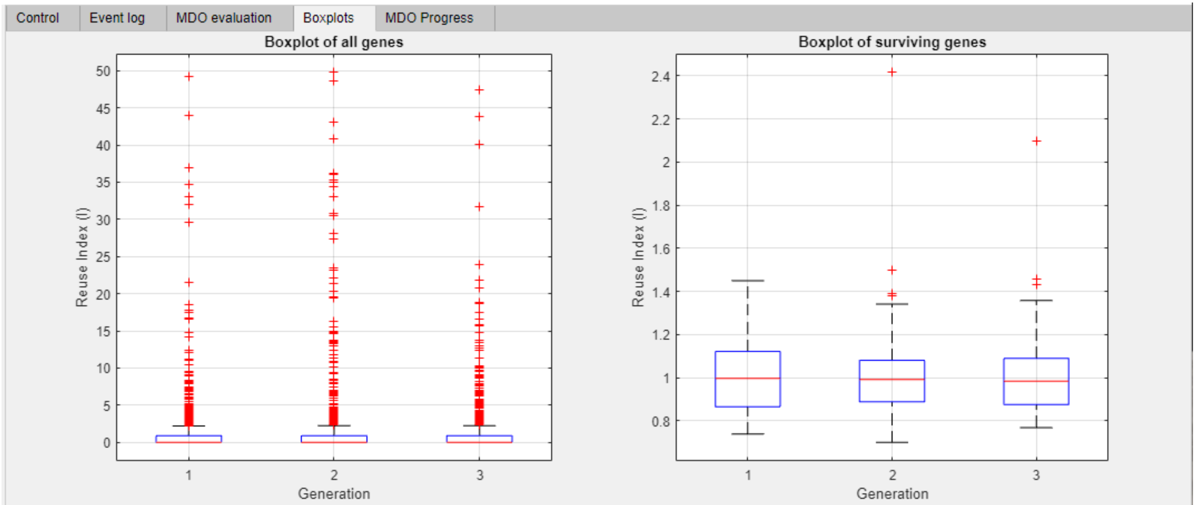

Figure 5.13: CRDT progress tab 3

The final tab, shown in Figure 5.14, shows the hardware selected by CRDT per generation. Every hardware element represents the number of times that element has been chosen. Every colour in the bars indicates a different generation. In this plot one can see the if there is a preference towards systems or if systems are not selected at all.

The meaning of the different numbers below the bars can be found in section 4.1.

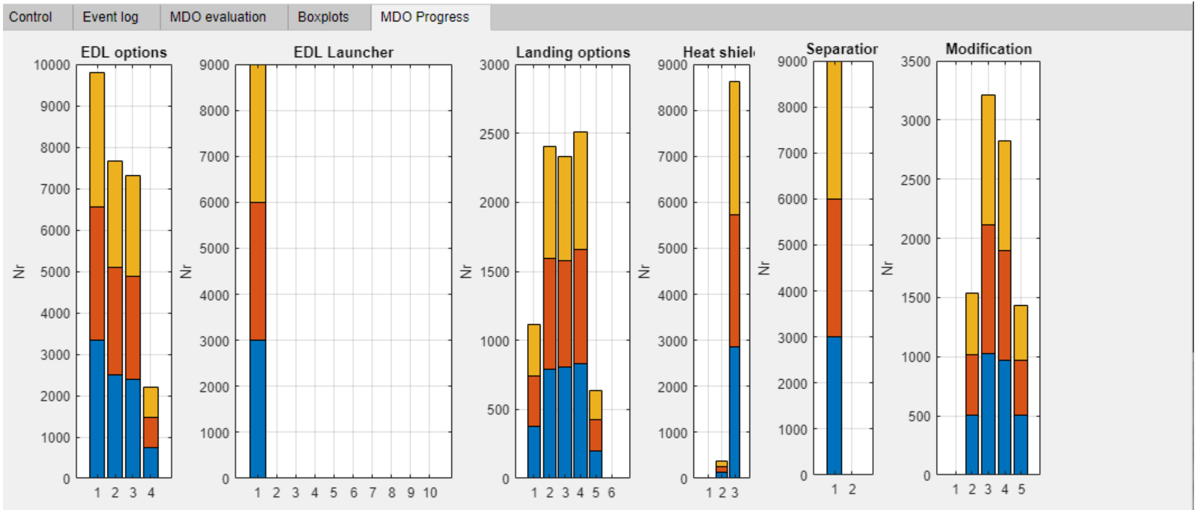

Figure 5.14: CRDT progress tab 4

5.4.5. Settings for Optimisation

To determine the optimal settings for the MDO inputs, a Monte Carlo optimisation is done. This is done by creating random combinations and using these settings to find the predefined target ID. The closer the final found configuration is to the target ID, the lower the value of The optimisation function is defined as the difference between the target ID and the closest found optimal ID. The flow diagram for this analysis can be found in Figure 5.15.

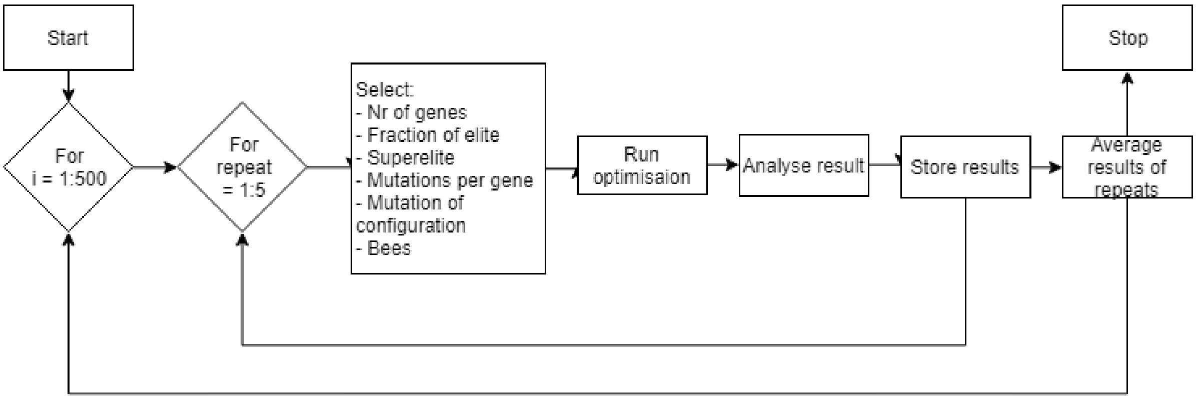

Figure 5.15: Monte Carlo optimisation used to determine MDO settings

For the first analysis the following input ranges have been used.

- Nr of genes = 100 - 3000
- Elite = 0.1 - 0.9
- SuperElite = 0 or 1
- Mutation per configuration = 0.1 - 0.9
- Mutation of configuration = 0.1 - 0.9
- Bees = 0.1 - 0.9

From the first run, it was found that the runs with SuperElites scored high and are thus not preferred. This means that the SuperElites are set to zero and will not be used. The lowest five configurations all had 2500 configurations per generation. For the remaining parameters, the range of the lowest ten MDO configurations was used. This leads to the following inputs.

- Nr of genes = 2000 - 4000
- Elite = 0.1 - 0.4
- SuperElite = 0
- Mutation per configuration = 0.5 - 0.9

- Mutation of configuration = 0.25 - 0.75
- Bees = 0.25 - 0.75

From this run it was found that a the preferred number of configurations is again approaching the upper limit. This leads to the conclusion that more configurations is preferred. The number of elites has been found to be between 0.2 and 0.25 where the number of bees is found to be between 0.3 and 0.4. Finally the mutations per configuration is found to be between 0.4 and 0.5, where the chance of mutation in a configuration is set to 0.7 and 0.8. The following setting for CRDT will be used throughout the thesis.

- Nr of genes = 2000 - 4000
- Elite = 0.25
- SuperElite = 0
- Mutation per configuration = 0.5
- Mutation of configuration = 0.75
- Bees = 0.35

5.5. Monte Carlo Analysis

When the genetic algorithm concludes and finds a feasible solution, the solution is transferred to the Monte Carlo analysis. This module varies the found solution and determines the Reuse Index of these variations. During the initial Monte Carlo analysis, the configuration ID and the mass/cost models are varied. All modifications are within limits set by the user. After the analysis, the module shows the results. These results are primarily for the original solution and show the mass and cost breakdown of the solutions. The results of the Monte Carlo analysis is shown as follows:

- Fraction of which variations that passed are within the user set constraints
- Boxplot showing the variation in:
  - Reuse Index
  - Reduction of payload capacity
  - Maximum deceleration
  - Maximum thermal loads

These results are automatically shown when the Monte Carlo analysis is done. They are shown within a MATLAB figure environment. A screen shot of a test run can be seen in Figure 5.16. On the top row, one can see the four boxplots showing the sensitivity of the solution. On the top right, the user can see a breakdown of the mass, cost and manhours of the found solution. This table can also be used to determine the hardware of the solution. In this example, one can see that the stage is recovered using an inflatable heat shield, a single parachute system, and uses retrorockets for landing. The mass and cost breakdown can also be found in the two pie charts on the bottom row. Finally, the Reuse Index as a function of the number of reuses can be found in the figure on the bottom right.

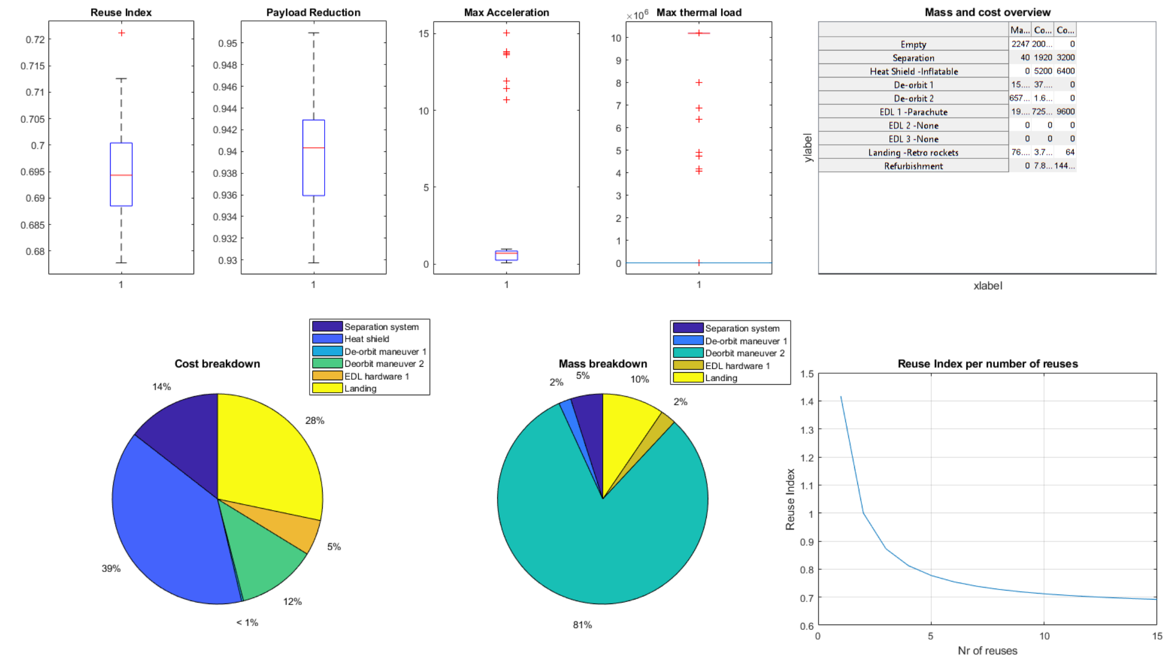

Figure 5.16: Example of first results page

5.5.1. Elaborate Results

The results of the sensitivity analysis are presented to the user in a second result screen. These can be found in figures Figure 5.17 through Figure 5.21.

In the first tab, shown in Figure 5.17, the user can see the solution found by CRDT. Furthermore, it shows the mass comparison of the reusable and expendable stage. Finally, the table on the right shows the inputs for the Reuse Index. All these results are for the found solution, not for the Monte Carlo analysis.

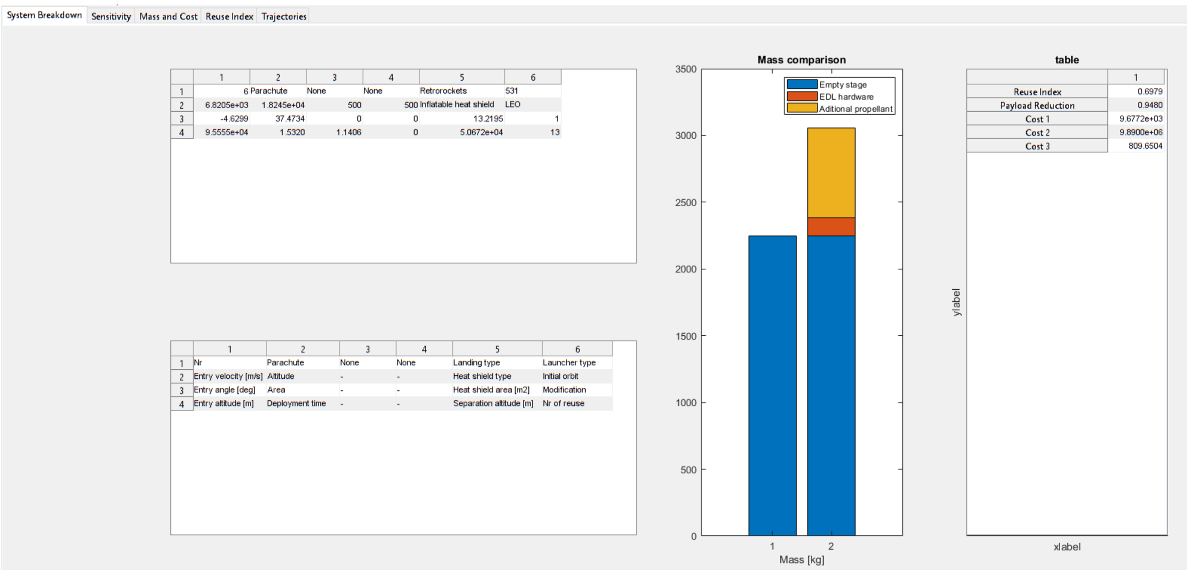

Figure 5.17: Example of detailed results page - tab 1

The second tab in Figure 5.18 shows the boxplots that were also shown in the initial results. However, an additional fifth boxplot showing the landing velocity can be found.

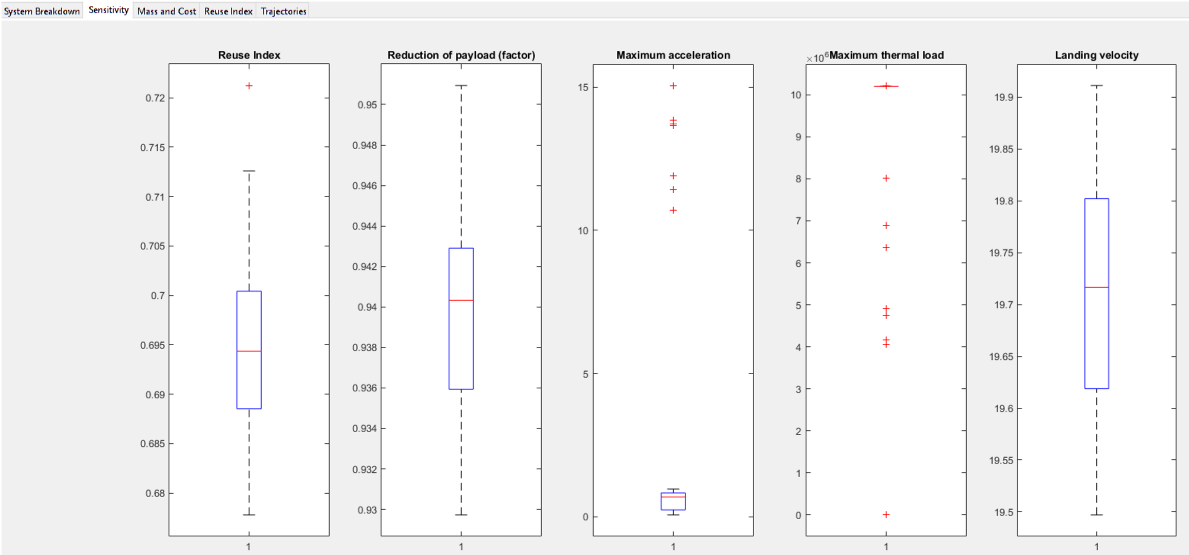

Figure 5.18: Example of detailed results page - tab 2

Figure 5.19 shows the third tab with the mass and cost breakdowns. The top two pie charts are identical to the ones in the initial results. The tab also adds the manhour pie chart and the total cost pie chart. Finally, it shows the table found in the initial results, containing the mass and cost breakdown in numbers.

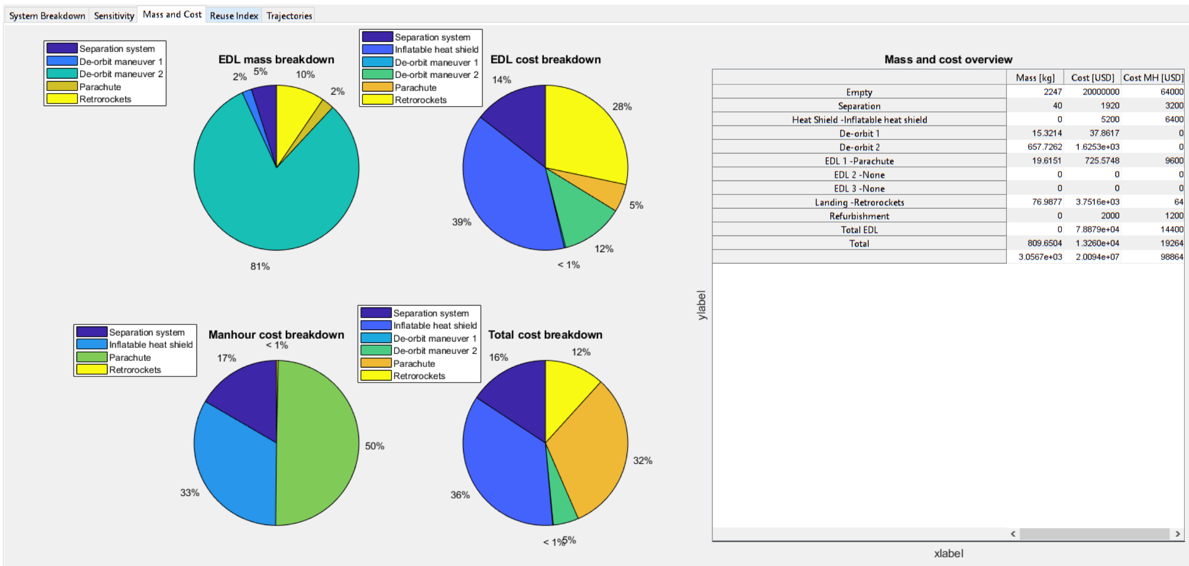

Figure 5.19: Example of detailed results page - tab 3

Tab 4, shown in Figure 5.20 shows the Reuse Index as a function of the number of reuses. This indicates the sensitivity to the number of total flights.

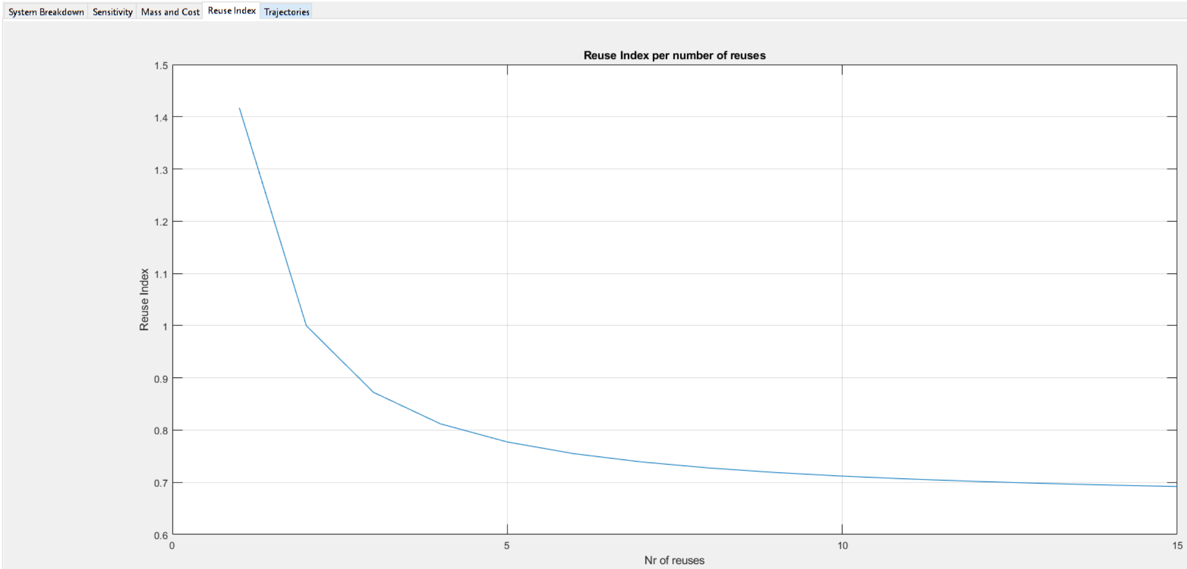

Figure 5.20: Example of detailed results page - tab 4

The final tab, shown in Figure 5.21 shows the trajectory plots of the initial solution. Here the user can see the following plots.

- Altitude - Time
- Time - Velocity
- Altitude - Velocity
- Dynamic pressure - Time
- Trajectory over round 2D earth
- Orbit over round 2D earth

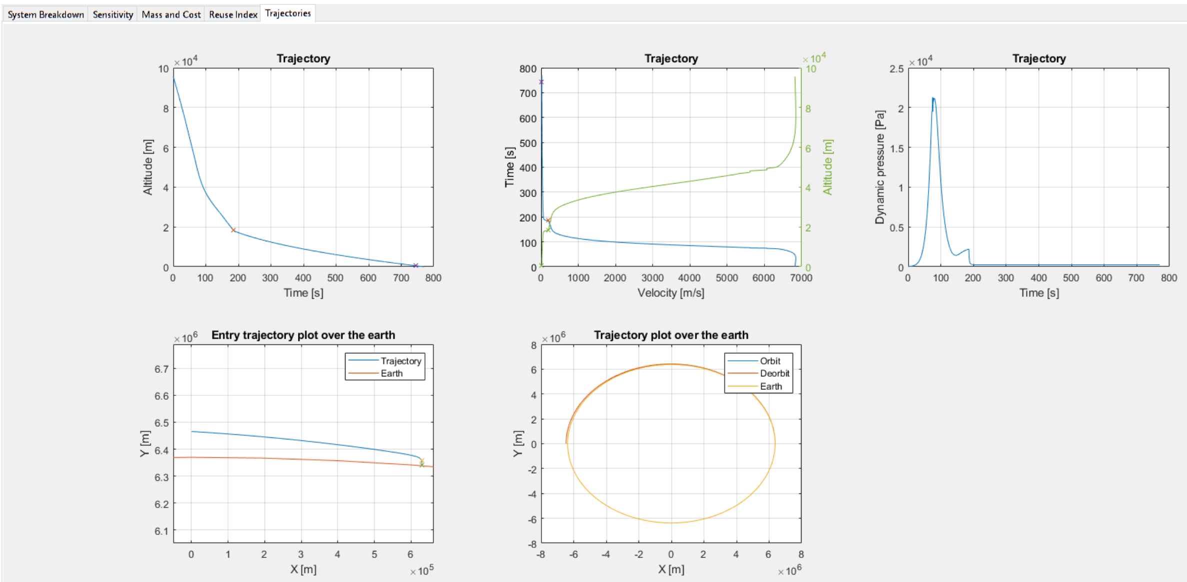

Figure 5.21: Example of detailed results page - tab 5

5.5.2. Sensitivity Analysis

The sensitivity analysis done directly after the genetic optimisation gives the user an overview of the sensitivity of the Reuse Index to variations in ID and mass/cost estimations. Based upon these results, the user can start a second sensitivity analysis, where the user has more control over the variations. The uncertainties are divided into five categories, which can be seen in the list below.

1. Uncertainty in stage geometry

2. Trajectory uncertainty
3. Onboard state estimation
4. Uncertainty in construction, trajectory, and state estimation (all three above)
5. Uncertainty in mass and cost estimations

In Table 5.2 the various variations are displayed. Each variation is assumed to be a normal distribution centred around the found optimum. The user is free to change the standard deviation for all inputs or put it to zero. The standard deviation is taken as a fraction of the mean.
As an example, when the deployment altitude is set to 10,000 meters and the uncertainty is put to 0.2 as can be seen in Equation 5.3 and Equation 5.4. The uncertainties proposed on the various models can be found in Table 4.10 and 4.9

$$\mu = 10000 \tag{5.3}$$

$$\sigma = 0.2 * 10000 \tag{5.4}$$

Table 5.2: Input for the Sensitivity Study

Parameter	**1**	**2**	**3**	**4**	**5**
Drag coefficient of all elements	x			x	
Initial mass	x			x	
Heat shield area	x			x	
Entry conditions		x		x	
Separation altitude			x	x	
Parachute deployment altitude			x	x	
Parachute area	x			x	
Drag plates deployment altitude			x	x	
Drag plate area	x			x	
Engine burn start altitude	x			x	
Engine burn time	x			x	
Engine throttle setting			x	x	
Individual mass cost models					x

6 Verification and Validation

This chapter gives an overview of the verification and validation work done on CRDT. Both are done in four phases. These steps are Launcher, Trajectory, Mass/Cost models and optimisation. The entire verification matrix can be found in Table 6.1. The launcher section contains all the modifications to increase the payload capacity such as stage elongation, added boosters, or both. Furthermore, it includes the separation system model. The trajectories section includes the comparison of the modified ParSim used in CRDT, and the original ParSim v3. Where this is not possible, such as for the de-orbit manoeuvre or the deceleration using the engine, the trajectory verification is done by comparison to analytic data. The verification of the mass and cost models is done per model. The verification is done by ensuring the model has been correctly implemented in CRDT. Where possible additional verification is done by comparison to historic data where possible. Finally the optimisation verification is done by running cases of which the optimum is known and comparing the results.

Table 6.1 shows the different verification steps performed. Each cell shows where the results are documented.

Table 6.1: Verification Matrix

Item	Dynamics	Mass	Cost
Parachute	subsection 6.3.4	subsection 6.4.4	subsection 6.4.4
Drag plates	subsection 6.3.3	subsection 6.4.5	subsection 6.4.5
Engine burn	subsection 6.3.5	subsection 6.4.3	subsection 6.4.3
Solid heat shield	subsection 6.3.1	subsection 6.4.1	subsection 6.4.1
Inflatable heat shield	subsection 6.3.2	subsection 6.4.1	subsection 6.4.1
Retrorocket landing	-	subsection 6.4.6	subsection 6.4.6
Airbag landing	-	subsection 6.4.6	subsection 6.4.6
Water landing	-	subsection 6.4.6	subsection 6.4.6
Mid air retrieval	-	subsection 6.4.6	subsection 6.4.6
Refurbishment	-		section 6.5
Launcher modification	subsection 6.1.1	subsection 6.1.1	subsection 6.1.1
Separation system	subsection 6.1.2	subsection 6.1.2	subsection 6.1.2

6.1. Launcher

Both types of modifications, the increase in payload performance and the addition of separation system, are verified in this section. The modifications to increase the payload performance are verified against existing data and by the correct implementation of the model.

6.1.1. Stage Modification

As stated in subsection 4.1.3, there are four types of modifications that are considered for the Atlas V Centaur launcher. The model described in section 4.1 has been implemented in CRDT and the results can be found in Figure 6.1 and Figure 6.2.

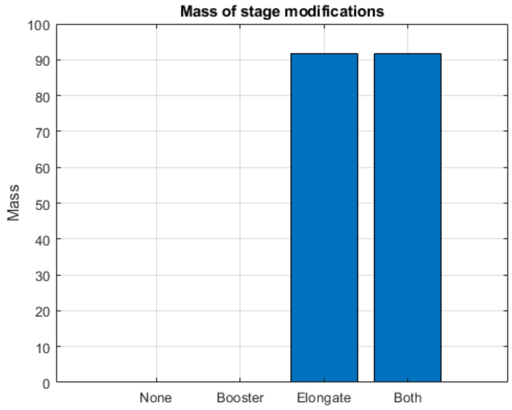

Figure 6.1: Mass in kg of stage modification

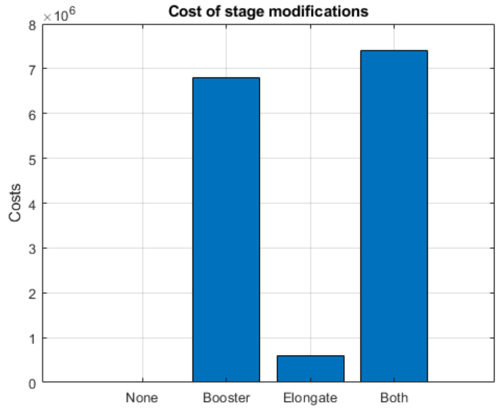

Figure 6.2: Cost in USD of stage modification

It can be seen that the extra AJ-60A strap-on booster does not add any mass to the upper stage. This is expected, as the mass is added to the first stage only. However, the total launch vehicle does become more expensive as the solid booster has to be included in the cost. The figure also shows that the stage elongation has a cost that is significantly lower compared to the addition of the solid booster. However, as it impacts the upper stage it also adds mass to the upper stage, which results in a payload reduction.

Figure 6.3 and Figure 6.4 show the mass and cost of the elongated stage for a range of added propellant mass. The x marks on the plots are the mass and cost values calculated using the relationship found in section 4.1. The line shown in the plot is calculated in ParSim based upon user inputs. One can see that the line overlies perfectly with the data points, thus it can be said that the model is correctly implemented. Note that the propellant mass shown in Figure 6.3 and Figure 6.4, is the mass of the added propellant.

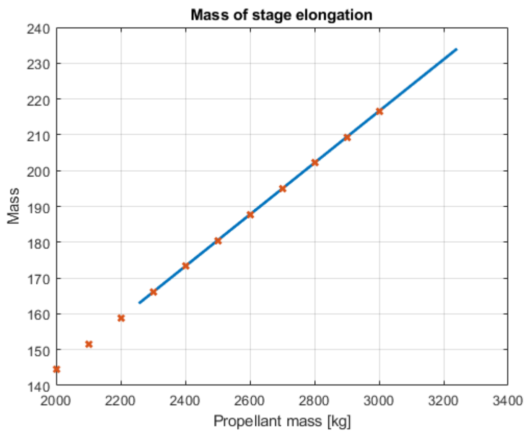

Figure 6.3: Additional Mass of stage elongation

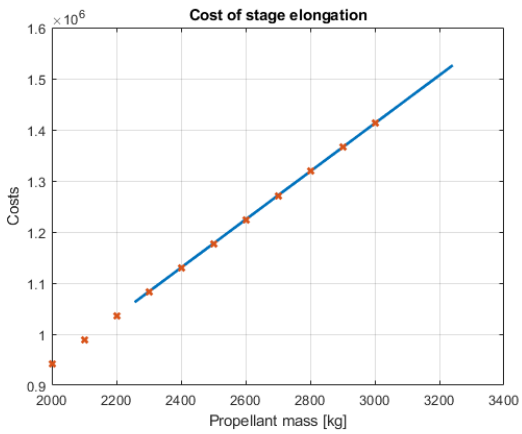

Figure 6.4: Additional Cost of stage elongation

Now the model is plotted against the validation data used to make the model. Furthermore, the two sigma lines are plotted. These results can be found in Figure 6.5 and Figure 6.6. As can be seen, the uncertainty increases when the stage is elongated or shrunk beyond the initial data points.

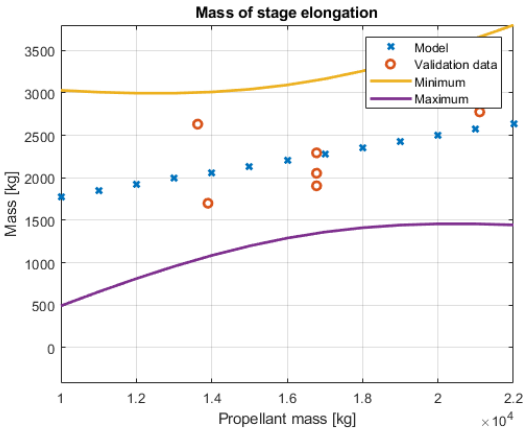

Figure 6.5: Mass of stage elongation

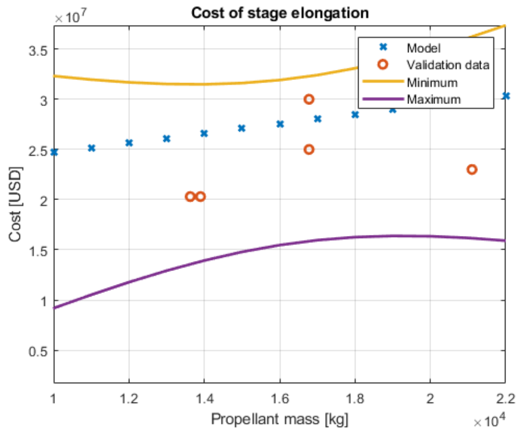

Figure 6.6: Cost of stage elongation

One should note that the spread of mass and cost estimates is significant even for the same propellant masses. This is due to parameters not being taken into account, such as mass and cost reductions of the avionics and feed systems over time. However, as CRDT is a conceptual design tool this uncertainty can be accepted.
Figure 6.7 shows the payload capacity of the various launchers and their modifications. As can be seen, the launcher with added booster has the same payload capacity as the launcher that is one variant higher. This shows the performance model of the booster modification is implemented correctly. Furthermore, it can be seen that the stage elongation does not effect the payload capacity of the stage. Again this is expected as the stage elongated is assumed only to compensate for the added propellants and not to add performance. The payload capability of the various Atlas V Centaur variants can be found in Table 7.1. Figure 6.7 shows that payload to LEO has been properly integrated and can thus be considered to be verified.

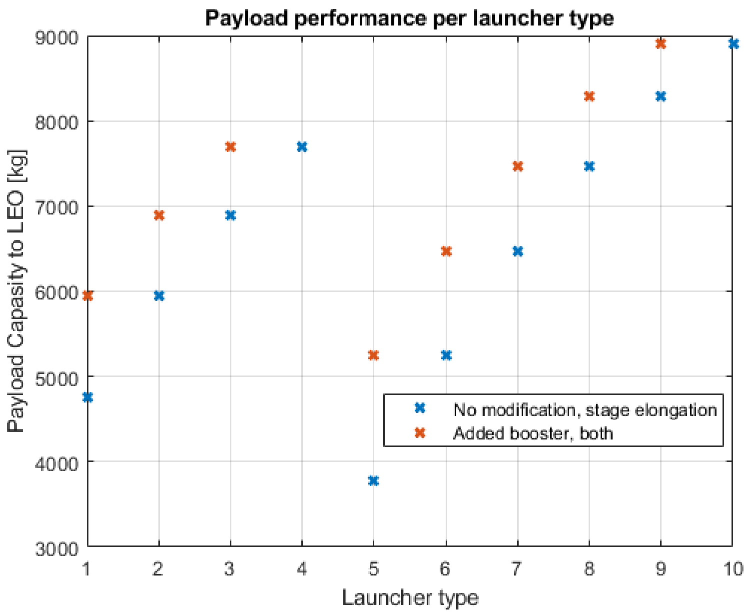

Figure 6.7: Payload capacity of the various launchers and modifications

The observations made in this section show that: the mass and cost of various modifcations behave as expected, the trends of the stage elongation with propellant mass is correct for the range required, and that the payload performance increase is correct. These three observations lead to the conclusion that launcher modification is implemented correctly and can be considered verified and validated.

6.1.2. Separation System

The second degree mass model for the separation system is compared to historic data. This can be seen in Figure 6.8. As can be seen the data overlies nicely with the model. The uncertainty of the mass model is 0.0718 using the convention shown in Equation 5.4.

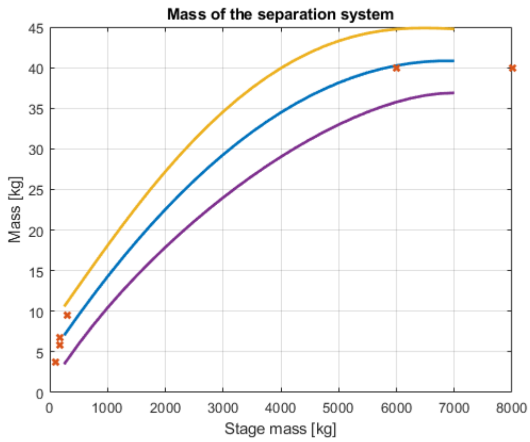

Figure 6.8: Used mass model for the separation system showing uncertainty

From Figure 6.8 it can be seen that there is little validation data to support the model, and that there are parameters not included in the model that play a role in the mass of a separation system. However, as a conceptual design model the mass model can be considered verified and validated.

6.2. De-orbit Maneuver

As mentioned in section 4.2 the de-orbit manoeuvre consists of three steps: two engine burns and one coasting phase. The delta-V required to change orbit can be determined using the equations mentioned in section 4.2. When using the script to calculate the delta-V required to change from a 300 km LEO orbit to a GTO orbit the code determines that this should be: 2.429 km/s. When performing the calculations by hand one can find a delta-V of 2.42 km/s. Thus it can be stated that the script produces an delta-V accurate up to 0.4%. For the propellants required to perform the engine burns, one is referred to subsection 6.4.3.

6.3. Trajectory

As the core of CDRT is based upon a modified version of ParSim v3, the initial verification is done on these modifications. For this a reference vehicle is taken, the characteristics of this vehicle can be found in Table 6.2. Each verification run was done by putting the decelerator hardware as Decel 1, Decel 2, and Decel 3 to ensure correct implementation of the entire vehicle ID.

Table 6.2: ParSim Verification Vehicle

Parameter		**Value**
Mass	kg	150
Drag coefficient	-	0.3
Frontal Area	m^2	8
Diameter	m	3.1914
Initial altitude	km	80
Flight path angle	deg	-2
Initial velocity	m/s	6000
Body length	m	2

6.3.1. Ballistic Entry

Even though the code for pure ballistic flight through the atmosphere has not been modified significantly in CDRT, it is important to verify the tool to ensure no errors have been introduced. This ensures the results produced by CDRT are reliable. The input for ParSim v3 can be seen in figure 6.9 and the input for CDRT can be seen in figure 6.10.

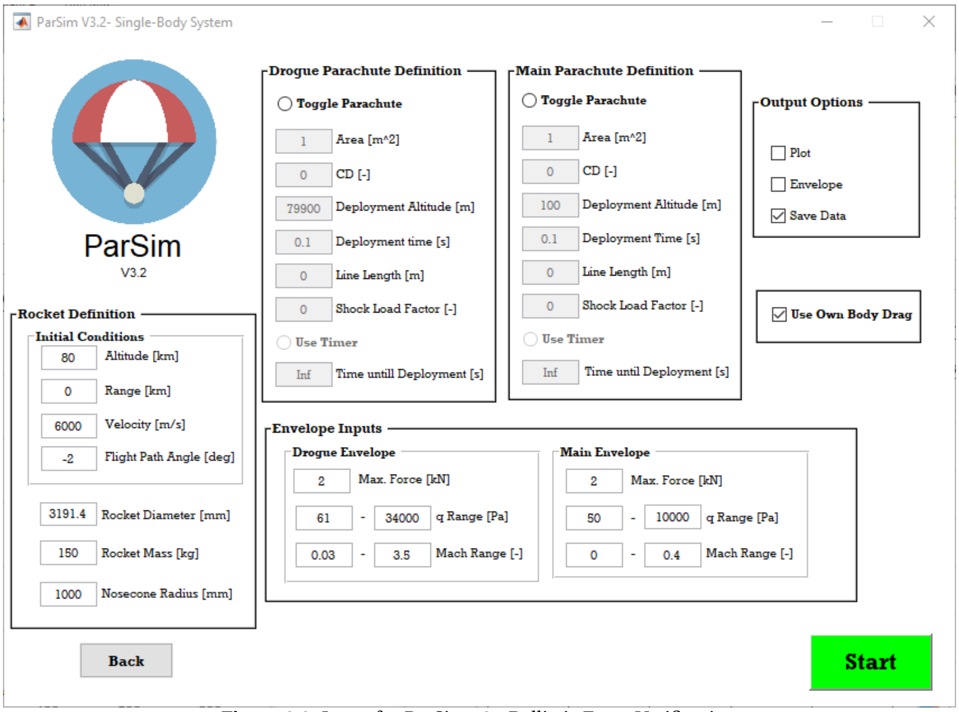

Figure 6.9: Input for ParSim v3 - Ballistic Entry Verification

1	0	0	0	0	1
6000	0	0	0	0	1
-2	0	0	0	0	1
80000	0	0	0	0	10

Figure 6.10: Input for CDRT - Ballistic Entry Verification

In Figure 6.11 and Figure 6.12 the comparison between CRDT and the original ParSim v3 can be seen. Figure 6.11 shows the altitude time plots, in which the difference due to the modifications is less then 3%. The results of Figure 6.12 show that the equilibrium velocity of the stage is the same in ParSim and CRDT. The difference originates during the high speed flight. This is most likely due to the modifications to accelerate the ParSim calculations.

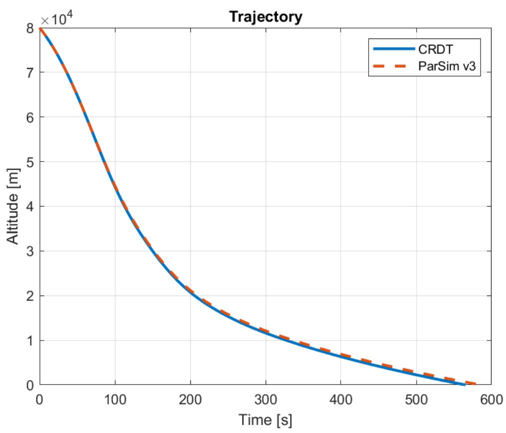

Figure 6.11: Altitude-time Comparison of Ballistic Entry in CRDT and ParSim

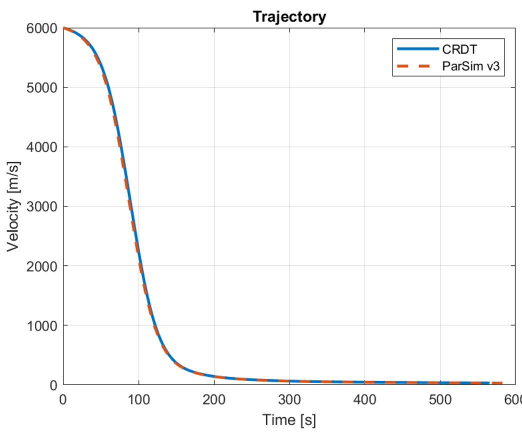

Figure 6.12: Velocity-Time Comparison of Ballistic Entry in CRDT and ParSim

When comparing the results one can state that the modifications do not impact the simulations results of Parsim in a significant way. Therefore, it can be said that the ballistic entry simulation is verified.

6.3.2. Inflatable Heat Shield

To verify the inflatable heat shield, the vehicle ID has been set as found in Figure 6.14. As ParSim v3 does not have the ability to model inflatable heat shields, the forward area of the test vehicle is changed to 16 m^2. The other parameters in Table 6.2 will remain the same. The inputs can be found in Figure 6.13.

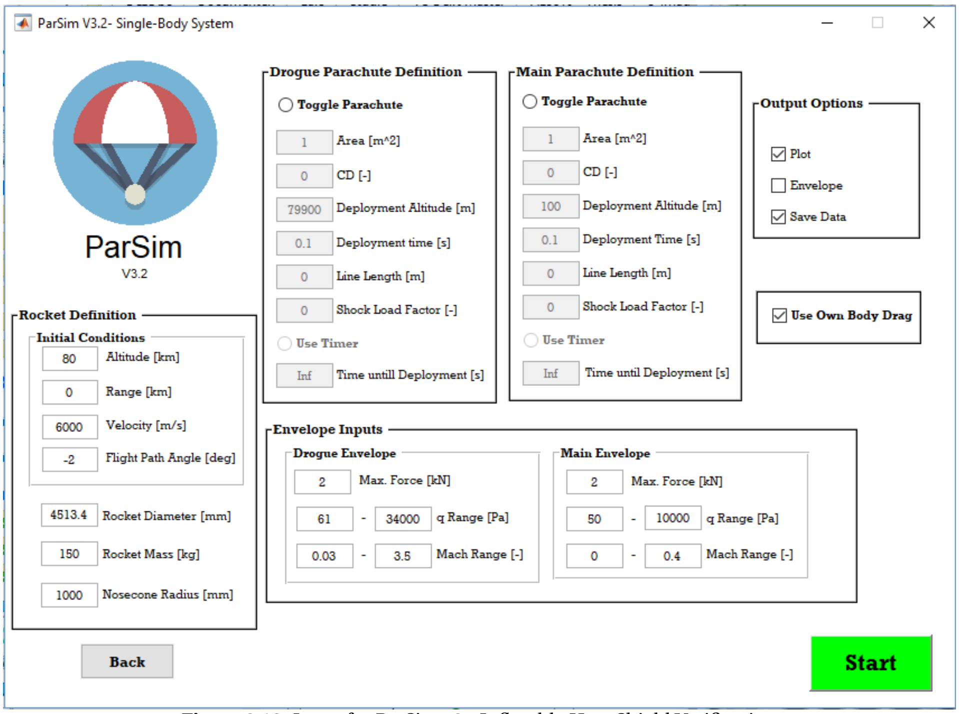

Figure 6.13: Input for ParSim v3 - Inflatable Heat Shield Verification

1	0	0	0	0	1
6000	0	0	0	2	1
-2	0	0	0	16	1
80000	0	0	0	0	10

Figure 6.14: Input for CDRT - Inflatable Heat Shield Verification

First a comparison is done between the bare stage and the stage with the inflatable heat shield. This is done to demonstrate the effect of the modification. As can be seen in Figure 6.15 the stage with the inflatable heat shield (dotted line) decelerates faster than the stage without (solid line). This is to be expected as the ballistic coefficient of the stage with the larger area is smaller.

In Figure 6.16 both ParSim and CDRT simulate the same configuration with the inflatable heat shield. As can be seen, there is a small difference between both tools.

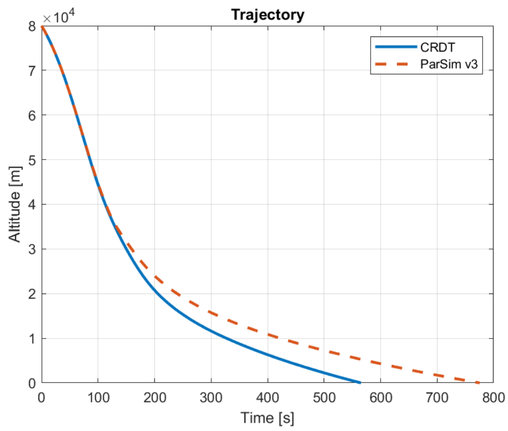

Figure 6.15: Effect of the Inflatable Heat Shield in Altitude-Time Plot

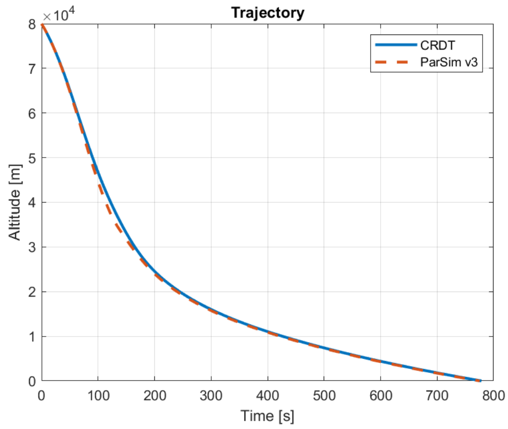

Figure 6.16: Verification of Inflatable Heat Shield Dynamics Model

There is almost no difference between the programs, and the ballistic coefficient decreases when the inflatable heat shield is added. Therefore, the implementation of the dynamics model of the inflatable heat shield is considered verified.

6.3.3. Drag Plates

The drag plates that have been added to the stage are 4 m^2 and are deployed at 37200 m. The vehicle ID can be found in Figure 6.17.

1	2	0	0	0	1
6000	37200	0	0	0	1
-2	4	0	0	0	1
80000	1	0	0	0	10

Figure 6.17: Input for CDRT - Drag Plate Verification

As with the inflatable heat shield, ParSim v3 cannot model drag plates. Therefore the inputs need to be tricked. This is done by changing the body drag coefficient at 37200 m altitude. The calculations showing the required body drag coefficient can be found in Equation 6.1 and Table 6.3. It is determined that the new drag coefficient is 0.6.

$$C_d A_{total} = C_d A_{body} + C_d A_{plate} \tag{6.1a}$$

$$C_d A_{plate} = C_d A_{total} - C_d A_{body} \tag{6.1b}$$

$$C_d A_{plate} = 0.6 * 8 - 0.3 * 8 = 2.4\ [m^2] \tag{6.1c}$$

$$A_{plate} = 2.4/0.6 = 4\ [m^2] \tag{6.1d}$$

Table 6.3: ParSim Drag Coefficient Input

Mach range	C_D
3 - inf	0.3
0 - 3	0.6

Again the initial comparison is between the bare stage and the stage with drag plates. This can be seen in Figure 6.18. As can be seen, the stage with drag plates takes longer to get to the ground. This is in line with what is expected.

By simulating drag plates in ParSim V3 using the method earlier described, one can compare the simulation results of CDRT with ParSim V3. These results can be seen in Figure 6.19. As can be seen, the drag plates decrease the ballistic coefficient; thus the stage decelerates faster than the original stage. Note that with an entry vehicle of only 150 kg, the mass of the drag plates has a significant impact on the ballistic coefficient. For trajectory comparison, the mass of the plates has been set to zero.

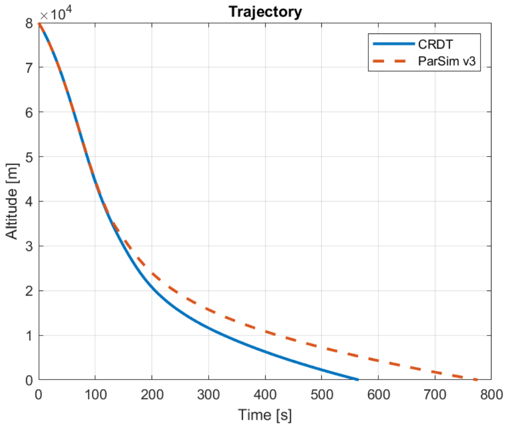

Figure 6.18: Effect of Drag Plates in Altitude-Time Plot

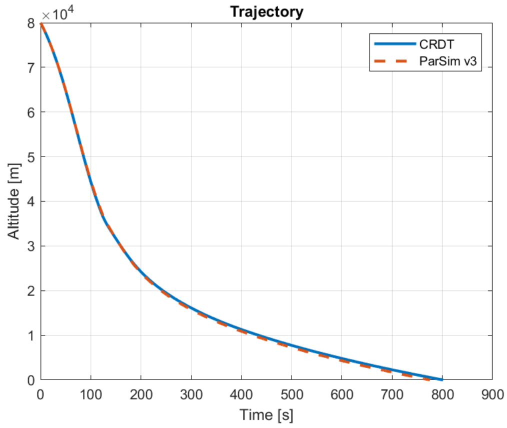

Figure 6.19: Verification of Drag Plate Dynamics Model

As can be seen, the lines of CRDT and ParSim v3 overlap nicely. This leads to the conclusion that the model of the drag plates has been implemented correctly.

6.3.4. Parachutes

The verification of parachutes is done in a similar manner as drag plates and the inflatable heat shield. However, it is easier as ParSim V3 was written for parachute simulations. For the parachute verification a single parachute of 40 m^2 has been chosen which deploys at an altitude of 8 km.

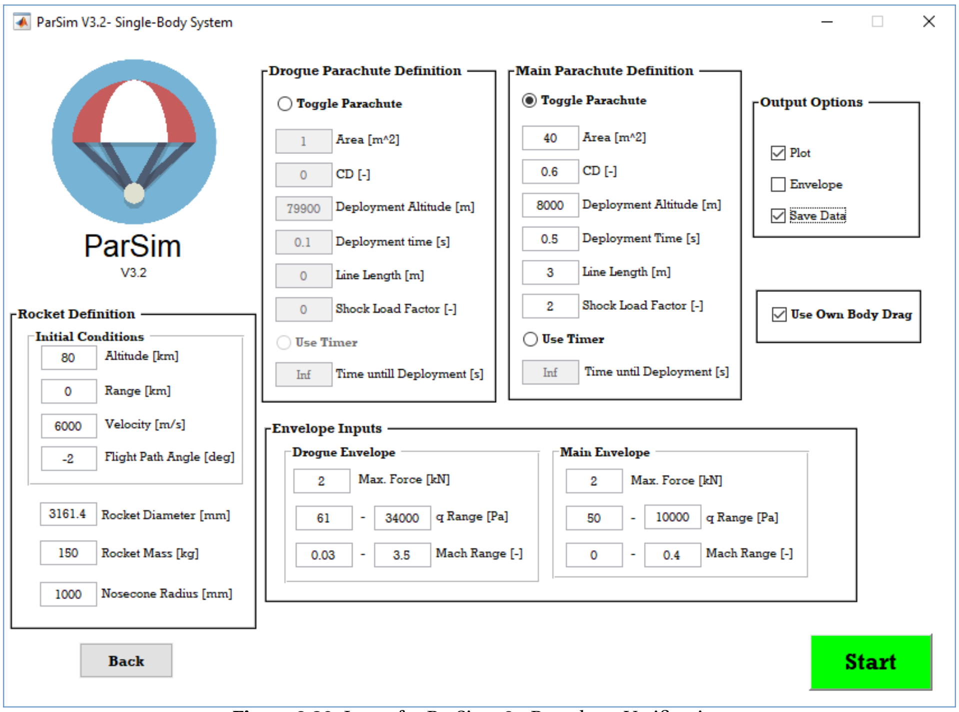

Figure 6.20: Input for ParSim v3 - Parachute Verification

1	1	0	0	0	1
6000	8000	0	0	0	1
-2	40	0	0	0	1
80000	1	0	0	0	10

Figure 6.21: Input for CRDT - Parachute Verification

Again first a comparison is done between the bare stage and the stage with parachutes. As seen in Figure 6.22 the parachutes (dotted line) cause a longer descent time, indicating a slower descent velocity. This is in line

with the expectation of a parachute system.
Figure 6.23 shows the comparison between ParSim v3 and CRDT. As can be seen the difference is quite small. The terminal velocity is identical, and the flight time has a difference of less than 3 percent.

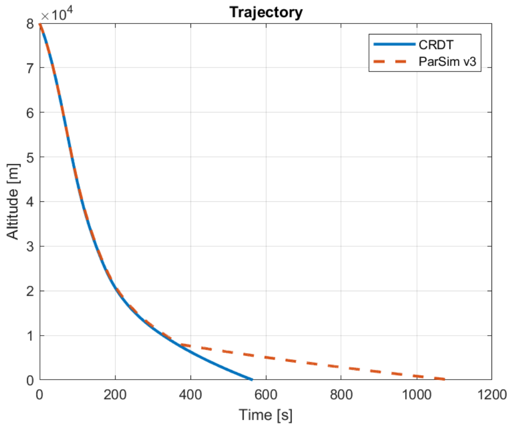

Figure 6.22: Effect of Parachutes in Altitude-Time Plot

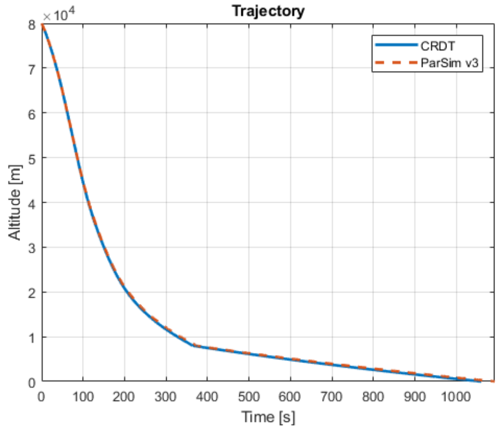

Figure 6.23: Verification of Parachute Dynamics Model

Given the expected behaviour of the parachute and the close comparison to ParSim it can be said that the CRDT parachute module is verified.

6.3.5. Engine Burn

The engine burn trajectory verification can be seen in Figure 6.24 and Figure 6.25. in these plots a one-second engine burn is performed at 85 km. As can be seen, the engine burn has little effect on the altitude-time plot, this is expected as the engine burn is performed parallel in the velocity vector. In the Velocity-Time plot, one can however see a clear decrease in velocity. As the burn is performed at 95km, the terminal velocity of both stages is the same, this is confirmed in Figure 6.25.

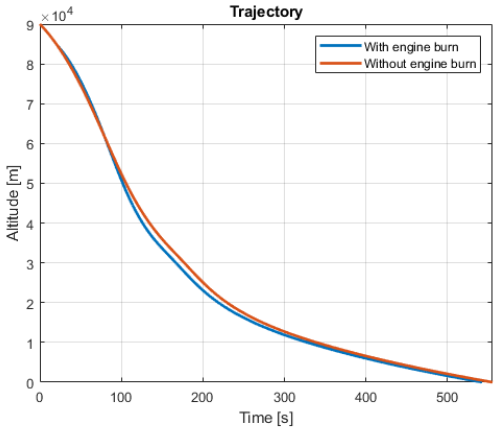

Figure 6.24: Effect of Engine Burn in Altitude-Time Plot

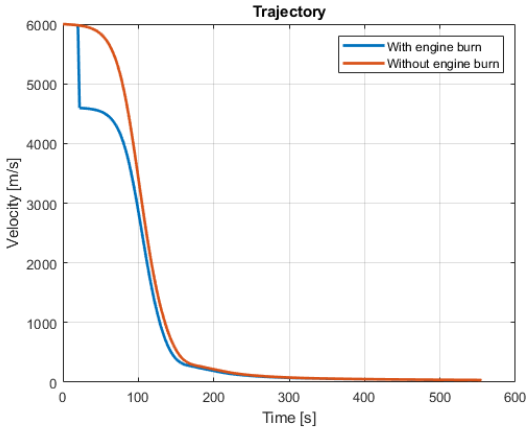

Figure 6.25: Effect of Engine Burn in Velocity-Time Plot

Given that the engine burn follows the expected behaviour, the engine module can be considered verified.

6.4. Mass and Cost Models

The verification and validation of the mass and cost models is done by comparing the model as implemented in CRDT to historic data. Where possible the data which was used for comparison is not the same data used to build the model. Where no data is available at all, the verification is done by comparing the model to analytically calculated results.

6.4.1. Heat Shield

To verify the mass and cost of the inflatable heat shield, a comparison to historic data is made. This data can be found in Table 6.4 and Figure 6.28 shows the comparison. Furthermore, Figure 6.26 and Figure 6.27 shows the comparison between the solid and inflatable heat shields.

Table 6.4 shows the size of the inflatable heat shield together with the mass of the bag and the inflation system. The percentage indicated in the table indicates the mass fraction of the bag to the total thermal protection system.

Table 6.4: Mass Comparison of Several Inflatable Heat Shields

Mission	Diameter [m]	Mass Bag [kg]	Mass Inflation System [kg]	Percentage	Source
IRVE	14	40	21 + 10 (cables)	56.6 %	[38]
LOFTID	6	62	140	30.7 %	[14]
HEART	8.3	169	72 + 241 (TPS)	35.1 %	[68]

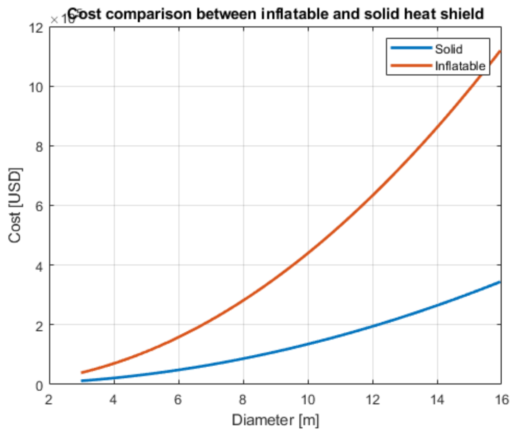

Figure 6.26: Cost comparison of solid and inflatable heat shield

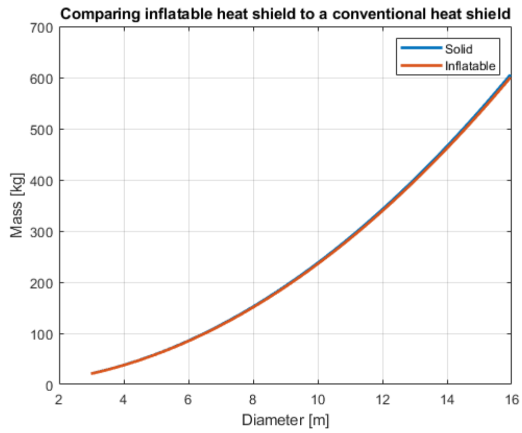

Figure 6.27: Mass comparison of solid and inflatable heat shield

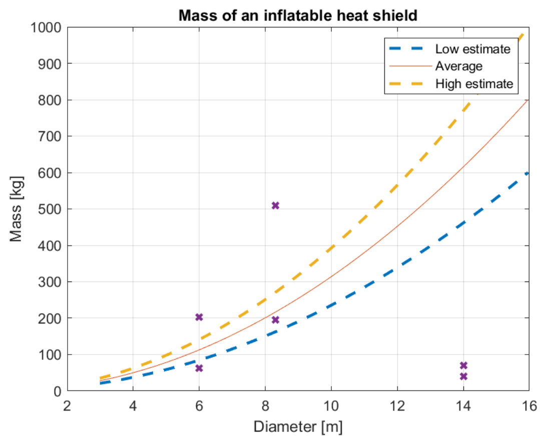

Figure 6.28: Mass range of inflatable heat shields

From Figure 6.28, it can be seen that the mass range of the inflatable heat shield is quite broad. When overlaying with the three reference missions in Table 6.4 one can see that this range is realistic . The only exception is the ESA IRDT mission using an inflatable heat shield. It is unknown why this system mass is as low as it is. However, one option could be that as it was an LEO mission the dynamic pressure and thus the structure mass was lower. Work done by DEIMOS space indicates that the ESA TRL in terms of inflatable systems has dipped over the recent years; this could indicate why the IRDT mission is an outlier in terms of mass [3].

Furthermore, it can be observed in Figure 6.27 that the solid heat shield is comparable to the mass estimate of the inflatable heat shield. When looking at the plot, it is clear that the solid heat shield is about 3 kg/m^2. This is comparable to the 3,03 kg/m^2 given in [49]. Thus the mass estimations of both the inflatable and solid heat shield can be considered verified and that the mass model for the inflatable heat shield is validated.

The cost comparison can be found in Figure 6.26, which shows that the inflatable heat shield is more expensive than the solid heat shield. This is expected as, amongst others, the TRL of the inflatable heat shield is lower. According to Rasky et all [49] one can see that the cost per flight equals 333 USD/ft^2 per flight. The results of this can be seen in Figure 6.29. From this figure, it can be said that the cost model of the inflatable and solid heat shield are verified.

6.4.2. Transcost Implementation

To verify the effect of the Transcost factors the f1 factor is set to "status 2" or High TRL and f2 factor set to "status 3" or High Team Experience. The effect of Transcost can be seen in Figure 6.30. As the TRL and team experience is high, the cost drops.

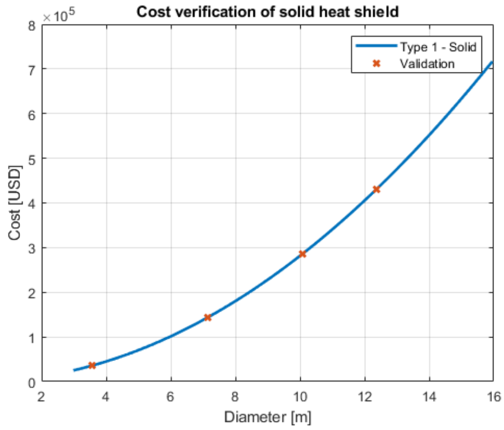

Figure 6.29: Cost verification of the solid heat shield

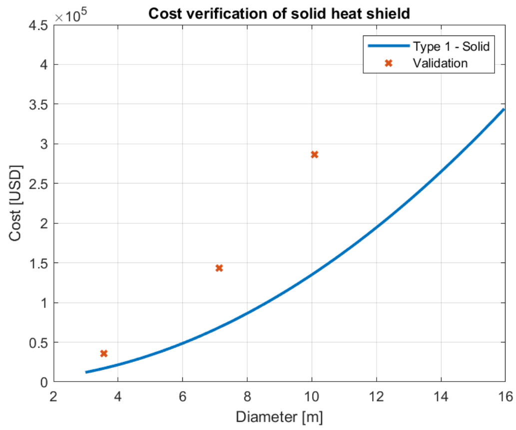

Figure 6.30: Demonstration of the effect of development cost

From Table 3.1 it can be seen that using the high TRL ($f_1 = 0.8$) and high team experience ($f_3 = 0.6$), one gets a $f_{development}$ of 0.48. When comparing the costs of Figure 6.30 one can find in Table 6.5 that the cost fraction is about 0.48. Therefore, it can be said that the cost model is verified.

Table 6.5: Comparison of TPS costs with and without Transcost

Value without Transcost	Value with Transcost	Fraction
1.49E5	0.75E5	0.49
2.80E5	1.40E5	0.50
0.40E5	0.20E5	0.50

6.4.3. Engine Burn

The verification of the two engine burn scripts is done separately and against each other. Figure 6.31 and Figure 6.32 show the mass comparison between analytical calculations and the results of engine burn scripts 1 and 2. Equation 6.2 and Equation 6.3 show the analytical equations used for the verification.

$$m_{burn1} = \dot{m} * t_{burn} \tag{6.2}$$

$$m_{burn2} = -m_1 * \left(1 - exp\left(\frac{\Delta V}{U_{vac}}\right)\right) \tag{6.3}$$

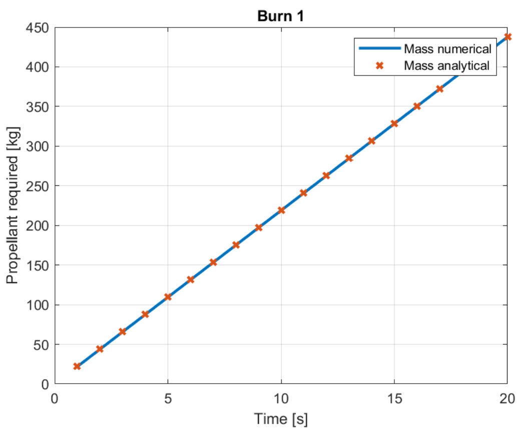

Figure 6.31: Validation of the Engine burn 1

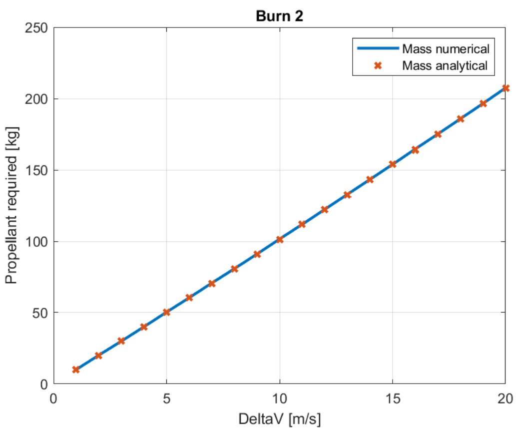

Figure 6.32: Validation of the Engine burn 2

To verify the cost calculations, the mass and cost of both methods are plotted against each other. The mass is shown on the horizontal axis and the cost on the vertical axis. This can be seen in Figure 6.33.

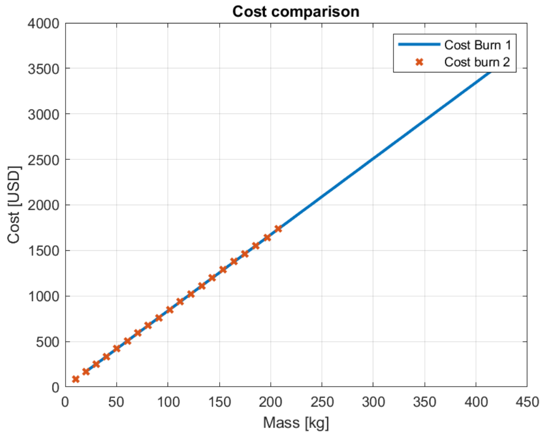

Figure 6.33: Validation of the engine burn cost function

As can be seen both models produce the same cost for the given masses. This leads to the conclusion that the cost models have been implemented properly.

6.4.4. Parachutes

The parachute mass modules are based upon historic data, where the cost models are built bottom up. Figure 6.34 shows the performance of the model compared to verification data.

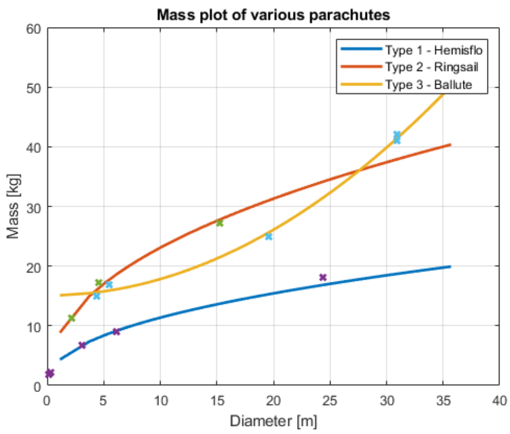

Figure 6.34: Verification of the parachute mass

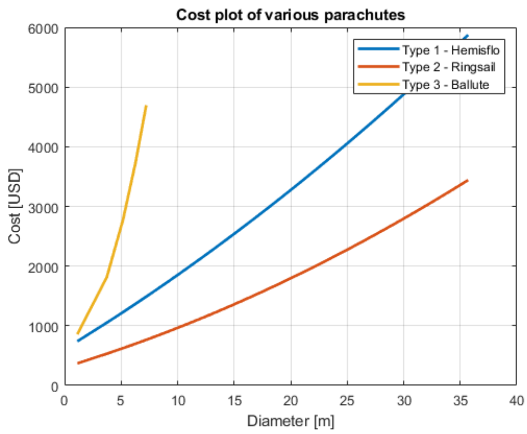

Figure 6.35: Verification of the parachute costs

As can be seen in Figure 6.34, the fit is quite good and the maximum error found is 8%. This leads to the conclusion that the mass models for the parachutes have been correctly implemented into CRDT, thus the model implementation verified.

As there is no cost data available, verification is done by comparing the cost models for the various parachutes to each other. As the Hemisflo parachute is made out of the more expensive Aramid materials it is expected that the parachute is more expensive than the Ringsail parachute. This is confirmed in Figure 6.35. When the Ringsail and Hemisflo parachutes are both assumed to be made out of nylon and the porosity of the Hemisflo is set to 0%, the costs of the two parachutes are equal. This can be seen in Figure 6.36. When the Hemisflo is made out of aramids and the Ringsail is made out of nylon, one can see in Figure 6.37 that there is again a difference in costs.

When looking at the Hemisflo and ballute parachutes one notices that the ballute is much more expensive than the other parachutes. This is mainly due to the high production area compared to the projected area.

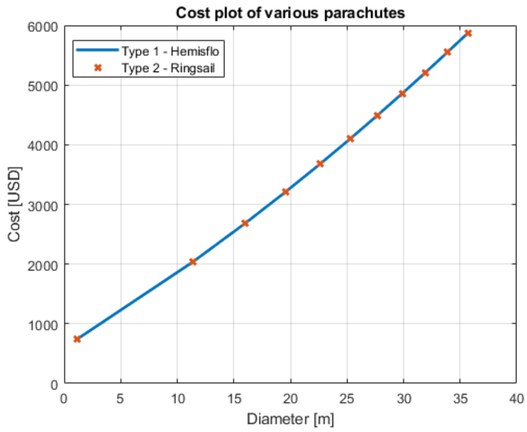

Figure 6.36: Parachute cost verification, nylon

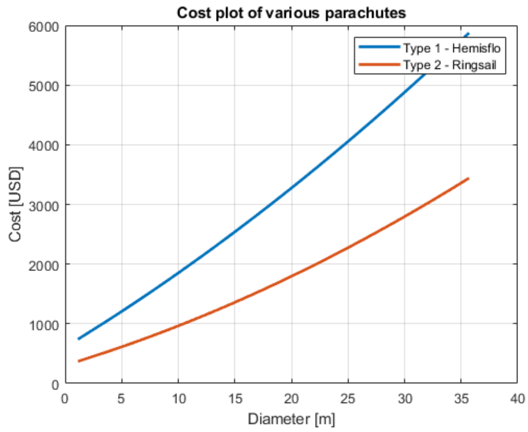

Figure 6.37: Parachute cost verification, nylon-aramid

Based upon the results the mass and cost models for the parachutes can be considered verified. The mass model matches the data. Furthermore, the costs behave as expected. The aramid costs are higher than the nylon parachute, and the ballute is more expensive than both.

6.4.5. Drag Plate

As mentioned in subsection 4.6.2 the drag plates follow a linear line as it is only a function of the plate area. As can be seen in Figure 6.38 this is true in the verification of the model. The same goes for the cost which can be seen in Figure 6.39.

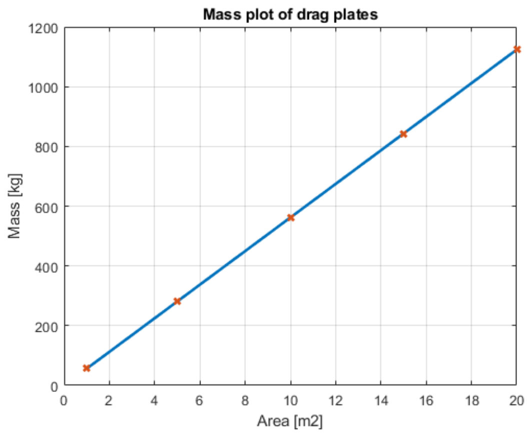

Figure 6.38: Verification of the drag plate mass

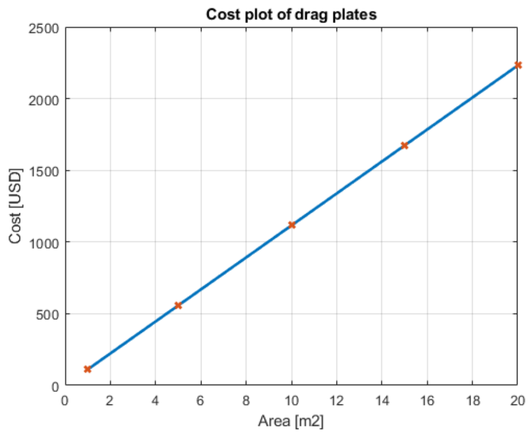

Figure 6.39: Verification of the drag plate costs

Given the perfect overlap of the analytical data with the data obtained from CRDT one can consider the drag plate module verified.

6.4.6. Landing

The verification of the mass of the retrorocket and airbag systems can be found in Figure 6.40. It can be seen that the masses of the retrorocket and airbag landing systems perfectly overlay the verification data. Furthermore it can be seen that the mass of the water landing is a horizontal line, as it is only a function of the stage mass and not the landing velocity. For the mid-air retrieval, there is no mass appointed as the parachute is caught by the helicopter and no additional mass is required.

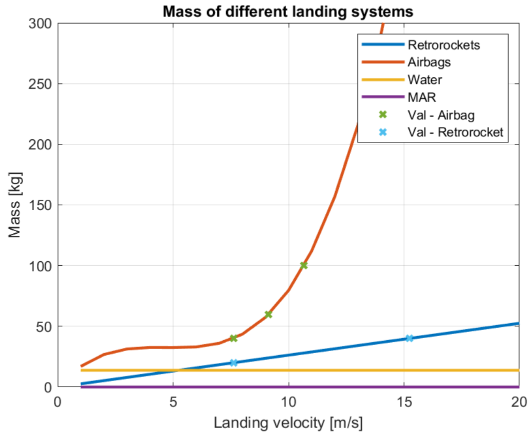

Figure 6.40: Mass comparison of all landing systems (stage mass = 2000 kg)

To demonstrate the effect of stage mass and landing velocity, 3D surface plots have been made for the retrorocket, airbags and water landing options. These can be seen in Figure 6.41, Figure 6.42, and Figure 6.43. Again the third order behaviour of the airbag system can be clearly seen in Figure 6.42. Furthermore it can be seen that the airbag system is heavier than the retrorocket system. This is in agreement with the model described in subsection 4.7.2. Finally, the linear behaviour of the water landing as a function of stage mass can be seen in Figure 6.43.

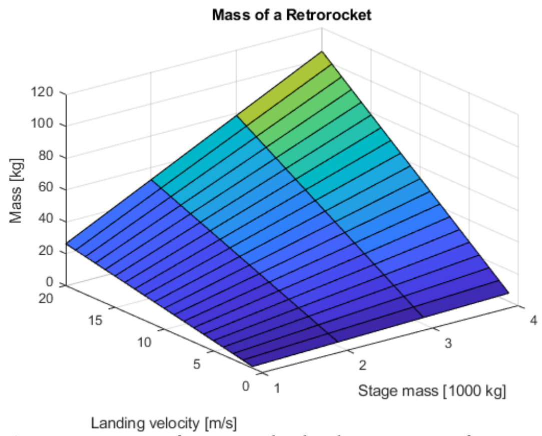

Figure 6.41: Mass of a retrorocket landing system as function of landing velocity and stage mass

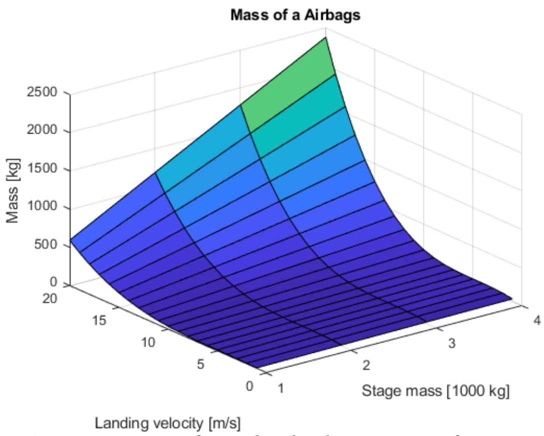

Figure 6.42: Mass of an airbag landing system as function of landing velocity and stage mass

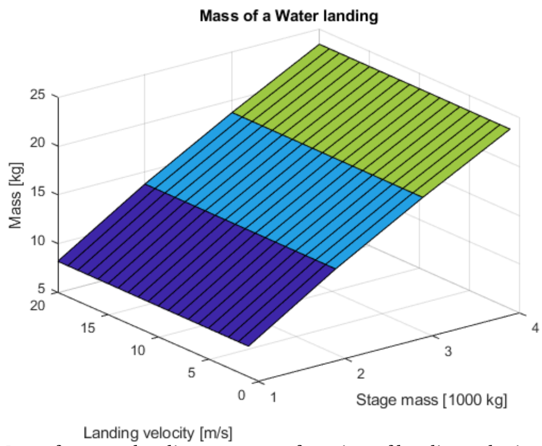

Figure 6.43: Mass of a water landing system as function of landing velocity and stage mass

The comparison of the cost of all landing options can be found in Figure 6.44. As all models depend on the mass of the landing hardware one can see a similarity between Figure 6.40 and Figure 6.44. As expected the airbag system is cheapest for low landing velocities, where the retrorockets become cheaper for landings at higher velocities. The flotation device can be seen to be cheaper than the retrorocket landing for velocities above 8 m/s. Again flotation system mass is not dependant on the landing velocity and only on the stage mass.

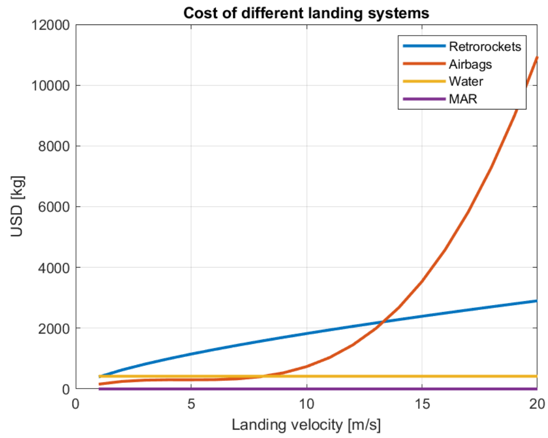

Figure 6.44: Cost comparison of all landing systems (stage mass = 2000 kg)

Given the good overlap of the anaytical data in Figure 6.40 and the behaviour of the cost seen in Figure 6.44 one can conclude that the landing models are verified.

6.5. Retrieval and Refurbishment

As mentioned in section 4.8 and section 4.9, the retrieval and refurbishment steps do not have an added mass, only cost and manhour costs. Figure 6.45 and Figure 6.46 show these costs. The following numbering is used.

1. Retrorocket landing, no separation
2. Airbag landing, no separation
3. Water landing, no separation
4. Mid-Air Retrieval, no separation
5. Retrorocket landing, with separation
6. Airbag landing, with separation
7. Water landing, with separation
8. Mid-Air Retrieval, with separation

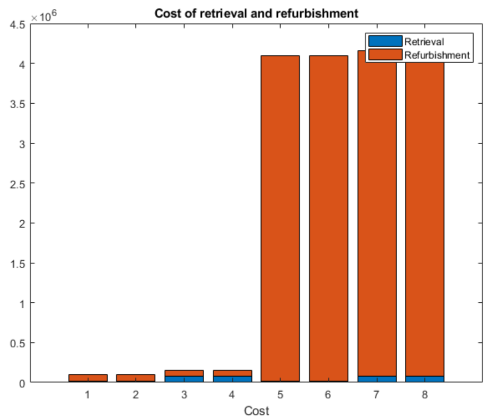

Figure 6.45: Cost of Retrieval and Refurbishment operations

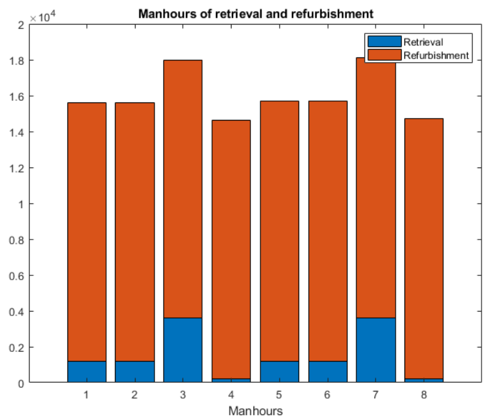

Figure 6.46: Manhour cost of Retrieval and Refurbishment operations

As can be seen in Figure 6.45 the options without separation are much cheaper. This is due to the necessity to rebuild part of the stage after separation. Furthermore, one can see the higher retrieval costs for the water landing and MAR. This is due to the higher costs of the boat or helicopter compared to a truck.

In Figure 6.46 one can see that there is not much difference in required manhours for the separated and non-separated systems. This is due to the fact that the inspection phase in refurbishment has a much higher contribution to the manhours. This can be seen in Table 6.6. Furthermore, one can see the higher manhour cost of a water landing compared to the land landing and MAR. Finally it can be seen that the MAR has the lowest cost in terms of manhours compared to both the land and water landing.

Table 6.6: Cost and Manhours of Retrieval and Refurbishment

Configuration	Cost [2018 USD]		Manhour cost	
	Retrieval	**Refurbishment**	**Retrieval**	**Refurbishment**
1	18000	78900	1200	14400
2	18000	78900	1200	14400
3	76000	78900	3600	14400
4	77500	78900	216	14400
5	18000	4078900	1200	14520
6	18000	4078900	1200	14520
7	76000	4078900	3600	14520
8	77500	4078900	216	14520

6.6. Optimisation

To ensure the optimisation algorithm functions correctly, one can perform an analytical analysis to determine the area in which the optimum can be found. The focus of this section is primarily on the hardware selection, thus on the integer side of the optimisation algorithm. The analytical solutions are compared to the runs performed in chapter 7. The focus of this section is on thermal protection, decelerator hardware, and landing hardware.

6.6.1. Thermal Protection

From the models, it can be seen that solid or inflatable thermal protection has about the same mass, but the inflatables have a higher cost. The inflatables, however, have the advantage of taking the function of both thermal protection and decelerator hardware. Therefore, research indicates a preference for inflatable heat shields [39]. When running cases in CRDT, more specifically the cases of section 7.3, it can be seen that CRDT disregards the solid options and only shows the inflatable configurations.

6.6.2. Decelerator Hardware

To verify the optimisation algorithm one needs to have an understanding of the mass and cost of the various decelerator hardware elements included in CRDT. Figure 6.47 shows the required landing velocity on the x-axis and the decelerator mass on the y-axis. Here one can see that for any landing velocity required, the drag plates are much heavier than a parachute system with the same requirements. Even when taking the mass of the retrorocket landing system into account, seen in Figure 6.48, one can see that the drag plates are always heavier than the parachute system. One can however see in Figure 6.49, that the cost of a drag plate decreases to below the cost of a parachute system at about 60 m/s. This has to do with the way the model is used for both costs. The cost of a drag plate reaches zero when the area of the drag plate reaches zero. For the parachutes however, the cost includes the suspension lines and riser, which are not area dependent.

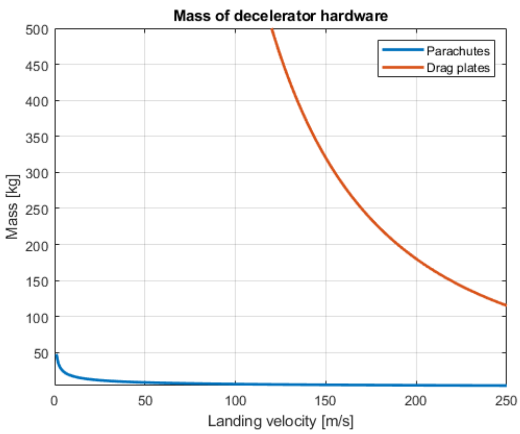

Figure 6.47: Comparison of decelerator hardware mass

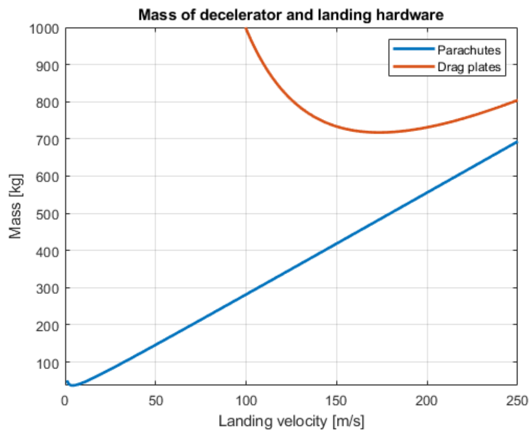

Figure 6.48: Comparison of decelerator hardware plus landing hardware mass

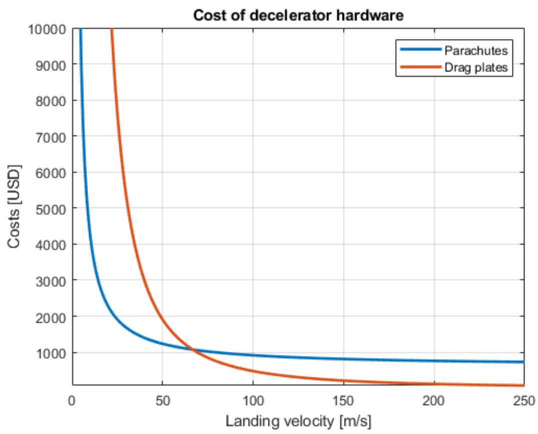

Figure 6.49: Comparison of decelerator hardware cost

A run allowing for both drag plates and parachutes has been done in section 7.3. There CRDT finds an option using the parachute system and does not consider drag plates to be a feasible option. This can be seen in Figure 6.50 where an LEO case is run with all decelerator options. In this bar plot every colour indicates a new generation and the height of a single bar indicates the amount of times a certain landing option was considered in the generation.

In the first generation, one can see a reasonably equal distribution between no decelerator (bar 1), parachutes (bar 2), and drag plates (bar 3). The propulsive deceleration has a low contribution. This is due to stage separation. After separation of the tank and engine, a propulsive deceleration is no longer possible. Over the various generations, indicated by different colours, one can see that drag plates slowly get less contribution to the generation. Parachutes however, gain a larger contribution to the generations.

These results lead to the conclusion that the optimisation case focusing on the decelerator can be considered to be verified as it converges to the lighter and cheaper parachutes.

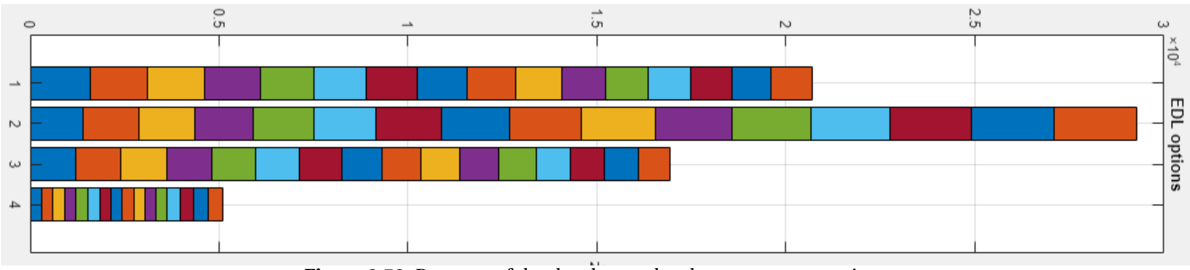

Figure 6.50: Progress of the decelerator hardware over generations

6.6.3. Landing Hardware

From the models found in Knacke, that every landing hardware has a mass optimum, there is the lowest mass. Figure 6.51 and Figure 6.52 show these results reproduced by CRDT. To complement the results Figure 6.53 and Figure 6.54 show the same results for the water landing and mid-air retrieval. Finally, Figure 6.49 show a comparison of the cost of all landing options.

As expected, both land landings have an optimum. For the retrorocket landing, this is a bit more clear. The airbag landing has an interesting part where the mass decreases again after a landing of less than 3 m/s discussed earlier in this chapter. From the figures it can be seen that any run should always find a retrorocket landing over an airbag landing. Second to the mass, the costs in Figure 6.49 also shows a preference to retrorocket landings. The case is ran as the LEO case in chapter 7 and the verification is shown in section 7.3.

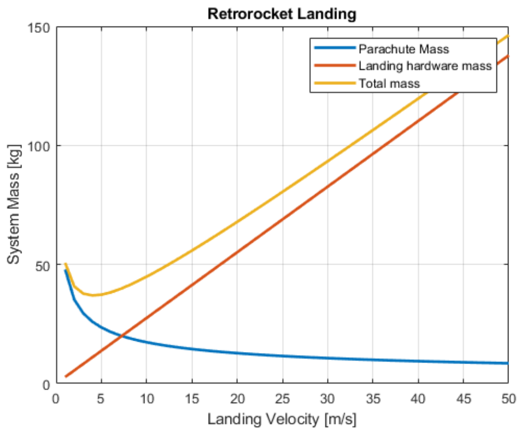

Figure 6.51: Comparison of retrorocket landing mass

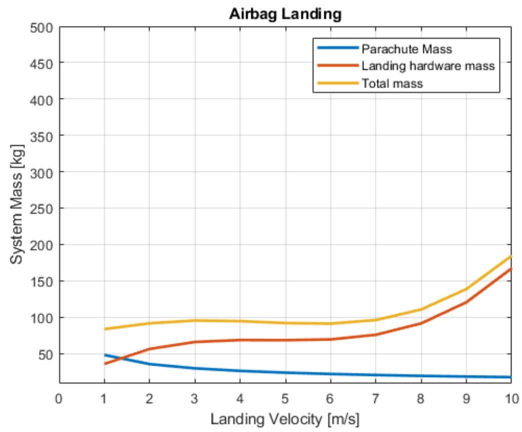

Figure 6.52: Comparison of airbag landing mass

The water landing and mid-air recovery follow the same trends observed earlier in this chapter. Interesting, however, is that the mid-air recovery is always lower in terms of mass. This means that, for any run using all landing options, the MAR should be found. This has been confirmed when running CRDT.

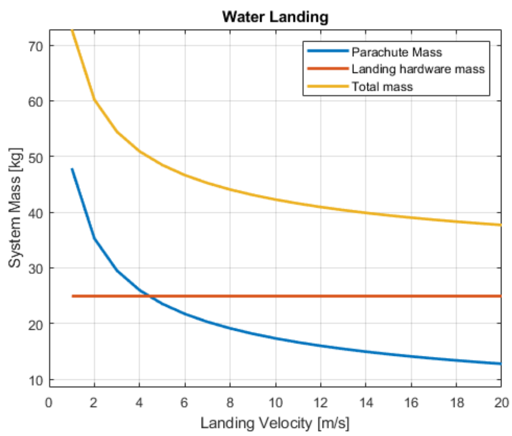

Figure 6.53: Comparison of water landing mass

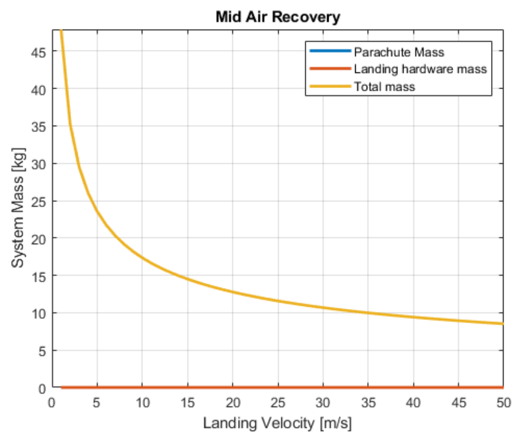

Figure 6.54: Comparison of MAR mass

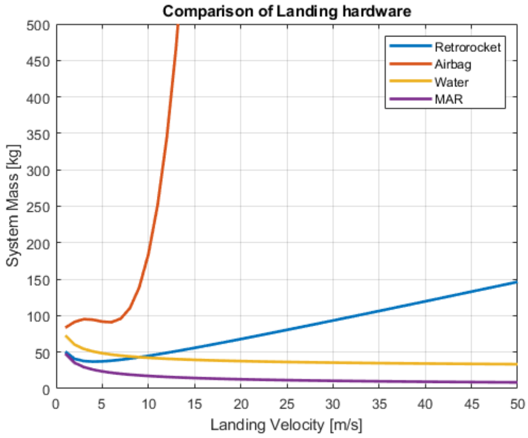

Figure 6.55: Comparison of decelerator hardware mass

The cost models found in Figure 6.44 confirm the results found in Table 7.7, section 7.3, the preferred solution in terms of cost is the retrorocket solution. When forcing a run to find an airbag landing configuration, one can see a higher Reuse Index but lower payload reduction factor indicating a higher cost.
Overall it can be said that for a land landing CRDT should and does find a retrorocket landing, as decelerator mass is lower, as allowable terminal velocity is higher, lower overall system mass for a given landing velocity, and the lower the cost for a given landing velocity.
When doing a run with all four landing options, one can see that CRDT does find the mid-air Recovery option. This is expected as it can be seen in Figure 6.54 and Figure 6.44 that MAR has a low mass and a low cost. The progress of a LEO case with all landing options can be found in Figure 6.56. In this bar plot every colour indicates a new generation and the height of a single bar indicates the amount of times a certain landing option was considered in the generation.
It can be seen that the tool always considered a landing option; this can be seen by the non-existence of bar 1. Furthermore, it can be seen that the mid-air Retrieval (bar 5) has fewer configurations in the first generation. This is due to the stricter requirements on MAR as it requires a parachute for the last decelerator option. Over the generations, it can be seen that the water landing (bar 4) and MAR have about the same contribution to the first as to the last generation. The dry landings using retrorockets (bar 2) populates the last generation more than the first in comparison to airbags (bar 3). This is expected due to the higher cost and mass of a dry landing compared to a water landing or mid-air recovery. When only comparing dry landings, one can see a preference for a retrorocket landing.

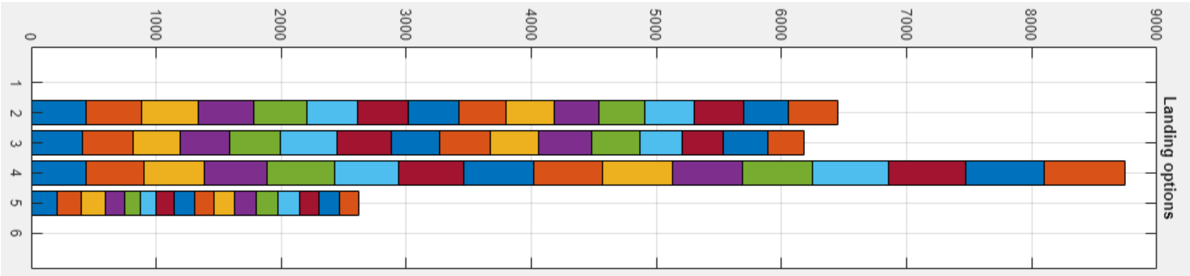

Figure 6.56: Progress of the landing hardware over generations

6.6.4. Constraints

Over the various optimisation verification runs performed, no solutions were found that broke constraints. This confirms that the script responsible for filtering configurations that are unfit for transfer to a new generation works as expected.

6.7. Tool

The requirements of CRDT have been set in section 2.6. Table 6.7 shows the status of the requirements after the development cycle.

Table 6.7: Requirements on the tool - Verification

ID	Requirement	Status
REQ - Tool - 01	The tool shall be able to determine the mass of the various EDL systems with 10 % accuracy	Partial (Note 1)
REQ - Tool - 02	The tool shall be able to determine the cost of the desired EDL systems with 10 % accuracy	Partial (Note 1)
REQ - Tool - 03	The tool shall be able to determine the performance of the various EDL system in terms of mechanical loads with 10 % accuracy	Partial (Note 2)
REQ - Tool - 04	The tool shall be able to determine the performance of the desired EDL system in terms of thermal loads with 10 % accuracy	Partial (Note 2)
REQ - Tool - 05	The tool shall be able to analyse a single configuration in less than 1 second	Done (Figure 5.11)
REQ - Tool - 06	The tool shall be able to analyse a single upper stage configuration	Partial (Note 3)
REQ - Tool - 07	The tool shall be able to find the configuration with the lowest Reuse Index given the users constraints	Done (section 6.6)
REQ - Tool - 08	The tool shall be able to analyse the sensitivity of a given configuration	Done (section 5.5)
REQ - Tool - 09	The tool shall present the results of an optimisation or sensitivity run to the user	Done (subsection 5.5.1)
REQ - Tool - 10	CRDT shall use a modified version of the DARE ParSim v3 to determine the stage performance	Done (section 5.3)
REQ - Tool - 11	Inputs shall be read from user modifiable files	Done (section 5.2)

Note 1

From section 4.10 it can be seen that most models have an uncertainty of 20% set to them and not the initially required 10%. The AIAA suggests that the mass contingency for the Conceptual and Preliminary Design Review (CoDR and PDR) can be found in Table 6.8.

Table 6.8: AIAA Suggested Mass Contingencies for a 500-2500 kg Spacecraft.

	CoDR	PDR
Class 1	25%	20%
Class 2	15%	10%
Class 3	1%	0.8%

In this table the classes indicate the amount of flight heritage a system has. Where class 1 is a completely new system, class 3 is a system based on an existing design. Class 2 is identify as a next generation system based upon a previous developed system.

The 10% requirements originated from the assumption that the Reusable Centaur is based upon the original Centaur and even the Reusable Centaur research performed for the Space Shuttle. It can be argued that the reusable upper stage has a low TRL and is thus more a class 1 mission in a PDR or even a CoDR state.

Note 2

In the paper presented at the IAC on the verification of the ParSim v3 tool, one can see that the error of the tool was less than 10%. The modifications to ParSim made within CRDT can be seen to match the ParSim results. It can be said with reasonable certainty that CRDT meets the requirements set. However, more validation data is desired to confirm this requirement.

Note 3

Within the code of CRDT, there is a file called "ParSim_0_SingleRun.m". This script allows users to either load an ID trough a CSV file or enter the ID into the code itself. This fulfills requirements REQ-Tool-06. The status has been put to partial as it does not allow for a user to run a single ID trough the graphical user interface.

6.8. Conclusion

Validation and Verification activities are continuous and never complete. However, with the verification and validation work performed, it can be stated that CRDT performs sufficiently for the purpose of this thesis. It can be determined that the various cost and mass models behave as expected and where validation data was available it could be seen that the models match the data. Primarily in the cost models, more particularly the manhour cost models, this proved to be complicated. However, within the scope of the conceptual design all models can be considered verified. The model for which validation data was available can be considered validated.

7

Case Studies

This chapter takes the tool to an actual problem. The Atlas V Centaur is taken as a reference vehicle as there is a lot known about the vehicle and the vehicle has been modified before. The latter allows to assess the mass and cost of stage elongation. The chapter discusses optimisation runs on four different orbits through CRDT, namely; low earth orbit, sun synchronous orbit, medium earth orbit, and geostationary transfer orbit. Per orbit there are three cases studied: no modifications to the launcher, elongated upper stage to compensate for the additional propellant, and extra booster to the first stage. For each case the results are presented and discussed. For the most relevant cases a sensitivity study is done showing the stability of the found solution.

7.1. Atlas V Centaur

The Atlas V Centaur from United Launch Alliance has been chosen for a case study to demonstrate the feasibility of upper stage reusability and the capabilities of the tool. The Atlas V Centaur has been chosen for reasons below. Finally, as the Centaur stage has gone through many iterations over the year, it is possible to make estimates as to how heavy and expensive an elongated Centaur stage would be, which was earlier discussed in subsection 4.1.3.

- The Centaur stage is a relative lightweight stage with a dry mass of just over 2200 kg. This makes a recovery more easy as it reduces the loads on the stage. [2].
- The Centaur stage uses the relatively expensive (compared to the rest of the stage) RL-10 engine thus making reusability more interesting (see subsection 2.4.2).
- The RL-10 engines are restartable and throttleable thus making them more ideal for EDL manoeuvres as it allows for more precise manoeuvres [22].
- Reusability and landing capabilities of the RL-10 family has been demonstrated in the DC-X vehicle [11].

The Atlas V Centaur launcher comes in various configurations. These are presented in Table 7.1. Here one can see the launcher type presented as a three digit number. The first digit describes the fairing diameter in meters, the second the number of strap-on solid boosters, and the third the number of engines on the upper stage. As all previous Atlas flights have been done with a single RL-10 engine, this will always be 1.

Table 7.1: Comparison of Payload Capabilities and Launch Cost the Different Atlas V configurations [2]

Launcher Type	LEO [kg]	SSO [kg]	GTO [kg]	Cost [USD]
401	9797	6670	4750	1.09E+08
411	12150	8465	5950	1.16E+08
421	14067	9050	6890	1.23E+08
431	15718	9050	7700	1.29E+08
501	8123	5945	3780	1.53E+08
511	10986	7820	5250	1.60E+08
521	13490	9585	6475	1.67E+08
531	15575	11160	7475	1.73E+08
541	17443	12435	8290	1.80E+08
551	18814	13550	8900	1.87E+08

The Centaur upper stage can be described with the parameters found in Table 7.2 and Table 7.3. The constraints on the landing velocity can be found in subsection 2.3.4. The maximum payload reduction factor constraint is chosen somewhat arbitrarily to be three. This means that the reusable configuration can only lift 33 % of the payload compared to the expendable configuration. The limits of the varying parameters can be found in Table 7.4.

Table 7.2: Centaur Stage Inputs [50, 2]

Parameter	Unit	Value
Empty Mass	kg	2247
Engine Mass	kg	561.75
Diameter	m	3.05
Length	m	12.68
$F_{t_{vac}}$ 100%	N	99200
Isp_{vac}	s	462
A_e	m^2	3.63
P_c	MPa	4.41
Expansion ratio	-	88.1
OF ratio	-	5.88
Cost	M USD	20
Cost engine	%	80
Nr yearly flights	Nr	10

Table 7.3: Centaur Stage Constraints

Parameter	Unit	Value
Acceleration	m/s^2	120
Landing velocity Nothing	m/s	5
Landing velocity Airbag	m/s	10
Landing velocity Retrorocket	m/s	100
Landing velocity Water	m/s	20
Landing velocity MAR	m/s	20
Max payload reduction factor (p)	-	3

Table 7.4: Centaur Stage Limits

Parameter	Min	Max
Entry velocity [m/s]	6000	8000
Entry angle [deg]	-10	0
Entry altitude [m]	80000	120000
Parachute deployment altitude [m]	1	80000
Parachute area [m^2]	1	40
Drag plate deployment altitude [m]	1	100000
Drag plate area [m^2]	0.1	5
Engine ignition altitude [m]	1	100000
Burn time [s]	1	20
Throttle setting [$-$]	0.75	1
Area of inflatable heat shield [m^2]	0.5	16
Separation altitude [m]	1	100000
Throttle setting	0.75	1.00

Note that the constraints shown in Table 7.3 one cannot find thermal limits imposed on the stage. This is due to the assumption that any form of thermal protection is suitable for a re-entry mission. Especially the inflatable heat shields have been developed for a Lunar or Mars return mission. This means that as long as the entry conditions are limited such as presented in Table 7.4 are met, the thermal flux constraints are never breached. Thermal constraints are important when not using any thermal protection, however this is not considered.

7.2. Overview of Cases

It is desirable to run each and every case to ensure one always finds an optimum. However, this would waste a significant amount of computing time as one can already remove some cases.

- As land landing is cheaper in retrieval, it is desired to always land on land (section 6.5). This is feasible for LEO and MEO as the inial orbits are circular, and thus, the Argument of Periapsis can be chosen. For GTO this is not deemed possible.
- The MEO and GTO cases will only be run with the hardware that was found in the LEO cases. This ensures a single configuration can be used for all flights.
- Drag plates are never considered as they are heavier than parachutes and cannot be used in combination with the inflatable heat shield.
- Due to the low allowable maximum terminal velocity of the "none" option for landing hardware, this is not taken into account.

The cases that will be run for the Centaur stage can be found in Table 7.5. For thermal protection, the inflatable heat shield will be used. To verify the optimisation algorithm, the solid heat shield is taken into account for the LEO runs. For all runs, engine burns and parachutes are taken into account. Drag plates are not considered in any case as they are heavier than the parachute options. All landing options are considered for the GTO mission as the operator cannot choose the location of the periapsis. For the LEO and MEO missions, only land landings are considered as they are significantly cheaper than the alternatives.
The launcher variant used for most LEO missions are the 401 and the 541. This is done as these are the most flown configurations. For the MEO flights, the 401 is used, as this configuration is the only variant used for the GPS missions. For the GTO flights, the 431 and 541 variants are used.

Table 7.5: Overview of Cases to be Performed

Category	Options	LEO	MEO	GTO
Thermal protection	Conventional	x		
	Inflatable	x	x	x
Decelerator	Parachute	x	x	x
	Drag Plate	x		
	Engine burn	x	x	x
Landing	Retrorocket	x	x	x
	Airbag	x	x	x
	Water landing			x
	Mid air recovery			x
Modification	None	x		
	Elongated stage	x	x	x
	Added booster	x	x	x
	Both	x	x	x
Launcher		401, 541	401	431, 541

The input and output files used for the cases can be found in the GIT repository and are made available upon request.

7.3. Low Earth Orbit (LEO) Missions

The LEO results are divided into four categories named LEO-1 trough LEO-4. The results and conclusions can be found in the sections below. The inputs are presented in Table 7.6. Cases

Table 7.6: Overview of the LEO Cases

Case nr	**LEO-1**	**LEO-2**	**LEO-3**	**LEO-4**
Configurations	2500	2500	2500	2500
Mutations	0.2	0.2	0.2	0.2
Elite	0.2	0.2	0.2	0.2
SuperElite	0	0	0	0
Bees	0	0	0	0
Thermal protection	All	All	Inflatable	Inflatable
Descent	All	All	Parachutes Engine	Parachute Engine
Landing	Land	Airbags	Airbag	Airbag
Launcher	401	401	401	541
Modifications	All	All	All	All

7.3.1. LEO-1

When running the LEO-1 case, one finds a solution using an inflatable heat shield and retrorockets for landing. The heat shield frontal area reaches the limit of 16 m^2, compared to the Centaurs' original frontal area of 6.5 m^2. This is expected as the lower the ballistic coefficient is, the lower the terminal velocity. Due to the large size of the inflatable heat shield and the high allowable landing velocity of retrorockets, no deceleration hardware is required.

The Reuse Index reaches goes one after three reuses. After 15 re-flights, the stage reaches a Reuse Index of 0.68. The system is required to add 520 kg of extra hardware with a total cost of 48,300 USD of reusable EDL hardware and 7,870,000 USD of non-reusable EDL hardware. This leads to a payload reduction factor of 1,0866. Furthermore, an extra AJ-60A strap on booster has been added to the launcher to compensate for the added mass.

7.3.2. LEO-2

The retrorocket landing solution found in the LEO-1 case has two major drawbacks, these are as follows:

- As the inflatable heat shield is on the forward surface, the retrorockets either need to fire through the heat shield or the stage needs to make a 180 degrees rotation.
- The onboard state estimation needs to be very precise to actuate the retrorockets at the exact altitude.

To mitigate these two drawbacks, a run has been done without retrorockets and only airbags as a landing option. When only selecting the airbag option, one finds a configuration that requires a parachute to decrease the terminal velocity of the stage. This is due to the constraints mentioned in Table 7.3 where the airbag system is only capable of handling an impact of at most 10 m/s. The dynamic pressure plots nicely show the effect of the parachute as the dynamic pressure in Figure 7.1b drops after 520 seconds, where the dynamic pressure in Figure 7.1a remains constant.

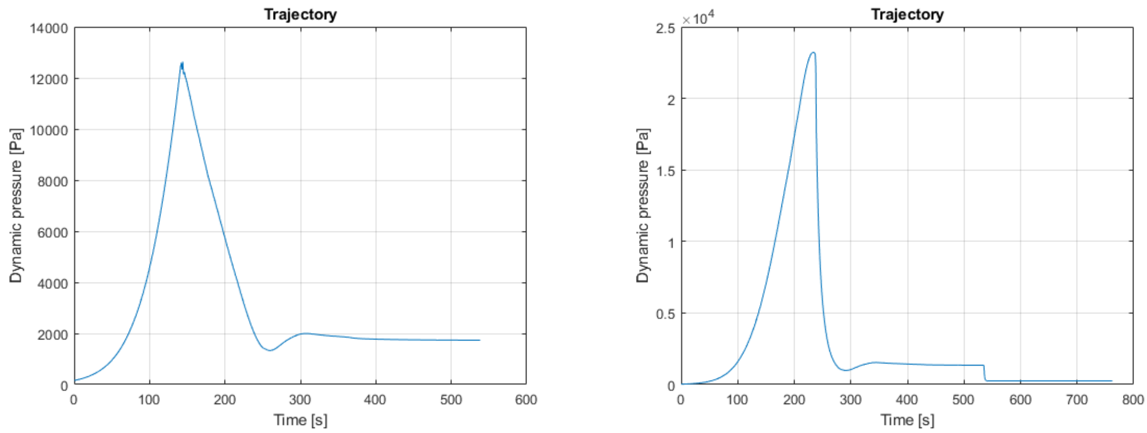

(a) Retrorocket landing (LEO-1 case)

(b) Airbag landing (LEO-2 case)

Figure 7.1: Dynamic pressure plot for both solutions

The solution LEO-2 has a Reuse Index of 1.14 after 15 flights and a total payload reduction of 1.749. As can be seen, the Reuse Index is above 1, which means the reusable variant is more expensive than the expendable variant.

7.3.3. LEO-3

When looking at earlier research, one can see that the inflatable heat shield can act as an airbag landing system [39]. Note that CRDT at the moment does not take this into account, however, it is recommended for further upgrades. To investigate this configuration the LEO-2 configuration is taken and the landing hardware gene is put to "0" or "no landing hardware". This solution is called the LEO-3 and has a Reuse Index of 0.70, and the payload reduction becomes 1.070. Note that CRDT indicates a violation of landing velocity constraints.

To demonstrate the Monte Carlo analysis some modifications are made to the LEO-3 configuration, now called LEO-3B and further in the sensitivity analysis. These modifications include increasing the parachute size to make it less prone to breaking constraints.

The uncertainty introduced onto the found solutions is 0.2 on all parameters. This means that all mass and cost models have a normal distribution were sigma equals 20 percent of the initial value. The numbering convention introduced in subsection 2.4.3 is used to indicate which uncertainty which is plot. For the final results published in the thesis, a more accurate uncertainty range is chosen. The Monte Carlo run was done using 1500 variations per run. The Monte Carlo analysis is further explained in section 5.5.

As can be seen in Figure 7.2, the Reuse Index is strongly influenced by the trajectory imperfections (boxplot 2). This is expected as the mass model for the inflatable heat shield is a function of the maximum dynamic pressure. As can be seen, this mainly negatively impacts the Reuse Index; the same results can be found in the combination plot (boxplot 4). As the mass and cost uncertainties are normally distributed, the Reuse Index can be brought down in the case where both the inflatable heat shield and the retrorocket models are less heavy and expensive than expected.

From the results, it can be seen that, with a sigma of 0.2 times the found value, the solution is quite robust. All variants in the box have a Reuse Index below 1, and even the whiskers of the plot remain below 1. Only for the trajectory imperfections and the mass/cost models, some outliers can be seen to breach the upper limit of 1 and are thus no longer cost-effective.

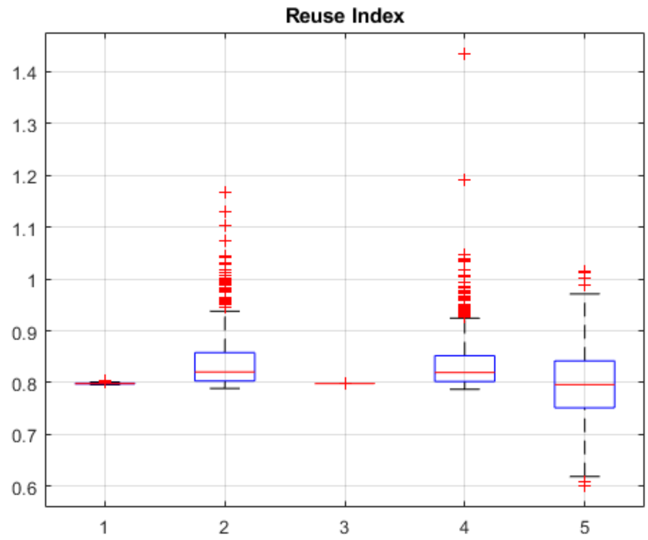

Figure 7.2: Uncertainty results - Reuse Index

7.3.4. LEO-4

As shown in Table 7.5, the LEO case also has to be run with the 541 configuration. This configuration flies to LEO for very heavy payloads. However, in the time frame 2010-2019 the 541 only flew to LEO once. When running the case, one can see that the Reuse Index goes down with 0.0137 for the mission. This brings the LEO-4 Reuse Index to 0.68.

When looking at payload reduction, one can see that it goes down to 1.049, which means that the LEO-4 case has less of an impact on the payload reduction than the LEO-3 case. However, given the few flights this variant has done to LEO it is questionable if 15 reuses can be reached in just this configuration. One could argue that, for a launcher with multiple variants, one should analyse the full mission spectrum to be able to get a proper indication of the cost reductions.

7.3.5. LEO overview

The results of the LEO cases can be found and compared in Table 7.7. As can be seen, the retrorocket landing has the lowest Reuse Index and therefore, the highest cost savings per kilogram. However, the LEO-3 case with no landing hardware has the lowest payload reduction. Depending on the user, one of these two solutions can be used for reusing a Centaur upper stage coming from low earth orbits. Note that the comparison is done for the Atlas 401 variant, thus LEO-4 is not taken into account. A more detailed mass and cost breakdown can be found in Table 7.8 and Table 7.9.

Table 7.7: Comparison of LEO Results

ID	Launcher variant	Solution	Reuse Index	Payload reduction
LEO-1	401 + booster	Inflatable heat shield, no decelerator, Retrorockets	0.68	1.087
LEO-2	401 + booster	Inflatable heat shield, Parachute, Airbags	1.14	1.749
LEO-3	401 + booster	Inflatable heat shield, Parachute, No (separate) landing hardware	0.70	1.070
LEO-4	541 + booster	Inflatable heat shield, Parachute, No (separate) landing hardware	0.68	1.049

Table 7.8: Mass and Cost Comparison of LEO-1, LEO-3 and LEO-4

ID	M(RHW) [kg]	C(RHW) [USD]	C(RR) [USD]
LEO - 1	520.85	48274	7806303
LEO - 3	347.45	43126	8276700
LEO - 4	347.45	43126	8276700

Table 7.9: Mass Breakdown of LEO-1, LEO-3 and LEO-4

ID	M(RHW) [kg]	Separation [kg]	Thermal protection [kg]	De-orbit [kg]	Parachutes [kg]	Landing [kg]
LEO - 1	520.85	24.35	48	47 + 218.8	0	182.6
LEO - 3	347.45	24.35	48	47 + 218.8	9.18	0
LEO - 4	347.45	24.35	48	47 + 218.8	9.18	0

7.4. Medium Earth Orbit (MEO) Missions

All launches to Medium Earth Orbit have been done using the Atlas V 401 launcher that has launched the GPS satellites. As the launcher has not been developed specifically for MEO, a solution is attempted to be found using the hardware found in the LEO case.

Table 7.10: Overview of the MEO Case

Case nr	MEO
Configurations	2500
Mutations	0.2
Elite	0.2
SuperElite	0
Bees	0
Thermal protection	Inflatable
Descent	Parachute
Landing	All
Launcher	401
Modifications	All

When running this case, CRDT shows a propellant mass required of 2191 kg. Of this propellant mass 875kg is required to lower the periapsis and 1316 kg is required for the entry burn. This means that 10 percent of the total propellants on board has to be used for the de-orbit manoeuvre. This leads to a negative payload capacity of the stage. Therefore, it can be concluded that reusing or even recovering a stage from MEO is not feasible.

7.5. Geostationary Transfer Orbit (GTO) Missions

When running the solution found for LEO-1 from a GTO orbit, one finds that the stage does not breach the constraints imposed. This leads to the preliminary conclusion that a GTO return is possible. Using the hardware found in the LEO-2 CRDT is run to determine if a solution can be found for a GTO with a lower Reuse Index. From the launch history of the Atlas V, one can see that most GTO flights are done using the Atlas V 431 and 541 configurations. Therefore the GTO runs are done for both configurations.

When comparing the results of the MEO case to the GTO case, one finds a required de-orbit propellant mass of 388.5 kg. Of this 47 kg is for the lowering of the periapsis and 341 kg is for the entry burn. The initial periapsis of the geostationary transfer orbit is 400 km, where the MEO periapsis is 22000 km.

Table 7.11: Overview of the GTO Cases

Case nr	GTO-1/2	GTO-3/4
Configurations	2500	2500
Mutations	0.2	0.2
Elite	0.2	0.2
SuperElite	0	0
Bees	0	0
Thermal protection	Inflatable	Inflatable
Descent	Parachute Engine burn	Parachute Engine burn
Landing	All	All
Launcher	431	541
Modifications	All	All

When running the Atlas 341 case one finds a payload reduction factor of 2.6793 and a Reuse Index of 1.678 for the LEO-1 solution, and 2.4131 and a Reuse Index of 1.5673 for the LEO-3 solution. This means that, for 15 flights, the stage does not have a reduction in cost. When looking at Table 7.11 one can see that even for the Atlas 541 case there is no solution with a reuse index below 1.

Only when setting the entry condition to 10000 m/s entry velocity at 80 km altitude, one finds a Reuse Index of 0.7378. However, it should be noted that the Exploration Flight Test-1 mission entered the atmosphere with about 9000 m/s, which was considered a high-speed test [44]. As the entry velocity goes outside of the allowable range, it cannot be said that this solution is feasible.

Table 7.12: Comparison of GTO Results

ID	Launcher variant	Solution	Reuse Index	Payload reduction
GTO-1	431 + stage elongation	Inflatable heat shield, no decelerator, Retrorockets	1.68	2.679
GTO-2	431 + stage elongation	Inflatable heat shield, Parachute, No (separate) landing hardware	1.57	2.413
GTO-3	541 + stage elongation	Inflatable heat shield, no decelerator, Retrorockets	1.26	1.259
GTO-4	541 + stage elongation	Inflatable heat shield, Parachute, No (separate) landing hardware	1.23	1.890

7.6. Sensitivity Analysis

To determine which parameters and which unknowns have the largest influence on the stage design, a sensitivity analysis is done by varying the inputs to CDRT. These variations are the stage mass, number of reuses, launcher type, refurbishment time, and number of manhours. These variations are done as they have the highest uncertainty.

7.6.1. Stage mass

When varying the initial Centaur empty mass between 1500 kg and 3000 kg one can get insight into how the Reuse Index behaves for different stage masses. These results can be found in Figure 7.3. As can be seen, it is advantageous to have the stage mass as low as possible.

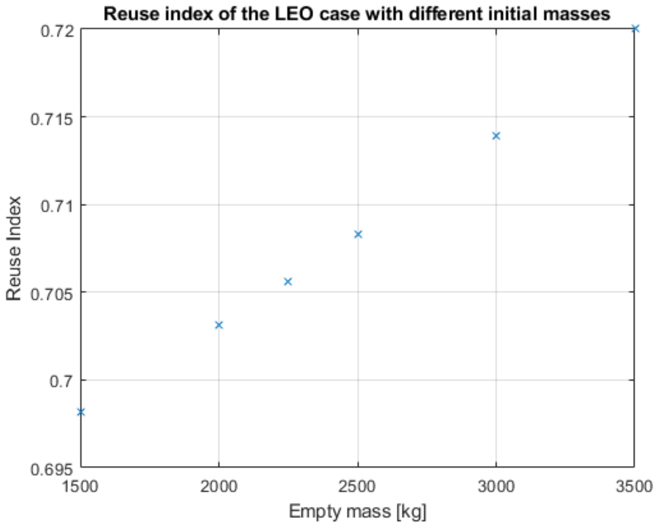

Figure 7.3: Reuse Index as function of empty mass (Case LEO-1)

This sensitivity analysis has been done for the LEO-3B solution, as this case had the lowest Reuse Index. However, similar results can be found for LEO-4 and LEO-1. This is due to the fact that the parachute area is a function of the stage ID, and not the vehicle mass.

7.6.2. Number of Reuses

When varying the number of reuses one can see that when increasing the reuses, the costs per kilogram decreases. This can be seen in Figure 7.4 for the LEO-3B case. Here it can also be seen that the slope of the line decreases, thus the cost decrease for an additional reuse becomes less. However, due to the nature of the Reuse Index the gradient will never become zero.

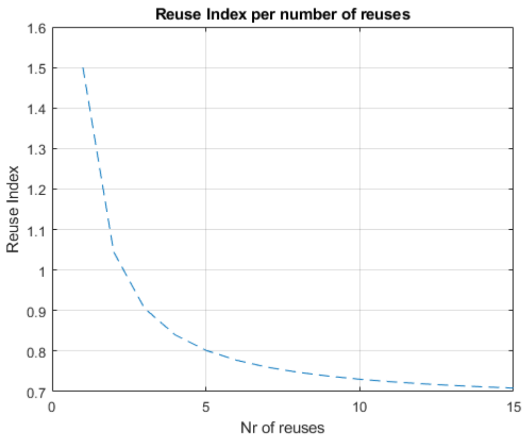

Figure 7.4: Reuse Index over nr of reuses

It can be argued that this is not realistic as it is likely that for more reuses, the refurbishment costs per reuse increase and the reliability of the stage goes down. This is comparable to the maintenance on a car after several years. However, neither are taken into account in the current Reuse Index.

7.6.3. Launcher Type and Modifications

To analyse the sensitivity variations are made to the LEO-1 result. These variations include changing the launcher type and modifications to the stage and determining the Reuse Index. The results of the sensitivity analysis can be found in Figure 7.5 and Table 7.13.

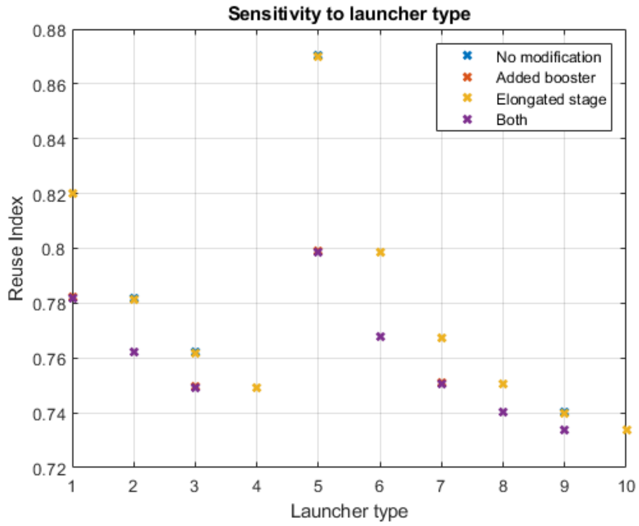

Figure 7.5: Sensitivity of the Reuse Index to the launcher type

Table 7.13: Sensitivity of the Reuse Index to the Launcher Type

Type	No modification	Added booster	Stage elongation	Both
401	0.8201	0.7821	0.8199	0.7818
411	0.7817	0.7624	0.7814	0.7621
421	0.7620	0.7497	0.7617	0.7494
431	0.7493	-	0.7491	-
501	0.8695	0.7983	0.8692	0.7980
511	0.7979	0.7673	0.7977	0.7670
521	0.7670	0.7504	0.7668	0.7502
531	0.7501	0.7399	0.7499	0.7397
541	0.7397	0.7333	0.7395	0.7331
551	0.7335	-	0.7331	-

As can be seen in the results, the Atlas V launcher divides in two categories. These categories are the 4XX and 5XX variants. As can be seen, the sensitivity analysis is strongly influenced by the payload capacity. When an extra booster is added, one can see that the Reuse Index is identical as the Reuse Index of the launcher one variant higher. However, when the stage is elongated, the Reuse Index increases somewhat. This has to do with the observation made in subsection 6.1.1 (Figure 6.1 and Figure 6.2) that stage elongation is punished in both mass and cost.

7.6.4. Manhours

The final sensitivity analysis is done on the manhours required and the cost per manhour. For this analysis, the LEO-1 case is taken.

Figure 7.6 show the variations to the manhours required for refurbishments. As can be seen, the Reuse Index is relatively insensitive to this variation. Even when taking 10 people, for 20 full-time days, thus 4800 manhours, one can see a Reuse Index of 0.687.

However, when varying the total amount of manhours, seen in Figure 7.7, one can see a much higher impact. When an uncertainty of 100% is imposed, one can see that the Reuse Index goes over 1, leading to a reusable stage that is more expensive than the expendable variant. An uncertainty of 100% is not unrealistic as the required amount of manhours is highly uncertain in this research.

Finally, the cost per manhour variations can be seen in Figure 7.8. This variation introduces the largest uncertainty in the research. It can be seen that uncertainty of 50% is already sufficient to let the Reuse Index go over 1.

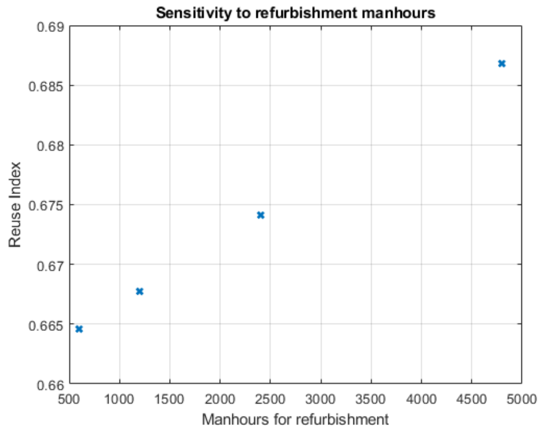

Figure 7.6: Sensitivity to manhours required for refurbishment

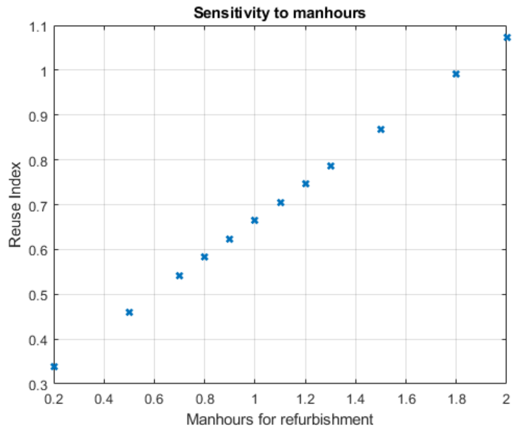

Figure 7.7: Sensitivity to total manhours required

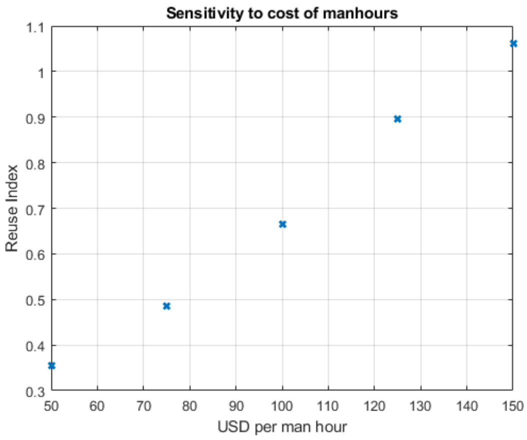

Figure 7.8: Sensitivity to the cost of one manhour

From the plots it can be concluded that the manhours and cost per manhour is a large uncertainties in the research. Depending on these two parameters, the reusable variant is either more or less expensive.

7.6.5. Higher LEO orbit

When running the LEO cases from SSO, one can find the results found in Table 7.14. The SSO orbit is assumed to be 800 km where the LEO orbit has an altitude of 400km.

Table 7.14: Comparison of SSO Results

ID	Launcher variant	Solution	Reuse Index	Payload reduction
SSO-1	401 + booster	Inflatable heat shield, no decelerator, Retrorockets	0.71	1.1418
SSO-3	401 + booster	Inflatable heat shield, Parachute, No (separate) landing hardware	0.72	1.1152
SSO-4	541 + booster	Inflatable heat shield, Parachute, No (separate) landing hardware	0.70	1.075

In all the SSO cases, the difference in Reuse Index originates from the propellant masses required. Where for the LEO the propellant mass for tge de-orbit manoeuvre was 47 + 218.8 kg, it becomes 95.2 + 221 kg for the SSO case.

However, it can be seen that all cases with a lower than 1 Reuse Index in the LEO case, also have a lower than 1 Reuse Index in the SSO case. The same conclusions can be reached as for the same launcher the SSO-1 has the lowest Reuse Index and SSO-3 has the lowest payload reduction.

7.7. Tool Performance

For CRDT it was found that the analysis of a single configuration takes between 0.2 and 0.5 seconds, with an average of 0.3 seconds. These simulations were run on either a desktop or laptop with an Intel I7 and 8+ GB of RAM. Both systems run Windows 10 and are between 2 and 4 years old.

This meant that all LEO runs were done in just over two hours. Three hours when taking the Monte Carlo analysis into account. When running the more detailed Monte Carlo analysis, one should assume an additional run time of between 45 and 60 minutes.

This means that a single case can be run in about half a day. Thus a designer can reach a preliminary conclusion within four hours.

8 Conclusion and Recommendations

This chapter contains the conclusions and recommendations found in this thesis. The conclusions provide answers to the research questions posed in the introduction and are elaborated on. The recommendations are divided into topics and are sorted in order of priority.

8.1. Conclusion

From the research done, it is concluded that a tool, CRDT, has been developed that meets the requirements imposed. The tool, focusing on reusable upper stages as an alternative to expendable upper stages, is capable of finding a conceptual solution based upon user inputs within half a day. This provides the designer with a powerful tool to provide initial designs of reusable stages. CRDT can easily be modified for suborbital, ballistic flights to simulate the flight of a first stage or a booster. The following conclusions regarding the development of the tool can be reached.

- **CRDT is capable of analysing a configuration in less then 0.5 seconds, leading to a final configuration in about half a day**
- **CRDT allows for flexibility in performance, mass and cost models**

When looking at the upper stage, one can see that the MEO case is not feasible for reusability. Furthermore, it can be seen that the GTO case is feasible but not desirable due to the high entry velocity required. This puts extra mechanical and thermal loads on the upper stage, which could lead to failure of the inflatable heat shield. For LEO orbits, it is concluded that reusability is possible. Cost reductions of 32% in terms of hardware cost can be reached in case of 15 reuses. Note that this is 32% on the hardware cost of the upper stage. This leads to a cost reduction per launch of about 9% on hardware cost and 6.3% on total cost.
The requirements on the mission of the reusable upper stage have been set in section 2.1 and are checked in Table 8.1. It can be seen that the original mission of the upper stage, to deploy a satellite in a desired orbit, has not been compromised. The launch cost reductions of 6.3% on the launch cost. In order to reach the required 10% one requires a Reuse Index of 0.52 for the upper stage. Finally, the requirements that the only impact on the stage mission is allowed to be the payload capacity is unproven as the reliability of the new system is unknown.

Table 8.1: Reusable Upper Stage Mission Requirements

ID	Requirement	Status
MIS - 01	The reusable upper stage shall deploy a payload to a desired orbit	Done
MIS - 02	A launch cost reduction of 10 % shall be achieved	Failed
MIS - 03	The addition of reusability shall only impact the stage performance in terms of payload capacity	Partial

- **Upper stage recovery is technologically feasible for LEO missions**
- **Indications show that upper stage reusability is economically feasible for the LEO cases, however cost reductions come closer to 6% on the total launch**

- **Upper stage reusability should be implemented after first stage or strap-on booster reusability has been implemented**

The found solution always calls for the addition of an extra booster to compensate for the performance loss. For atmospheric entry, the tool always finds a solution with an inflatable heat shield, which also acts as a decelerator. For landing the tool finds either a retrorocket landing or an airbag landing. The latter is mainly interesting when the inflatable heat shield can also be used as an airbag or when the onboard state estimation is not sufficiently accurate to fire the retrorockets.
It can be concluded that inflatable heat shields are a promising piece of technology, and the industry focus should be put on maturing the technology. Not only for the reusable upper stage, but also for future exploration missions is the inflatable heat shield an invaluable piece of technology.
Furthermore, it is concluded that the uncertainty in manhours and the cost per manhour is the leading uncertainty in the cost estimations.

- **Development of inflatable heat shield technology for the return of the upper stage**
- **Uncertainty in manhour cost models should be reduced to increase the accuracy of the results**

8.2. Recommendations

Throughout the thesis work, several items cause uncertainty in the results or assumptions that simplify the problem. These are the primary source for the recommendations made in the following section. All recommendations are supported by sections from the report and should be a focus point for future research in the field of reusability.

Reuse Index

The Reuse Index as proposed by ULA gives a good first order estimate of whether a reusable launch vehicle is economically interesting. However, in the opinion of the author, the Reuse Index is missing three primary elements. These are as follows:

1. Variable reusability of EDL hardware.
2. Reliability of the launcher.
3. Distinction between hardware and operation costs.

The current Reuse Index assumes that EDL hardware is either non-reusable or reusable for the same amount of flights as the stage. However, not every EDL element can be reused equally. Say a parachute deployed at high dynamic pressures might not be as reusable as a parachute deployed at subsonic conditions. Similar reusable heat shields have proven to be challenging, and might not last for as many flights as the stage itself.
As shown in section 2.2, the overall reliability of a reusable launch vehicle is lower than for the expandable variant. One should take the reliability of both the ascent and the descent flight into account. The reliability might even go down over the number of flights, this needs to be factored in.
Finally, the operation cost should be placed separately into the Reuse Index as they can be easily forgotten. furthermore, the operation and refurbishment costs might be a function of the system configuration. For instance, refurbishment costs of a parachute landing in saltwater will be higher then the refurbishment of a parachute system for a land landing. Using the proposed equation found in Equation 8.1 one can see that the reusable EDL costs, C(RHW), now comes with a Reuse Index on subsystem level. This Reuse Index can be found in Equation 8.2.

The proposed Reuse Index also takes the reliability of the launcher into account. The mean time between failure, represented by λ is divided into two categories. The mean time between failures of the launcher and the mean time between failures of the recovery.
The reliability of the launcher is a function of the cost of the refurbishment. The more the launch operator spends on refurbishments, the higher the reliability. However, this comes at a financial penalty. In the new Reuse Index, seen in Equation 8.1, the reliability of the original launcher (λ_E) is compared to the reliability of the reusable upper stage (λ_R) and the reliability of the recovery process (λ_{Rec}). The reduction of reliability is factored in through the λ_{Red}.

The new Reuse Index also divides the C(RR) into the non-reusable EDL hardware costs, operational costs (C(OP)), and refurbishment costs (C(REF)). Even though the original Reuse Index already allowed for this, it becomes more clear where the various costs originate form.

$$I = p\left(k\left(\frac{F_{unit}}{n} + \left(\frac{\sum_{i=1}^{i_{max}} C(RHW)_i I_i}{C(B)}\right) + \frac{C(RR) + C(OP) + C(REF)}{C(B))}\right) + (1-k)\right)$$
$$exp(\lambda_E - ((\lambda_R * \lambda_{Rec}) - n * \lambda_{Red})^n) \quad (8.1)$$

Where:

$$I_i = \left(\frac{C(Hardware)}{n_{hardware}} * F_{Hardware} + C(REF)\right) / C(Hardware) = \frac{F_{Hardware}}{n_{hardware}} + \frac{C(REF)}{C(Hardware)} \quad (8.2)$$

In Equation 8.2 the following assumptions have been made:

- Decrease in production number of EDL hardware, thus higher initial cost ($F_{Hardware}$)
- Reusable EDL hardware is fully reusable (C(RWH) = 0, k=1)
- No additional mass due to making EDL hardware reusable (p = 1)

Full Launcher Analysis

From the literature study and discussions at EUCASS2019, it was seen that reusability of only the second stage is not a solution to ensure a decrease in launch cost. This is supported by the conclusions of this thesis, as it was shown that a reduction of only 6.3% is feasible with only upper stage reusability.
The reusable launcher design should be included in the design of the entire launcher taking into account the first stage, second stage, add on boosters, and the fairing. Design studies should include ascent trajectory optimisation, de-orbit optimisation, descent trajectory optimisation, and hardware optimisation. One possibility for this research is an update to the Tu Delft Astrodynamics Toolbox (Tudat).

Full Mission Analysis

As mentioned in section 2.5, the Reuse Index does not take into account that certain launcher has multiple variants and missions. This means that the analysis as done in this thesis focuses on a single Atlas variant flying to a single orbit. It was shown in subsection 7.3.4 that for the Atlas 541 case to LEO this is unrealistic as this flight only happened once in the past decade.
It is recommended to do a full mission analysis taking into account the different missions done by the launcher. This includes the number of launches per year distinguishing the payload mass and desired orbit as the demand side. On the supply side, the launcher variants in both expandable as reusable configuration have to be set. The optimiser should now first determine the optimal reusable launcher mentioned above, and then analyse if a launcher fleet can be created with the available launcher variants to satisfy the market. It should be noted that a reusable launcher can be flown expendable in the last flight. During the full mission analysis, one can use the new Reuse Index to take the reliability of the launcher fleet into account.
Early work on this has been done by DLR which shows that for a reusable first stage for a European launcher it can be re-launched six times as the market requires the sixth flight to be a GTO flight, thus not allowing for first stage reusability [65].

Refurbishment and manhours

As mentioned in the conclusion and section 7.6, the most significant uncertainty comes from the manhours and the refurbishment time. It is recommended to keep a close eye on missions such as Callisto and publications on reusability. The more knowledge becomes available; the more accurate these estimations can be made.

CRDT

As mentioned in section 4.10, CRDT does not include the uncertainty of the mass and cost models into the genetic optimisation. It is recommended to include this uncertainty into the optimisation to help filter remove the bias created by the models' uncertainty. Proposed is that, before a configuration is analysed, a random noise is applied. This noise will fall within the range of the uncertainty range of the respective models. The gene with the added noise is analysed by ParSim, and the remainder of the optimisation is done as it is currently done.

Orbital dynamics
Mentioned in Table A.3, the drag on the vehicle in space is not taken into account during the de-orbit. However, performing an aerobraking manoeuvre might be advantageous as one can reduce the propellant mass and cost. It is recommended to update the orbital dynamic models to allow for more complex de-orbit flights. This should include atmospheric drag higher in the atmosphere and multiple burns and coast phases.

Dynamics model
CRDT assumes a ballistic entry as described in subsection 2.3.2. This is a consequence of the dynamics module of CRDT being based on ParSim. This means it does not allow for the simulation of any lift generation in the vehicle. The generation of lift, even in an Apollo-like vehicle, can result in much lower mechanical and thermal loads in the vehicle [4]. It is proposed and recommended to upgrade CRDT with the DARE TumSim tool. TumSim is a six degrees of freedom simulation tool developed for Stratos III, parallel to ParSim. Second, by enabling a higher variety of entry flights, TumSim can be used to determine the stability of combinations shown in Figure 4.2, where they are now being assumed. Furthermore, the mass and cost of the reaction control engines can be more accurately determined. As using TumSim as a dynamics model requires more inputs from the user, such as aerodynamic coefficients of the vehicle, it is proposed to use the CRDT-TumSim tool as a more preliminary design tool where the CRDT-ParSim tool takes the role of a conceptual design tool.

Thermal protection
At the moment CRDT includes one inflatable and one conventional heat shield. It is recommended to include other types of thermal protection, such as non-reusable conventional heat shields in the trade-off. Furthermore it is recommended to keep an close eye on the development of deployable and inflatable heat shields. As the technology matures, the mass and cost modes will become more accurate.

Decelerators
The parachute type is, at the moment, only a function of the deployment altitude. It is recommended to make the parachute type a variable in the system ID so it can be used in the optimisation. Finally, it is recommended to enhance the performance model of the parachute and drag plates to include opening times, parachute reefing, and stepwise opening of the drag plates. Regarding the propulsive deceleration, it is recommended to allow for a throttle setting variable during the burn, where at the moment the throttle setting is a constant.

Landing and retrieval
Recent work by Arianespace and SpaceX have shown that a ship with a capture net is a feasible landing solution. This is not taken into account in CRDT and is recommended for implementation.

Mass and cost models
The solutions found by CRDT are as good as the mass and cost models included. From chapter 4 and chapter 6 it can be seen that some of the models have a very high uncertainty or in some cases even an unknown uncertainty. It is recommended to start a more detailed and in-depth study in the mass and cost models and their uncertainties.
Finally, it is recommended to keep an eye on the research performed on the Callisto and ReFEx missions. These missions are performed by DLR and CNES to study the effect of reusability and focus, amongst other things, on the costs of retrieval and refurbishment.
The Transcost model is implemented with a constant development factor. However, it can be that a company has experience with parachutes up to a particular area but can make them larger. This means that the development factor for the smaller parachutes is lower than for, the larger parachutes. This requires the implementation of a development factor, which is a function of, amongst others, area.

9 Lessons Learned

The work presented in this thesis nicely combines the work I did within DARE in my various functions, with the increasing demand for lower launch costs. During the literature study and thesis, there have been many developments in stage reusability, which confirmed some of my estimations. However, it also showed that making the mass and cost models was more difficult than I estimated beforehand. It was however reassuring to hear that agencies such as ESA, DLR, and CNES having difficulties with this as well and set up projects such as Callisto and ReFEx to help mitigate their lack of knowledge [58]. I am proud that I could contribute to the discussions at EUCASS and FAR.

The development of a simulation and optimisation program as large and complex as CRDT proved difficult but enjoyable challenge. Even keeping an overview of the project is a challenge. I strongly recommend anyone doing the same to draw a clear simulation diagram. In this diagram, one can keep track of the status of the various simulation blocks, as well as the inputs and outputs of the various simulation blocks.

For anyone who is working on a thesis or large project in general, I recommend using tools such as ASANA and Instagantt to keep track of the planning and tasks. I feel that at some moments, I did not have a sufficient overview of the entire project leading me to forget items. It is recommended to make a Gantt Chart and keeping it updated throughout the thesis. One should not forget to include all elements, such as writing and proofreading, in this planning.

On the writing of the thesis itself, I recommend writing down observations, thoughts and findings directly. I felt that this gave me a good sense of progress and helped me keep track of to do's.

Reusability is an excellent method to reduce the cost of a launch, but it is not the only method. Other methods such as standardisation in a launcher and automatisation of production processes can be a great source of cost reductions. It is recommended to always look at the broad picture, but definitely not to forget reusability as a design option.

Bibliography

[1] 3M. *Nextel - Ceramic Textiles Technical Notebook.*

[2] United Launch Alliance. *Atlas V Launch Services User's Guide.* 2010.

[3] B. Bonetti et al. "European Flexible Heat Shields: Advanced TPS Design and Tests for Future In-Orbit Demonstration". In: *FAR 2019* (2019).

[4] D.E. Boylan and B.J. Griffith. "Simulation of the Apollo command module aerodynamics at high altitudes". In: *Journal of Spacecraft and Rockets* (1969).

[5] A.M. Brandis and C.O. Johnson. "Characterisation of Stagnation-Point Heat Flux for Earth Entry". In: *AIAA 45th AIAA Plasmadynamics and Lasers Conference* (2014).

[6] C. D. Brown. *Elements of Spacecraft Design.* 2002. ISBN: 1-56347-524-3.

[7] Sierra Nevada Corporation. *Space Technologies, Product Catalogue.* 2015.

[8] National Research Council. *Ceramic Fibers and Coatings: Advanced Materials for the Twenty-First Century.* 1998. ISBN: 978-0-309-05996-1.

[9] H.D. Curtis. *Orbital Mechanics for Engineering Students.* 2010. ISBN: 978-0-08-097747-8.

[10] J.W. Cuzzipoli. "Panel Session V - Kistler K-1 Reusable Aerospace Vehicle". In: *The Space Congress Proceedings* (2004).

[11] *DC-X.* 2017. URL: `http://www.astronautix.com/d/dc-x.html` (visited on 03/20/2019).

[12] *Debating reusability.* `http://www.thespacereview.com/article/3583/1`. 2019-06-18. 2018.

[13] R.A. Diaz-Silvia, M.M.Sarigul-Klijn, and N Sarigul-Klijn. "Rotary Decelerators for Spacecraft: Historical Review and Simulation Results". In: *AIAA Space Forum* (2013).

[14] R. A. Dillman et al. "Planned Orbital Flight Test of a 6m HIAD". In: Presented as the 2018 International Planetary Probe Workshop, Boulder, Colorado, 2018.

[15] D. Dowen, S. Christiansen, and O. Arulf. "Development of a reusable, low-shock clamp band separation system for small spacecraft release applications". In: *Proceedings of the 9th European Space Mechanisms and Tribology Symposium* (2001).

[16] N. G. Drenthe. *SOLSTICE - Small Orbital Launch Systems a Tentative Initial Cost Estimate.* 2016.

[17] ESA. *Requirements on Space Debris Mitigation for ESA Projects.* 2008.

[18] EUROCKOT. *CH4 - Spacecraft Interfaces.* 2001.

[19] *Falcon 9 Launches Bulgaria's 1st Commercial Satellite, Toasty Booster Survives hard Landing.* 2017. URL: `https://spaceflight101.com/falcon-9-bulgariasat-1/falcon-9-launch-landing-success-with-bulgariasat/` (visited on 07/18/2017).

[20] V. Finchenko et al. "Inflatable Re-Entry and Descent Technology for Manned Martian Mission". In: *IAC-2004* (2004).

[21] V.B. Gantovnik et al. "A Genetic Algorithm for Mixed Integer Nonlinear Programming Problems Using Separate Constraint Approximations". In: *AIAA* (2003).

[22] V.J. Giuliano. "CECE: A Deep Throttling Demonstrator Cryogenic Engine for NASA's Lunar Lander". In: *43rd AIAA/ASME/SAE/ASEE Joint Propulsion Conference & Exhibit* (2007).

[23] *Glenn Research Center's Role in Skylab 3.* 2008. URL: `https://www.nasa.gov/centers/glenn/about/history/skylab3.html` (visited on 10/15/2019).

[24] M. Gravlee, J.G. Reed, and C. Bridges. "Oribtal Disposal of Launch Vehicle Upper Stages". In: *AIAA SPACE 2014 Conference & Exposition* (2014).

[25] M. Gravlee et al. "Partial Rocket Reuse Using Mid-Air Recovery". In: *AIAA SPACE 2008 Conference & Exposition* (2008).

[26] D.A Heald. *Reusable Centaur Study - Final Report (Report NO CASD-NAS-73-032)*. 1974.

[27] K. Hori, Y. Hoshino, and H. Shimizu. *Vectran: Development of high functionality Fibers and its Applications at Kuraray Co, Ltd.* 2014.

[28] S. J. Hughes et al. "Hypersonic Inflatable Aerodynamic Decelerator (HIAD) Technology Development Overview". In: *AIAA 21st Aerodynamic Decelerator Systems Technology conference* (2011).

[29] M. R. Grover III, B. D. Cichy, and P. N. Desai. "Overview of the Phoenix Entry, Descent, and Landing System Architecture". In: *Journal of Spacecraft and Rockets* (2011).

[30] P. Jenniskens et al. "Preparing For Hyperseed MAC: An Observing Campaign To Monitor The Entry Of The Genesis Sample Return Capsule". In: *Earth, Moon, and Planets* 95 (Aug. 2006), pp. 339–360. DOI: 10.1007/1-4020-5075-5_34.

[31] H.W. Jones. "The Recent Large Reduction in Space Launch Cost". In: *48th International Conference on Environmental Systems* (2018).

[32] J.Stein et al. "Recent Developments in Inflatable Airbag Impact Attenuation Systems for Mars Exploration". In: *44th AIAA/ASME/ASCE/AHS/ASC Structures, Structural Dynamics, and Materials Conference, Structures, Structural Dynamics, and Materials* (1984).

[33] *Kapton (Polyimide) Film - Type HN*. https://catalog.cshyde.com/viewitems/films/kapton-polyimide-film-type-hn. 2019-04-16. 2018.

[34] T.W. Knacke. *Parachute Recovery System Design Manual*. 1992. ISBN: 0-915516-85-3.

[35] D. E. Koelle. *Handbook of Cost Engineering and Design of Space Transportation Systems*. TCS - TransCost-Systems, 2013.

[36] D. E. Koelle. "The transcost-model for launch vehicle cost estimations and it's application to future system analysis". In: *Acta Astronautica* 11 (1984).

[37] *Launch costs to low Earth orbit, 1980-2100*. https://www.futuretimeline.net/data-trends/6.htm. 2019-07-08. 2018.

[38] L. Marraffa et al. *Inflatable Re-Entry Technologies: Flight Demonstration and Future Prospects*. 2000.

[39] L. Marraffa et al. "IRDT - Inflatable Re-entry and Descent Technology". In: *Hot Structures and Thermal Protection Systems for Space Vehicles* (2003).

[40] *MathWorks Announces Release 2018a of the MATLAB and Simulink Product Families*. 2018. URL: https://nl.mathworks.com/company/newsroom/mathworks-announces-release-2018a-of-the-matlab-and-simulink-product-families.html (visited on 09/16/2019).

[41] MatWeb. *Aluminum 7075-T6; 7075-T651*. 2006.

[42] K. L. Miller et al. "Trailing Ballute Aerocapture: Concept and Feasibility Assessment". In: *39th AIAA/ASME/SAE/ASEE Joint Propulsion Conference and Exhibit, Joint Propulsion Conferences* (2003).

[43] E. Mooij. *Lecture Notes AE4870B: Re-entry Systems*. 2016.

[44] NASA. *NASA facts: Exploration Flight Test=1*. 2014.

[45] NASA. *NASA Technology Roadmaps. TA 9: Entry Descent and Landing Systems*. 2015.

[46] L. Pepermans. *A Literature Study on the Feasibility of Upper Stage Reusability of a Low Earth Orbit Launch Vehicle for Medium Payloads*. Unpublished, available upon request. 2018.

[47] L. Pepermans et al. "Flight Simulations of the Stratos III Parachute Recovery System". In: *IAC-18* (2018).

[48] *Pyrogel XT Blanket Cut-to-Size*. http://www.buyaerogel.com/product/pyrogel-5-mm-cut-to-size/. 2019-04-16. 2018.

[49] D. Rasky, F.S. Milos, and T.H. Squire. "Thermal Protection System Materials and Costs for Future Reusable Launch Vehicles". In: *Journal of Spacecraft and Rockets* 38 (2011).

[50] Aerojet Rocketdyne. *RL10 Propulsion System*. 2019.

[51] J. A. Samareh. "Estimating Mass of Inflatable Aerodynamic Decelerators Using Dimensionless Parameters". In: *IPPW-8* (2011).

[52] A. Schwing. *Costing Methods*. 2008.

[53] M. Snijder. *Cost effectiveness of the first stage recovery of a small satellite launcher*. 2017.

[54] RUAG Space. *PAS 381S (15") Separation System.*

[55] RUAG Space. *PAS 610S (24") Separation System.*

[56] RUAG Space. *Payload Adapter Systems for EELV.*

[57] *SpaceX targeting 24-hour turnaround in 2019, full reusability still in the works*. 2018. URL: `https://spacenews.com/spacex-targeting-24-hour-turnaround-in-2019-full-reusability-still-in-the-works/` (visited on 03/20/2019).

[58] S. Stappert et al. “A Systematic Comparison of Reusable First Stage Return Options”. In: *EUCASS-18* (2019).

[59] K. Takase et al. *Successful Demonstration for Upper Stage Controlled Re-entry Experiment by H-IIB Launch Vehicle*. Mitsubishi Heavy Industries Technical Review Vol. 48 No. 4 (December 2011).

[60] A.P. Taylor and P.R. Delurgio. “An overview of the landing system for the K-1 launch vehicle, parachutes and airbags”. In: *14th Aerodynamic Decelerator Systems Technology Conference, Aerodynamic Decelerator Systems Technology Conferences* (1997).

[61] *The Cost of Trucking*. 2018. URL: `https://www.imiproducts.com/blog/the-cost-of-trucking/` (visited on 04/17/2019).

[62] *ULA Rocketbuilder*. 2019. URL: `https://www.rocketbuilder.com/` (visited on 08/16/2019).

[63] *U.S. Inflation Rate*. `http://www.in2013dollars.com/1960-dollars-in-2018?amount=1`. 2019-08-13. 2019.

[64] A. Del Vecchio et al. “EXPERT – The ESA Experimental Re-Entry Vehicle: Overview of the Experiments and Payloads qualified and accepted for the flight”. In: *39th AIAA Fluid Dynamics Conference* (2009).

[65] J. Wilken and S. Stappert. “Investigation of a European Reusable VTVL First Stage”. In: *EUCASS 2019* (2019).

[66] M. Strothmann - Gurth und Wolf. personal communication. 17-09-2018.

[67] P. Woodruff, C. Yanaros, and A. Witkowski. “Low Density Supersonic Decelerator Ballute Design and Packing”. In: *23rd AIAA Aerodynamic Decelerator Systems Technology Conference* (2015).

[68] H. Wright et al. “HEART FLIGHT TEST OVERVIEW”. In: *IPPW-9* (2012).

[69] B.T.C. Zandbergen. *Thermal Rocket Propulsion version 2.05*. 2016.

A

Overview of CRDT Model Assumptions

This appendix gives an overview of all assumptions made in the creation of CRDT.

Table A.1: Assumptions - Launch vehicle

ID	Assumption
Veh - 01	The only performance loss of the launch vehicle is in terms of payload mass to orbit
Veh - 02	The performance of the first stage is not affected by the reusable upper stage
Veh - 03	The performance of the strap-on boosters is not affected by the reusable upper stage
Veh - 04	The ascent trajectory is not affected by the reusable upper stage

Table A.2: Assumptions - Upper Stage

ID	Assumption
Stage - 01	No mass is lost during re-entry other than propellant mass
Stage - 03	Refurbishment is sufficiently good to not influence launcher reliability
Stage - 04	The empty upper stage can operate in a user defined thermal range
Stage - 05	The empty upper stage can operate in a user defined dynamics pressure range

Table A.3: Assumptions - De-orbit

ID	Assumption
DO - 01	Two engine burns are sufficient for de-orbiting
DO - 02	The stage is de-orbited in half an orbit.
DO - 03	Atmospheric drag is negligible during the de-orbit manoeuvre
DO - 04	The bare stage has sufficient Attitude Determination and Control System capabilities to perform the de-orbit manoeuvre so modifications are not required
DO - 05	The engines can be started multiple times

Table A.4: Assumptions - Descent

ID	Assumption
Desc - Body - 01	The stage is aerodynamically stable during the descent
Desc - Body - 02	The stage has a constant angle of attack of 0 degrees during flight
Desc - Body - 03	The stage does not generate any lift (L=0)
Desc - EDL - 01	Figure 4.2 is followed
Desc - Para - 01	Parachute inflation force is taken as a constant factor
Desc - Para - 02	The parachutes are stable, thus the deceleration force is parallel to the velocity vector
Desc - Para - 03	Parachute lines are sufficiently long for the wake effects to be neglected
Desc - Para - 04	Vehicle angle of attack is zero when the parachute is deployed
Desc - Para - 05	No mass is lost during parachute deployment
Desc - Para - 06	The deployment altitude of the parachute determines what kind of parachute is used (h < 7500 m - Ringsail, h < 35000 m - Ribbon Parachute, h > 35000 m - Ballute)
Desc - Para - 07	Maximum Mach number of the Ringsail parachute equals 1.5
Desc - Para - 08	Maximum Mach number for the ribbon parachute equals 3
Desc - Para - 09	Ballute has no maximum Mach number
Desc - Para - 10	Dynamic pressure is no limit for parachutes
Desc - Plate - 01	Drag plate deployment is instantaneous
Desc - Plate - 02	Drag generated by the drag plates is symmetric
Desc - Plate - 03	Drag plates are not limited by Mach number
Desc - Plate - 04	Drag plates are not limited by dynamic pressure
Desc - Prop - 01	Engine has no start up behaviour, thus deliverers required thrust at t-0
Desc - Prop - 02	Engine thrust is always in line with the velocity vector
Desc - Prop - 03	Engine has no problems starting whilst wind blows into the engine
Desc - Prop - 04	Vehicle angle of attack is zero when the engine is fired
Desc - Prop - 05	No propellant is left behind after the engine burn

Table A.5: Assumptions - Entry

ID	Assumption
AE - 01	There is no loss of mass during entry phase
AE - 02	The stage is aerodynamically stable during re-entry
AE - 03	A ballistic entry trajectory is flown
AE - 04	The stage is assumed to have sufficient GNC capabilities for the entry manoeuvre
AE - 05	The stage is assumed to have sufficient ADCS capabilities for the entry manoeuvre

Table A.6: Assumptions - Landing

ID	Assumption
Land - 01	Landing system mass is a function of landing velocity, stage mass at landing, and landing system type
Land - 02	Maximum landing velocity of the landing system type is dependent on the landing system type
Land - 03	Mid-air retrieval is only possible in case a parachute is deployed at 5 km or higher
Land - 04	When using a landing system the vehicle always lands safely

B

USD Inflation

The following inflation models for the US Dollar have been used in CRDT [63].

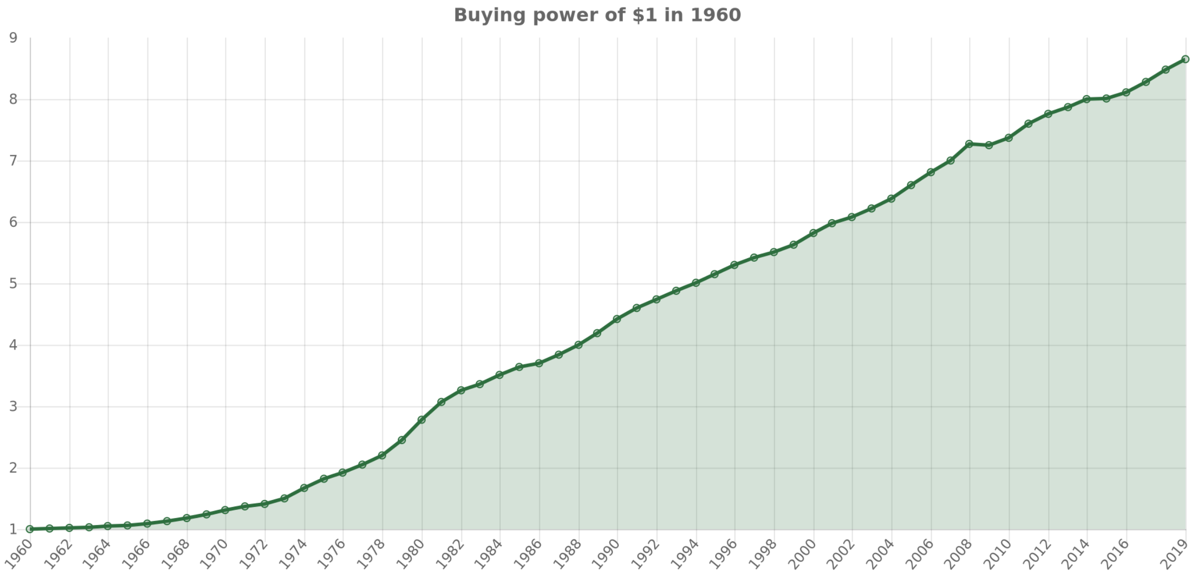

Figure B.1: Inflation of the US Dollar since 1960

Table B.1: Inflation of the US Dollar since 1960

Year	Amount	Inflation rate	Year	Amount	Inflation rate	Year	Amount	Inflation rate
1960	1	0.017182131	1980	2.783783784	0.134986226	2000	5.817567568	0.033613445
1961	1.010135135	0.010135135	1981	3.070945946	0.10315534	2001	5.983108108	0.028455285
1962	1.02027027	0.010033445	1982	3.260135135	0.061606161	2002	6.077702703	0.015810277
1963	1.033783784	0.013245033	1983	3.364864865	0.032124352	2003	6.216216216	0.022790439
1964	1.047297297	0.013071895	1984	3.510135135	0.043172691	2004	6.381756757	0.026630435
1965	1.064189189	0.016129032	1985	3.635135135	0.035611165	2005	6.597972973	0.03388036
1966	1.094594595	0.028571429	1986	3.702702703	0.018587361	2006	6.810810811	0.032258065
1967	1.128378378	0.030864198	1987	3.837837838	0.03649635	2007	7.004797297	0.028482143
1968	1.175675676	0.041916168	1988	3.996621622	0.041373239	2008	7.27375	0.038395501
1969	1.239864865	0.054597701	1989	4.189189189	0.048182587	2009	7.247871622	-0.003557777
1970	1.310810811	0.057220708	1990	4.415540541	0.054032258	2010	7.366756757	0.016402765
1971	1.368243243	0.043814433	1991	4.601351351	0.042081102	2011	7.599290541	0.031565286
1972	1.412162162	0.032098765	1992	4.739864865	0.03010279	2012	7.756554054	0.020694499
1973	1.5	0.062200957	1993	4.881756757	0.029935852	2013	7.870168919	0.014647595
1974	1.665540541	0.11036036	1994	5.006756757	0.025605536	2014	7.997837838	0.016221878
1975	1.817567568	0.09127789	1995	5.148648649	0.028340081	2015	8.007331081	0.001186976
1976	1.922297297	0.057620818	1996	5.300675676	0.029527559	2016	8.108344595	0.012615129
1977	2.047297297	0.065026362	1997	5.422297297	0.022944551	2017	8.281081081	0.021303545
1978	2.202702703	0.075907591	1998	5.506756757	0.015576324	2018	8.483338964	0.024424092
1979	2.452702703	0.113496933	1999	5.628378378	0.02208589	2019	8.65347973	0.020055873

Table B.2: Exchange rates to USD

Value (2019)	Dollar
1 EUR	USD 1.11
1 YEN	USD 0.0095

C

Overview of CRDT

C.1. Flow Diagrams

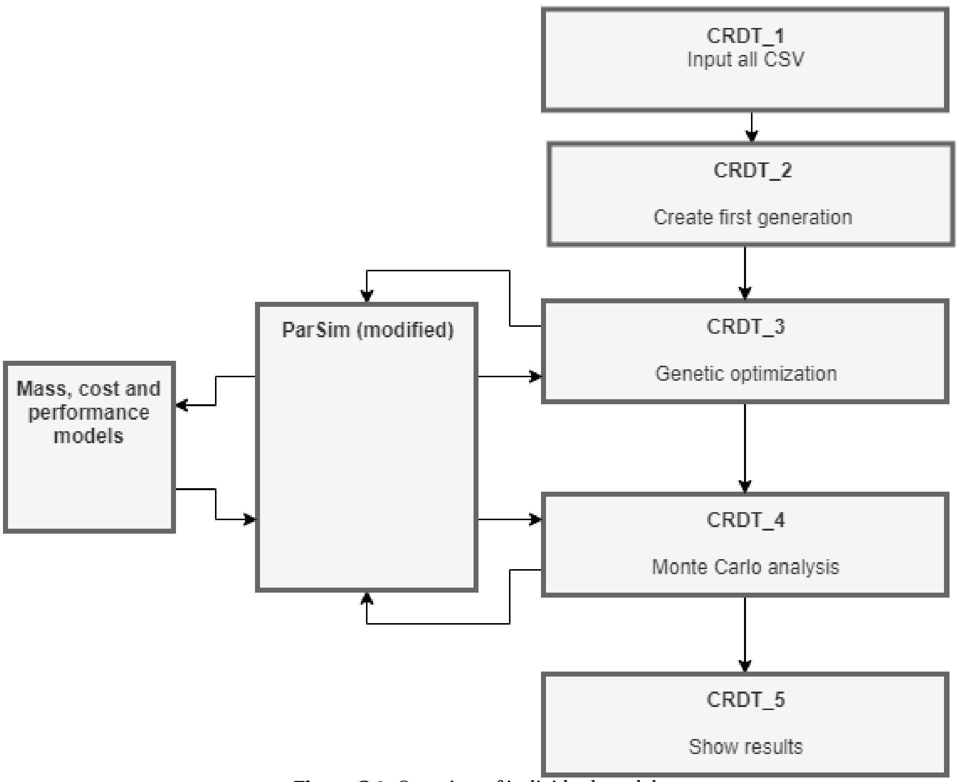

Figure C.1: Overview of individual models

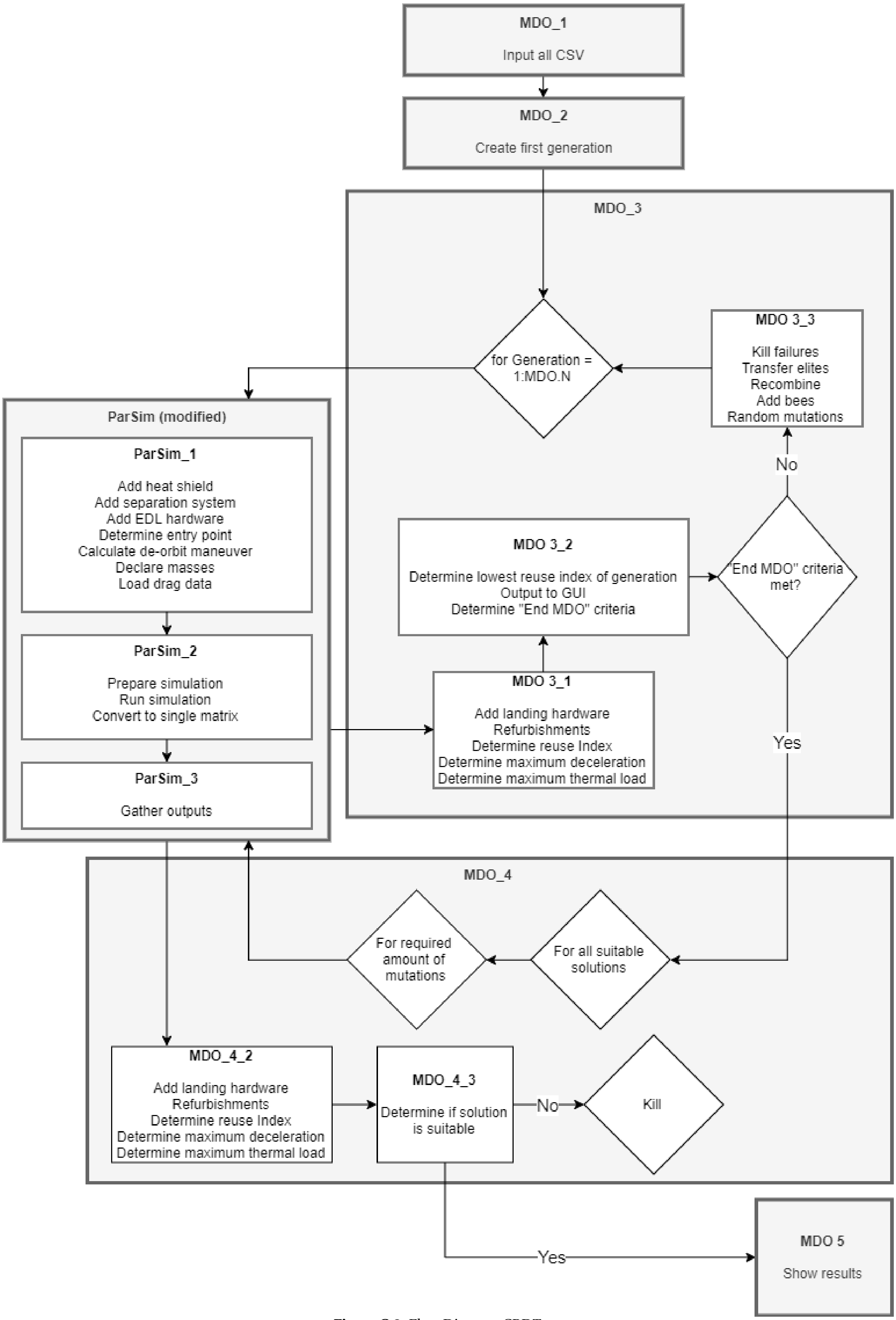

Figure C.2: Flow Diagram CRDT

C.2. De-orbit Burn Script

```
function [Mass,Cost] = MassBurn_Deorbit(dt,deltaVreq,Constants,System,Costs)

mt = System.Body.MassEmpty;
tb = 0;
deltaV = 0;

while abs(deltaVreq) > deltaV
    %       F = alim * Constants.g0 * mt;

    % Determine propellant required
    mdot = System.Body.Engine.ThrustVac/(System.Body.Engine.Isp*Constants.g0);
    mt = mt + mdot*dt;

    % DeltaV reached in this step
    detaV_step = (System.Body.Engine.ThrustVac/mt) * dt;

    % Total deltaV and burn time
    deltaV = deltaV + detaV_step;
    tb = tb + dt;
end

% Determine propellant mass
Mass = mt - System.Body.MassEmpty;

% Determine cost
Cost = Mass*1/(1+System.Body.Engine.OF) * Constants.CostLOX + ...
    Mass*System.Body.Engine.OF/(1+System.Body.Engine.OF) * Constants.CostH2;

f1 = Costs.Development(4,1);
f2 = Costs.Development(4,2);
f3 = Costs.Development(4,3);

Dev_factor = DevelopmentCosts(f1,f2,f3);
Cost = Cost*Dev_factor;

end
```

D

Complete overview of Inputs and Outputs

The following appendix gives an overview of the complete inputs and outputs of CRDT.

D.1. Inputs

1) Constants:

1. Gravitational acceleration at sea level
2. Stefan-Boltzmann constant
3. Mass of the Earth
4. Radius of the Earth
5. Gravitational constant
6. Heat capacity ratio of air
7. Standard gravitational parameter of Earth

2) Material Parameters:

1. Aramid ribbon cost per length
2. Aramid sheet cost per area
3. Aramid suspension line cost per length
4. Aramid riser cost per length
5. Nylon sheet cost per area
6. Nylon suspension line cost per length
7. Nylon riser cost per length
8. Aluminium cost per mass
9. Cost of a manhour
10. Hypalon cost per area
11. Hypalon mass per area
12. Pyrogel cost per area
13. Nextel cost per mass
14. Nextel mass per area
15. Kapton cost per area
16. Vectran mass per area
17. Vectran cost per mass
18. Cost liquid hydrogen per mass
19. Cost liquid oxygen per mass

3) Manhour costs:

1. Ringsail parachutes
2. Ribbon parachutes
3. Drag plates
4. Engine
5. Solid heat shield
6. Inflatable heat shield
7. Airbag
8. Retrorocket
9. Water landing
10. Mid air retrieval
11. Refurbishment
12. Separation system
13. Replacement of parts

4) Development parameters:

1. Separation system
2. Parachutes
3. Dragplates
4. Engine burn
5. Solid heat shield
6. Inflatable heat shield
7. Land landing
8. Water landing
9. Mid air recovery

5) System limits:

1. Acceleration limit, engines only
2. Acceleration limit, entire stage
3. Maximum landing velocity, no landing hardware
4. Maximum landing velocity, Retrorockets
5. Maximum landing velocity, Airbags
6. Maximum landing velocity, Water landing
7. Maximum landing velocity, Mid air recovery
8. Maximum allowable payload reduction
9. Maximum thermal flux
10. Maximum thermal flux heat shield

6) Initial orbit:

1. LEO
2. SSO
3. MEO
4. GTO

7) Launcher performance:

1. LEO payload per variant
2. SSO payload per variant
3. MEO payload per variant
4. GTO payload per variant
5. Launch cost per variant

8) Allowable range of following parameters:
1. Entry velocity
2. Entry angle
3. Entry altitude
4. Maximum deployment altitude of parachutes
5. Maximum deployment altitude of drag plates
6. Maximum deployment altitude of engine burns
7. Maximum parachute area
8. Maximum drag plate area
9. Engine throttle setting
10. Engine burn time
11. Heat shield area
12. Separation altitude

9) Stage definition:
1. Initial empty mass
2. Post separation mass
3. Diameter
4. Stage length
5. Radius of nose cone

10) Engine definition:
1. Maximum vacuum thrust
2. Vacuum specific impulse
3. Nozzle exit area
4. Chamber pressure
5. Nozzle expansion ratio
6. Oxygen/Fuel ratio
7. Engine to stage mass ratio
8. Total propellant mass

11) Stage costs:
1. Stage cost
2. Engine cost

12) GUI inputs:
1. Allowed heat shield types
2. Allowed decelerator types
3. Allowed landing hardware types
4. Nr of genes
5. Chance of mutation
6. Nr of elites
7. Nr of SuperElite
8. Nr of Bees
9. Initial orbit
10. Launcher variant
11. Allowed stage modifications
12. Nr of reuses

D.2. Outputs

1) Stage breakdown:
1. Configuration ID
2. Mass breakdown
3. Mass comparisons between original and reusable stage
4. Cost breakdown
5. Performance loss due to reusability
6. Reuse index

2) Sensitivity plot:
1. Reuse Index
2. Payload reduction
3. Maximum acceleration
4. Maximum thermal flux
5. Landing velocity

3) Figures:
1. Altitude - time plot
2. Velocity - time plot
3. Dynamic pressure - time plot
4. Deceleration - time plot
5. Orbit plot